

POLITECNICO DI TORINO

Corso di Laurea Magistrale in Ingegneria per l'Ambiente e il Territorio

Tesi di Laurea Magistrale

**Mathematical modeling of
cholera epidemics in South Sudan**

Modellazione matematica delle
epidemie di colera nel Sudan del Sud



Relatore:

Prof. Francesco LAIO

Relatori esterni:

Prof. Andrea RINALDO

Doct. Damiano PASETTO

Candidata:

Carla SCIARRA

matricola: 219921

Supervisor esterni presso

École Polytechnique Fédérale de Lausanne:

E. Bertuzzo, F. Finger, D. Pasetto, A. Rinaldo



Anno Accademico 2015-2016

This work is subject to the Creative Commons Licence.
Questo testo è soggetto alla Creative Commons Licence.

from the speech addressed at Board Meeting of the Vaccine Fund, May 2002:

"... We must ensure that children and parents and communities are educated and taught: unless all of our communities understand the importance of immunization, we will not succeed in preventing the millions of deaths that are occurring unnecessarily. And we must ensure that vaccines and health care are accessible and affordable for all families."

Nelson Mandela

Abstract

Cholera is one of the main health issue around the world, especially in Africa, where every year thousands of people die due to this enteric disease. International agencies, as the World Health Organization and the United Nation are making big efforts to help people in need and to stop this infection and, even if progresses have been made, a lot of work is still required.

Epidemiological models of cholera outbreaks, like the *SIRB* that is proposed in this thesis, have been developed in the last decades to better understand the routes of transmission of the infection and to provide key tools in elaborating intervention strategies in case of an emergency.

The mathematical approach used in this thesis work to simulate the epidemics consists of a spatially-explicit model driven by rainfall and human mobility. This methodology, which has already been successful in the reproduction of several cholera outbreaks, has several advantages: as first, the model considers the hydrological network in which the “cause bacteria” *Vibrio cholerae* can survive and move, which is one of the possible ways the epidemics can spread in infection-free areas; as second, the model accounts for the aggravating effect of the rain, which increases the bacteria concentration in the water through the run-off of excreta and latrines; as last the model considers human mobility, by which the bacteria can be suddenly spread far away by a daily traveler.

In this work, we analyze and model the cholera epidemics that affected South Sudan, the newest country in the world, during 2014 and 2015. South Sudan possibly represents one of the most difficult context in which adapt the deterministic mathematical cholera model, due to the unstable social and political situation that clearly affects the fluxes of people and the sanitary conditions, increasing the risk of large outbreaks. Despite the limitation of a static gravity model in describing the chaotic human mobility of South Sudan, the *SIRB* model, calibrated with a data assimilation technique (Ensemble Kalman Filter), retrieves the epidemic dynamics in the counties with the largest number of infected cases, showing the potentiality of the methodology in forecasting future outbreaks.

Contenuto

Il colera è una delle più importanti problematiche sanitarie nel mondo, specialmente in Africa, dove ogni anno migliaia di persone muoiono affette da questa malattia enterica. Le agenzie internazionali, come l'Organizzazione Mondiale della Sanità e le Nazioni Unite, lavorano per fermare l'epidemie, e nonostante i progressi, tanto lavoro è ancora necessario. I modelli epidemiologici del colera, come il *SIRB* che viene utilizzato in questa tesi, sono nati con l'intento di studiare i meccanismi di trasmissione della malattia e di fornire strumenti utili all'elaborazione di strategie in caso di emergenza.

L'approccio matematico utilizzato è un modello spazialmente esplicito in cui le principali forzanti risultano essere la pioggia e la mobilità umana. La validità di tale metodo è stata comprovata dall'applicazione su altri casi studio. Tra i vantaggi principali del modello proposto, in primis, quello di considerare la rete ambientale in cui il "batterio causa" *Vibrio cholerae* può sopravvivere e muoversi, spostando così l'infezione in posti in cui prima non ve n'era presenza; inoltre, il modello tiene conto dell'effetto aggravante delle piogge che possono, tramite lisciviazione degli escrementi e delle latrine, aumentare la concentrazione dei batteri nell'acqua; infine, viene presa in considerazione la mobilità umana, tramite la quale la malattia può essere spostata improvvisamente da un pendolare quotidiano su lunghe distanze.

In questo lavoro, sono state analizzate e studiate le epidemie di colera che hanno coinvolto il Sudan del Sud nel biennio 2014-2015. Il Sud Sudan è forse uno dei contesti più difficili nel quale adattare la formulazione matematica deterministica che è stata proposta, dovuto alle instabili condizioni socio-politiche che evidentemente influenzano i flussi di persone e le condizioni sanitarie del paese, aumentando il rischio che malattie trasmissibili possano diffondersi in tutta la nazione. Nonostante le limitazioni nel descrivere la caotica mobilità umana in Sud Sudan, il modello *SIRB*, calibrato con una tecnica di data assimilation (Ensemble Kalman Filter), riesce a simulare le dinamiche delle epidemie nelle zone dove si registra il più alto numero di infetti, mostrando quindi la potenzialità della metodologia nel prevedere future epidemie.

Contents

Abstract	v
Contenuto	vi
List of figures	ix
List of tables	x
Acronyms	x
1 Introduction	3
1.1 Cholera epidemiology	3
1.2 Modeling the epidemics	4
1.3 South Sudan epidemics	5
1.4 Objectives and structure	5
2 Background of South Sudan cholera epidemics	7
2.1 Geography and land administration	7
2.1.1 Geography, topography and hydrography	7
2.1.2 Administrative division	9
2.2 Climate	10
2.3 Economic, social, political and demographic aspects	11
2.3.1 Population	11
2.3.2 Water and sanitation	13
2.4 Cholera epidemics	13
2.4.1 Year 2014	14
2.4.2 Year 2015	15
3 Cholera epidemiological model	17
3.1 Model assumptions	17
3.1.1 SIR model	18
3.2 SIRB Model	19
3.3 Model parameters and calibration	22
3.3.1 The Bayesian approach	24
3.3.2 Ensemble Kalman Filter	26
4 Model setup and epidemiological data	29
4.1 Epidemiological records	29
4.2 Framework	29
4.3 Centroids	32
4.4 Population	37
4.5 Distances	39
4.6 Rainfall data	39
4.7 Adapting the model	42
4.8 Calibration set-up	42
4.9 Initial conditions and time of the simulations	43
4.10 Pseudo-code	45

5 Results and discussion	48
5.1 Prior definition	49
5.1.1 First attempts for year 2014	49
5.1.2 Prior for South Sudan	52
5.2 Year 2014	53
5.3 Year 2015	58
5.4 Discussion	62
6 Conclusions	65
Bibliography	72

List of Figures

1.1	<i>Vibrio Cholerae</i> bacteria	3
1.2	Paths and states of cholera epidemics	4
1.3	Time series of suspected cholera cases	6
2.1	South Sudan geography	8
2.2	South Sudan topography	9
2.3	South Sudan hydrography	10
2.4	South Sudan administrative division	11
2.5	South Sudan Köppen-Geiger climate classification	12
2.6	Water, sanitation and hygiene data	13
2.7	Vaccination sites and epidemic attack rate for 2014	14
2.8	Cholera epidemic: map for 2014	15
2.9	Cholera epidemic: map for 2015	16
3.1	Schematic representation of the SIRB model	21
3.2	Schematic representation of DA technique	28
4.1	Modifications for the Payam of Juba	30
4.2	Spatial domain of the model	31
4.3	Population distribution from WordPop	33
4.4	Population distribution, re-sized raster	34
4.5	Payam raster image for centroid computation	35
4.6	Grid to compute centroids	36
4.7	Position of the Payams' centroids	37
4.8	Rain analysis on January 1 st , 2014	40
4.9	Payam raster image for rainfall analysis	41
4.10	Detail on the comparison between Payam vector and raster representation	42
5.1	EnKF, simulations for 2014 using prior Haiti, global behavior	50
5.2	EnKF, simulations for 2014 using prior Haiti, cumulative curve	50
5.3	EnKF, simulations for 2014 using prior Haiti, County-level cases	51
5.4	EnKF, simulations for 2014 using prior Haiti, parameters behavior	52
5.5	EnKF, simulations for 2014 using the new prior, global behavior	54
5.6	EnKF, simulations for 2014 using the new prior, cumulative cases	54
5.7	EnKF, simulations for 2014 using the new prior, County level cases	55
5.8	EnKF, simulations for 2014 using the new prior, parameters behavior	56
5.9	Open Loop, simulation for 2014 using the new prior, global behavior	57
5.10	EnKF, simulations for 2015 using the new prior, global behavior	58
5.11	EnKF, simulations for 2015 using the new prior, cumulative cases	59
5.12	EnKF, simulations for 2015 using the new prior, County level cases	60
5.13	EnKF, simulations for 2015 using the new prior, parameters behavior	61
5.14	Open Loop, simulation for 2015 using the new prior, global behavior	62
5.15	Response of the gravity model	63

List of Tables

3.1	Parameters of the model	23
3.2	Reduced parameters of the model	24
4.1	Fixed parameters	43
4.2	Initial conditions and times	44
5.1	Range of the parameter prior distribution from Haiti case study	49
5.2	Range of the parameter prior distribution for South Sudan case study	53
5.3	RMSE comparison for simulations of year 2014	57
5.4	RMSE comparison for simulations of year 2015	61

Acronyms

DA	Data Assimilation
DREAM	DiffeRential Evolution Adaptive Metropolis
EnKF	Ensemble Kalman Filter
IDPs	Internally Displacement Persons
KF	Kalman Filter
MC	Monte Carlo
MSF	Médecins Sans Frontières
PoC	Protection of Civilians
PDF	Probability Density Function
RMSE	Root Mean Square Errors
SIRB	Susceptible-Infected-Recovered-Bacteria
SS	South Sudan
SSMoH	South Sudanese Ministry of Health
SSNBS	South Sudan National Bureau of Statistics
UN	United Nations
UNHCR	United Nations High Commissioner for Refugees
UNICEF	United Nations Children’s Emergency Fund
WASH	Water, Sanitation and Hygiene
WHO	World Health Organization

All the maps in this work were processed with the use of ArcGIS 10.3 from data and shapefiles made available from the South Sudan Government, the South Sudan National Bureau of Statistics and the World Health Organization. In order to maintain the authenticity of these information, we tried to minimize the number of modifications to the least possible yet adequate to allow us to analyze the new acquired information. Misfits between shapefiles and different spelling of toponyms are possible. Results and data of the model have been processed using MATLAB 2015.

Introduction

1.1 Cholera epidemiology

Cholera is an enteric disease caused by the bacteria *Vibrio Cholerae*, usually of serogroup O1 and O139 (Kaper et al., 1995) (Fig.1.1). The infection is subject of studies since the XIX century when the disease spread in the Indian subcontinent, although proofs of a possible cholera infection can be found back in the 5th century BC in Sanskrit (Harris et al., 2012). Nowadays, cholera is a public health issue around the world, above all in developing countries, most of the time occurring in the African continent (Bhattacharya et al., 2009). The bacterium naturally lives in the human intestine but it also survives and reproduces in the aquatic environment, causing spread of the infection thanks to the waterways and the river networks. In fact, it has been shown that the bacteria are found in association with zooplankton and aquatic vegetation, resulting autochthonous in some coastal regions (Colwell, 1996; Lipp et al., 2002).



Figure 1.1: *Vibrio Cholerae* bacteria. (Mekalanos J. and Lehman A., 2012)

Transmission of the disease occurs through ingestion of contaminated water or food (Miller et al., 1985). Once ingested, the bacteria *V. Cholerae* colonize the small intestine and elaborate *cholera toxin*, a protein toxin that triggers fluid and electrolyte secretion by intestinal epithelial cells (Nelson et al., 2009). Recently, laboratory analysis have suggested that the passage of the bacteria into the gastrointestinal tract can raise in hyperinfectious status (Fig.1.2), facilitating the *human-to-human* transmission of the illness (Bertuzzo et al., 2008). Other studies are now highlighting the role of animals in carrying the bacteria and the house environment as a reservoir of bacteria (Kaper et al., 1995).

The infection can be asymptomatic or can affect the human host with watery diarrhea that lasts a few days. Other symptoms can be nausea and muscle cramps. In some cases, severe diarrhea can lead to dehydration and electrolyte imbalance, until death (WHO, 2010). The disease can be defined as *endemic* or *epidemic*. It is endemic in cases in which the infection recurs in time and

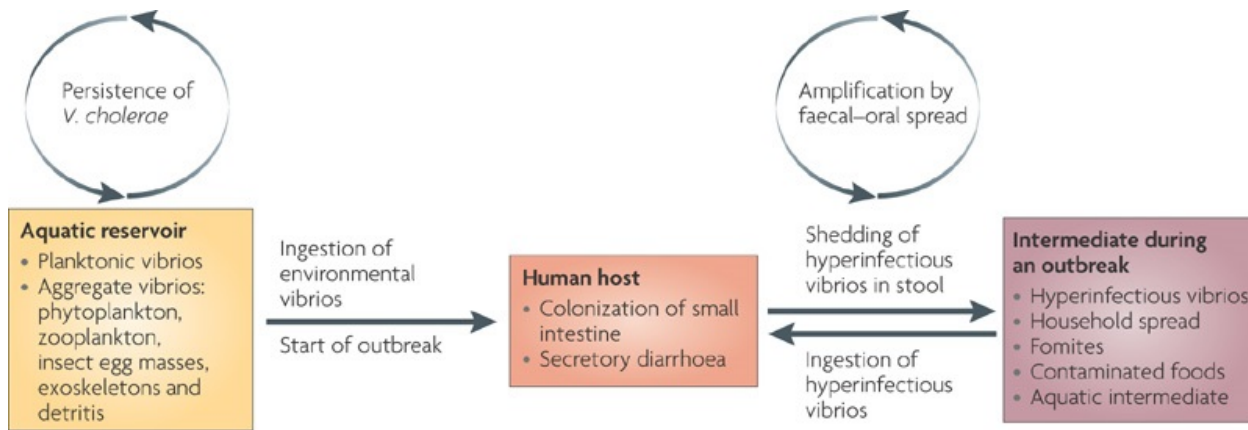


Figure 1.2: Schematic representation of cholera transmission paths and states. Susceptible people can contract the disease by ingestion of environmental vibrios. Symptomatic infection enhances, via excreta, the local concentration of the pathogen, powering the route of transmission with hyperinfectious states and amplifying the faecal-oral spread of the disease (Nelson et al., 2009).

place, whereas epidemic denotes cholera occurring unpredictably.

The role that environmental factors play in the spreading phenomena of cholera infection is then evident. As the bacteria can move in the aquatic environment, each change in the hydrological cycle may affect the pathogenic concentration in water: rain and its seasonal behavior, droughts and floods, can enhance or reduce the transmission process.

Nevertheless, relevance has to be given to the environmental matrix in which the disease spreads into disease-free regions (Bertuzzo et al., 2008), together with consideration on human mobility and travelers carrying the disease in long-distance journeys. Susceptible people traveling on a daily basis may contract the disease in destination sites and take the disease back to the possibly uninfected communities where they regularly live. At the same time, infected individuals not showing severe symptoms, can carry the illness releasing bacteria via their faeces (Mari et al., 2012). Finally, symptomatic infected individuals locally increase the bacteria concentration, which is then spread along the hydrological network.

1.2 Modeling the epidemics

Epidemiological models for large-scale diseases as cholera, likewise measles, SARS and other contagious diseases, are relatively recent and are now taking off for their capability to understand the process dynamic and forecasting, analyze intervention scenarios and attack strategies to reduce the spreading phenomena. The first cholera model was proposed by Capasso and Paveri-Fontana (1979) to describe the epidemic in Bari (Italy) during 1973. Codeço (2001) extended the model, considering the dynamics of the susceptible population, together with the dynamics of the infected population and the free-living pathogens. Particular progress in the mathematical modeling of cholera epidemics has been made in response to the dramatic Haiti outbreak in 2010, in the attempt of aiding the real-time emergency management in allocating health care resources and evaluating intervention strategies (Bertuzzo et al., 2014).

The model used in this work to study the dynamic of cholera epidemics in South Sudan, has been developed in the Laboratory of Eco-Hydrology at the École Polytechnique Fédérale de Lausanne, together with the cooperation of the Polytechnic University of Milan and the University of Padua within the project DYCHO - *Dynamics and Controls of large-scale Cholera Outbreaks* -, supported by the Swiss National Science Foundation. This deterministic model simulates the dynamics of Susceptible, Infected, Recovered individuals, and Bacterial concentrations – *SIRB model* – in a spatially-explicit setting of local human communities. In this way the model results can be compare

with the real epidemiological data (Bertuzzo et al., 2014) collected in different zones of the infected region. With respect to the standard zero-dimensional SIR models, the spatially-explicit framework has the advantages to consider the environmental matrix along which the disease can spread and the river network in transporting and redistributing *V.Cholerae* (Bertuzzo et al., 2010). An additional advantage of the proposed formulation is to include rainfall data and human mobility as drivers of transmission.

A first formulation of this model has been used to simulate the 2000 cholera epidemic in KwaZulu-Natal province in South Africa (Bertuzzo et al., 2008; Mari et al., 2012). Other applications of the spatially explicit and rainfall-driven model include cholera epidemics in Haiti in October 2010 (Bertuzzo et al., 2011, 2012, 2014; Rinaldo et al., 2014; Mari et al., 2015; Pasetto et al., 2016) and in Lake Kivu Region, Democratic Republic of Congo, between 2004-2011 (Finger et al., 2014). A last conception of the model has been applied for 2005 cholera epidemic in Senegal by Finger et al. (2016), using mobile phone data to fully catch the influence of mass gatherings in the spreading of the disease.

1.3 South Sudan epidemics

In this thesis we study the epidemics that affected South Sudan in 2014 and 2015. Epidemiological records have been made available by the South Sudan Minister of Health - *SSMoH*. In recent years, 4 major cholera outbreaks have occurred in South Sudan. The unstable social conditions of the Nation, together with poverty and lack of sanitation, enhanced the risk until the outbreak of a new infection in 2014.

Despite the oral cholera vaccination campaign into the Protection of Civilians camps at the beginning of 2014, whose population-level effectiveness was highly affected by mass population displacements (Azman et al., 2016), the first cholera case was confirmed in April 23, 2014 in the capital Juba. Four weeks later, the SSMoH declared the outbreak. In total, 6,269 suspected cases were recorded, including 156 deaths. The epidemic ended in October 2014, not evolving in endemic. Unfortunately, the country passed through a similar condition during the following year. The 2015 epidemic, if compared to the previous year, affected less the country in terms of number of cases and duration (Fig. 1.3). First case showed up in May 18, 2015 and the totally recorded suspected cases were 1,575, with 46 deaths. The epidemic ended in September 2015.

1.4 Objectives and structure

This thesis has three aims. First, with our work we would like to contribute to the understanding of the South Sudan epidemic dynamics, by analyzing the context in which the disease spreads. The second task of the thesis consists in the setup of the spatially-distributed cholera model for the SS epidemics, objective particularly challenging due to the critical country conditions, the internal civil wars and the scarcity of mobility data. Different advanced calibration procedures have been proposed to assess the probability distribution of the model parameters governing the epidemic processes. The third and final goal is to analyze the results of the simulations in order to suggest future directions for further understanding of cholera dynamics in South Sudan, and possibly extending the discussion to general large-scale epidemics.

The report is organized as follows:

Chapter 2: *Background of South Sudan cholera epidemics*, delineation of the area affected by the epidemics. The geography, hydrology and climate of the country will be shortly described as well as the time and space characteristics of 2014-2015 epidemics.

Chapter 3: *Epidemiological model*, details on the mathematical structure of the rainfall-driven, spatially-explicit model of cholera epidemics. This chapter contains as well a brief yet concise

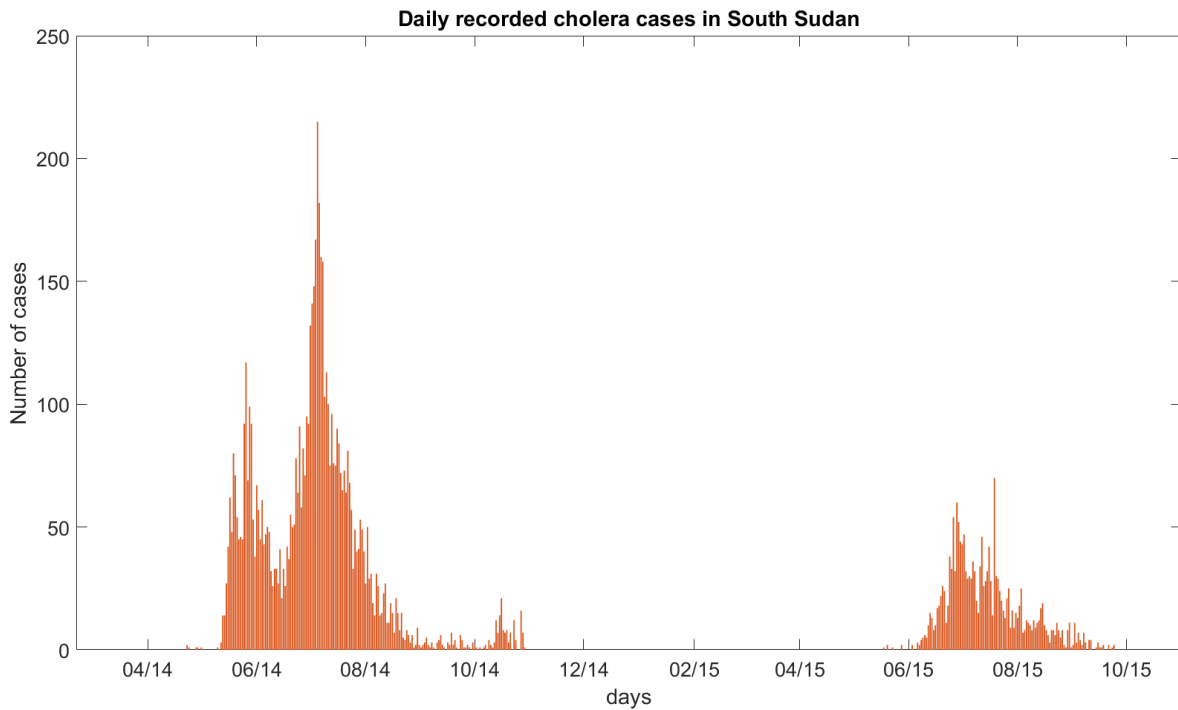


Figure 1.3: Time series of all suspected cholera cases registered by SSMoH and WHO all over South Sudan territory.

digression on the *Ensemble Kalman Filter*, the data assimilation technique here adopted for the calibration of the model against the epidemiological data.

Chapter 4: *Model setup and epidemiological data*, chapter dedicated to the description of the model setup and input data (rainfall and population). Particular attention is dedicated to the domain discretization, based on the available epidemiological records.

Chapter 5: *Results and discussion*, presents and discusses the model responses associated to different calibration procedures for both years of analysis.

Chapter 6: *Conclusions*, drives toward main conclusions of this thesis work, highlighting the benefits of using the spatially-explicit model for the simulation of the epidemics and suggesting some possible model improvements for future works.

Background of South Sudan cholera epidemics

Originally belonging to Sudan, the Republic of South Sudan is the newest nation in the world. The territory of Sudan, referring to both Northern and Southern parts, has always been land of great interest by conquerors due to the presence of the Nile and, recently, due to oil reservoirs. After years of Arab domination and British-Egyptian rule, Sudan gained its independence in the second half of the XX century. From then onward two civil wars (1955-1972; 1983-2005), due to heterogeneity in ethnicity and in religion between the two sudanese parts, affected the entire population, leading to more than 2 millions deaths and 4 millions refugees. In 2005, at the end of the Second Sudanese Civil War, the so-called ‘Comprehensive Peace Agreement’ among the two factions established the terms of autonomy of the Southern Sudan. The country obtained independence from the Northern part thanks to a referendum on self-determination in July 2011, becoming the 54th country of the African Continent (Treccani, 2016; Collins, 2015; SSNBS, 2012).

2.1 Geography and land administration

2.1.1 Geography, topography and hydrography

South Sudan is a landlocked country situated in Central Africa. It shares its borders with Sudan to the north, Ethiopia to the east, Kenya, Uganda and the Democratic Republic of Congo to the south, and Central African Republic to the west. The capital city is Juba, which is also the most populated one, located in the south east. The total extension of the country is about 644,329 km² (CIA, 2015). Due to political and governance conflicts, borders are actually not well defined, as instance the Abyei area and the north-western borders. For the purpose of this thesis, we do not take into account the disputed areas. Figure 2.1 shows South Sudan placement and borders.

The country is predominantly flat. There are only two upland areas:

- the *Imotong Mountains*, situated on the Uganda borders, characterized by high peaks. Here the Mount Kinyeti, the highest point in South Sudan, raises up to 3,172 meters (Collins, 2015; Global Security, 2016)
- the *Ironstone Plateau*, at the feet of the ‘Nile Congo watershed’ on the west side borders, whose peaks’ elevation is among 800 and 1,700 meters. (Collins, 2015)

Figure 2.2 shows the topography of the area under study.

At the hearth of the nation a clay plain is present, where the Mountain Nile flows from south to north. This area, named *Al-Sudd*, is characterized by swamps, lagoons, side channels, and several lakes created by the Mountain Nile and its tributaries (mainly the Sobat River from Ethiopia and the Bahr Al-Ghazal River from the west) (CIA, 2015; Collins, 2015) (Fig.2.3). In this area, the Nile becomes the White Nile thanks to the debit of the other streams.



Figure 2.1: Position of South Sudan territory and its capital Juba in the African continent. Dashed lines show disputed areas and undefined borders. Data provided by SSMoH and OpenStreetMap (2015).

The Al-Sudd swamp is the main drainage area, covering more than 100,000 km², almost the 15% of the country's total area. The label 'Sudd' is the local term defining the vegetation that covers the entire region (Collins, 2015).

In 1978 the Jonglei Canal was planned to bypass Al-Sudd swamp and provide a straight well-defined channel for the Nile to flow. The building of the structure stopped due to the political instability and during the rain season, this part of the country is not viable using means of land transport (Treccani, 2016; SSNBS, 2012).

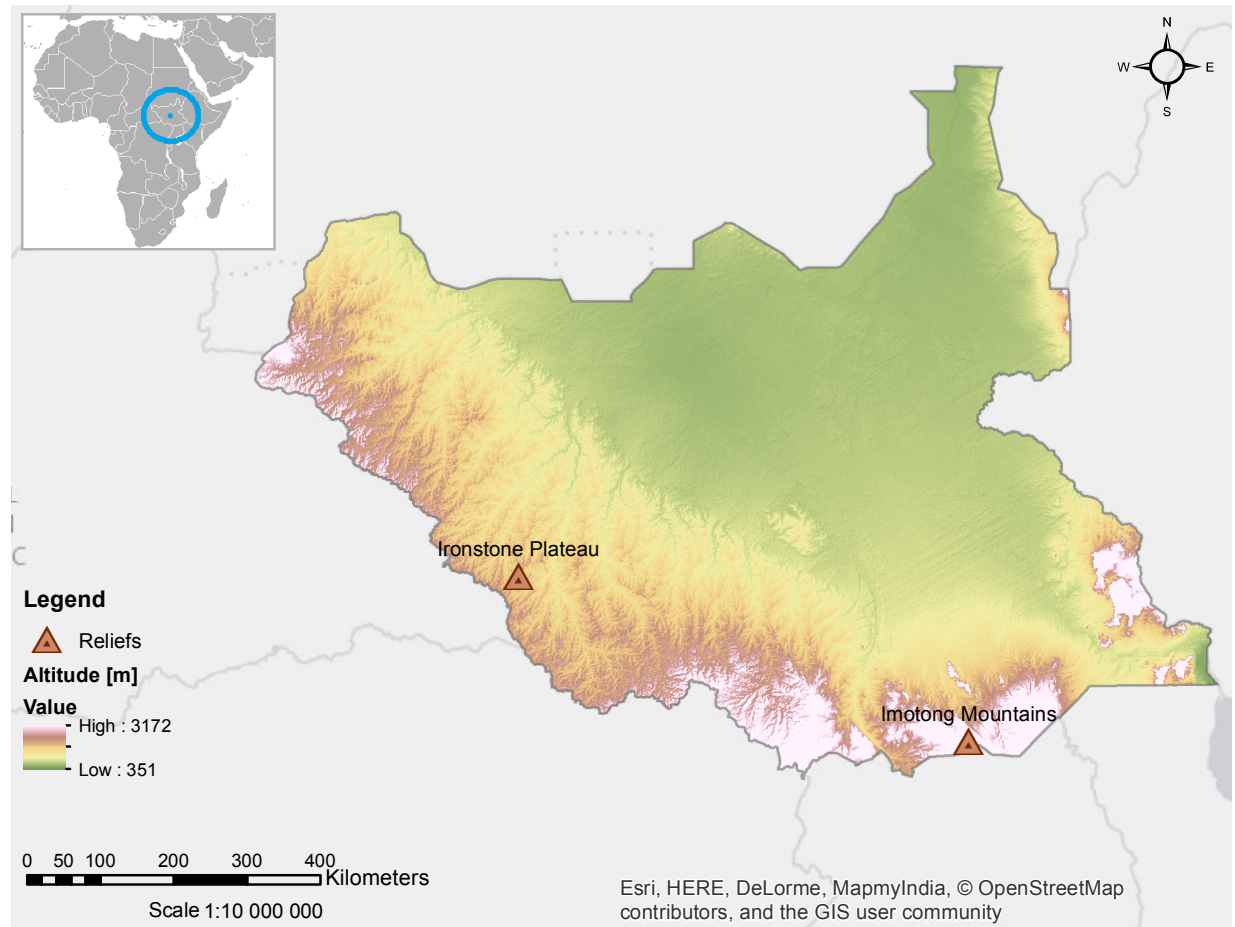


Figure 2.2: Digital Elevation Model of South Sudan provided by SSMoH and position of the upland areas. Resolution 90 meters. Data provided by SSMoH and OpenStreetMap (2015).

2.1.2 Administrative division

For administrative purposes, the nation is divided in ten states (Fig.2.4), following the three historical regions of Sudan: *Bahr el Ghazal*, *Equatoria*, and *Greater Upper Nile*. Each state is then divided in *counties*, themselves divided in *payams*, which are aggregates of villages. The minimum number of inhabitants required per payam is 25,000. They can be further subdivided into a variable number of *Bomas* (Grawert, 2010).

A new subdivision has been proposed by President Salva Kiir in December 2015 for establishing 28 states, whose borders are defined following ethnicity and the historical three regions (Sudan Tribune, 2015). For the aim of this thesis, and following all the official reports found, we will consider the structure showed in Figure 2.4, i.e. before December 2015.

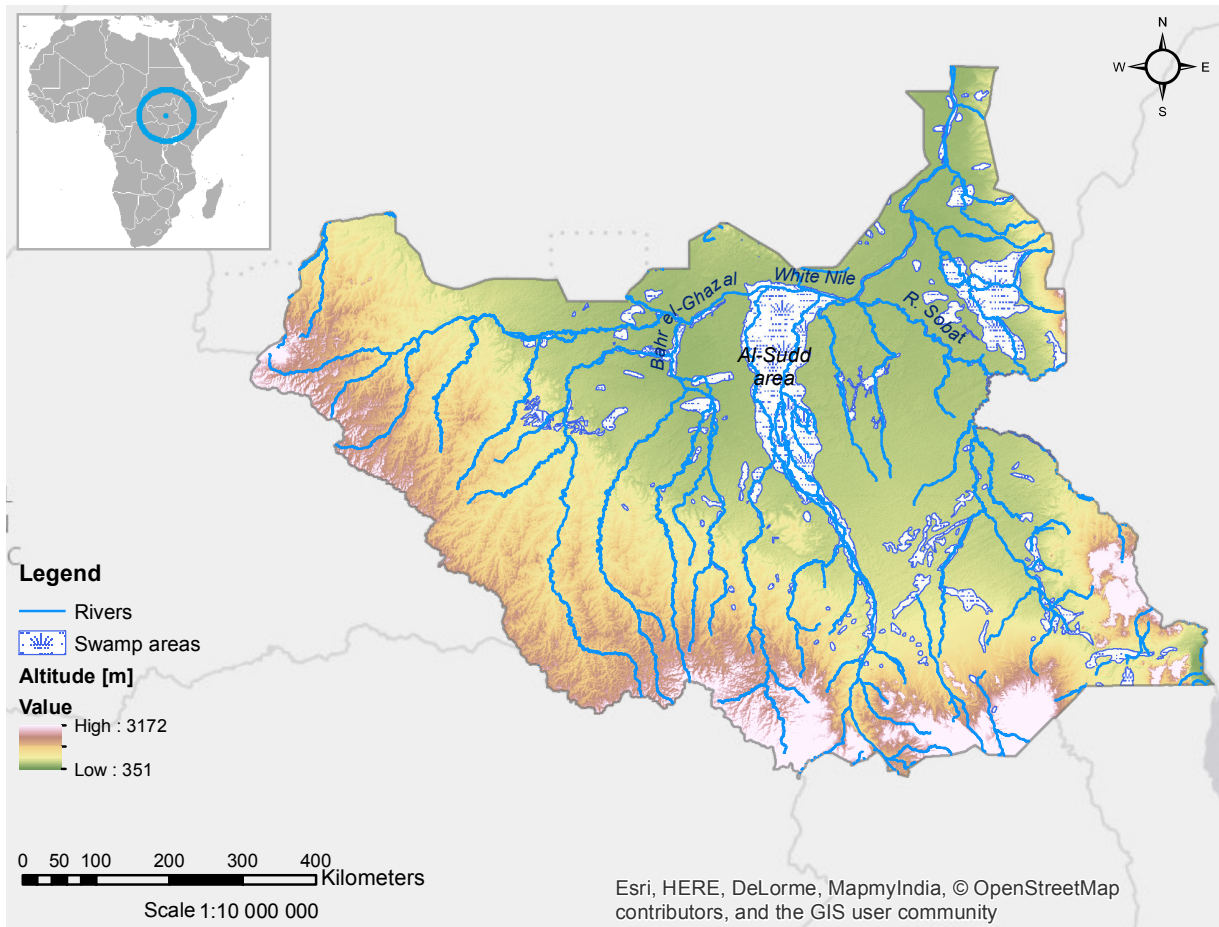


Figure 2.3: Hydrographic network of South Sudan. Al - Sudd swamp area is highlighted. Data provided by SSMoH and OpenStreetMap (2015).

2.2 Climate

The southern sudanese territory is vast, so that diverse climates are present along it. Analyzing the country in latitude, according to the Köppen-Geiger Climate classification based on temperature and precipitation (Fig. 2.5 on page 12), we can distinguish dry, arid and semiarid climates in the north (12°N, Group B) and, wet savanna climate in the south (3°N, Group A) (Collins, 2015; VUVM, 2011). Specifically, a small north-eastern part on the borders with Sudan is classified as *BWh*, presenting warm desert climate conditions; while on the west side of the same border, classification states a warm semi-arid climate *BSh*.

The majority of the country is although influenced by the annual fluctuations of the *Inter-Tropical Convergence Zone*, determining a tropical savanna climate group (*Aw*) (Global Security, 2016). Cool and dry winds from north-east blow at the beginning of the year, meeting after few months the moist southwesterlies winds. The wet season starts roughly in April and lasts until November, though its length is variable. Rainfalls result to be heavier in the southern upland areas, due to orographic phenomena. In the tropical savanna region, temperature has not spatial variability, and its values increase going towards the end of the dry season and reaching more than 35 °C in March. July is the coldest month, when temperature falls down to 20 °C or less (World Atlas, 2016; Global Security, 2016).

The meteorological situation has effects on the social and economical southern sudanese aspects and on the environment. As instance, the tropical forest that grows during the wet season is cut and burnt during the dry season, compromising the ecosystems. Roads, that in some cases only consist in rough tracks or not even that, become impassable during the rainfalls.

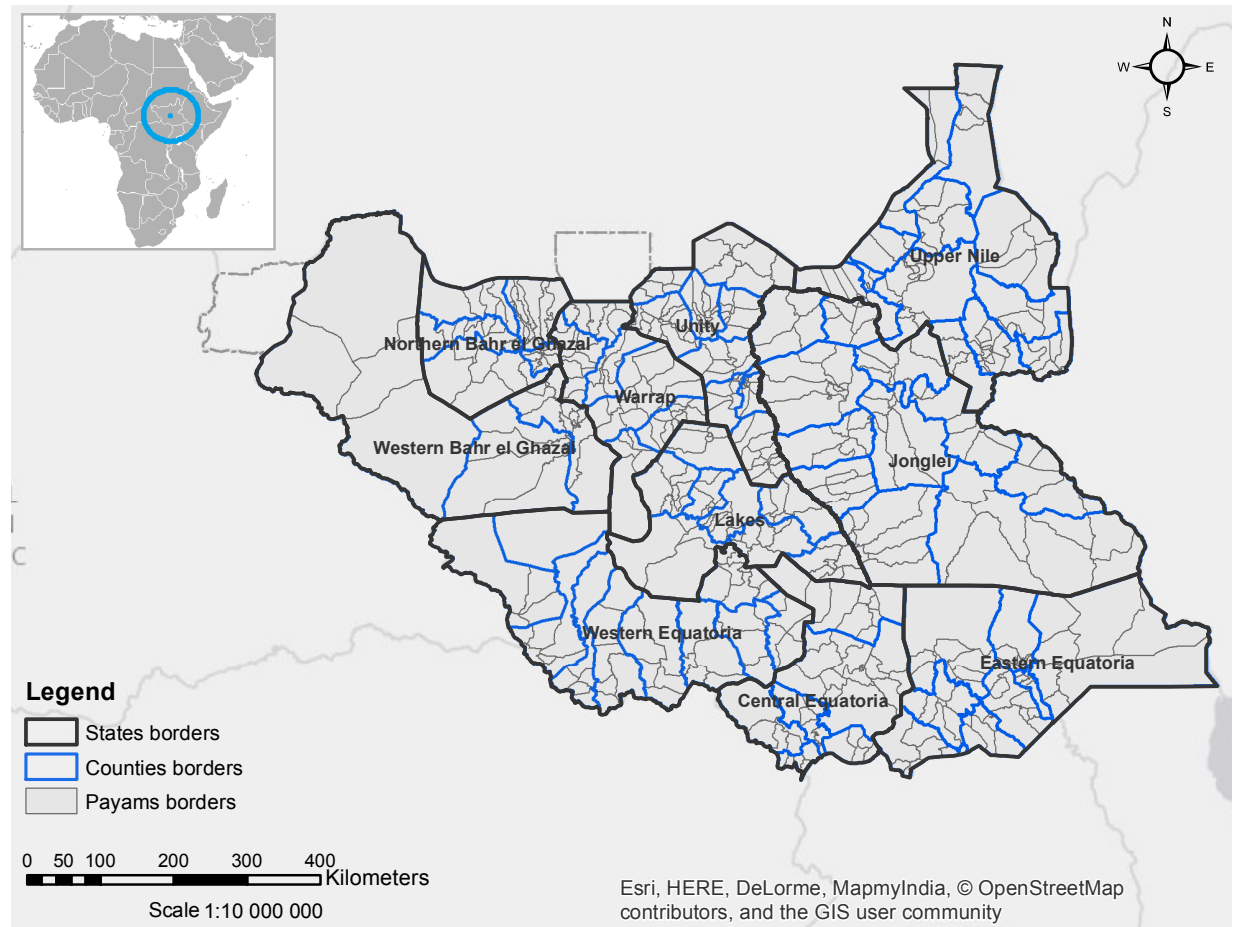


Figure 2.4: Administrative division of South Sudan up to November 2015. The map shows the 10-states division, together with the organization in counties - thick dark grey line - and Payams - thin black line.

2.3 Economic, social, political and demographic aspects

The Republic of South Sudan is one of the poorest and less developed country in the world, appearing at the 169th place in the Human Development Index scale (SSNBS, 2012).

Subsequently to the establishment of the secession, conflicts were born in the area of Abyei, on the borders with Sudan, as a result of disputes for the control of oil reservoirs. Moreover, the government was not able to manage a country with so many internal fractures because of ethnicity. Corruption and conflicts of interests rule the country. The political party that brought the nation to the independence, the Sudan People's Liberation Movement (SPLM), is now divided and fighting for power, wasting money in army. At the same time, violent rebels fight against the government. In December 2013, violence broke out in the streets of the capital Juba, giving start to another internal war (Kelly, 2016) that keeps going (BBC, 2016).

The lack of infrastructures that characterizes the country complicates the relationships with the surrounding countries. Roads are mainly unpaved; a single-track railroad connects the city of Weu in Western Bahr el Ghazal to Babonosa in Sudan. International flight connections are present from Juba and Malakal. Internal flight connections, supported by UN are scheduled (SSNBS, 2012; UNMISS, 2015).

2.3.1 Population

At the time of writing, the exact value of the population of South Sudan is unknown. The last census was organized in 2008 during the Sudanese administration, when the population reached by

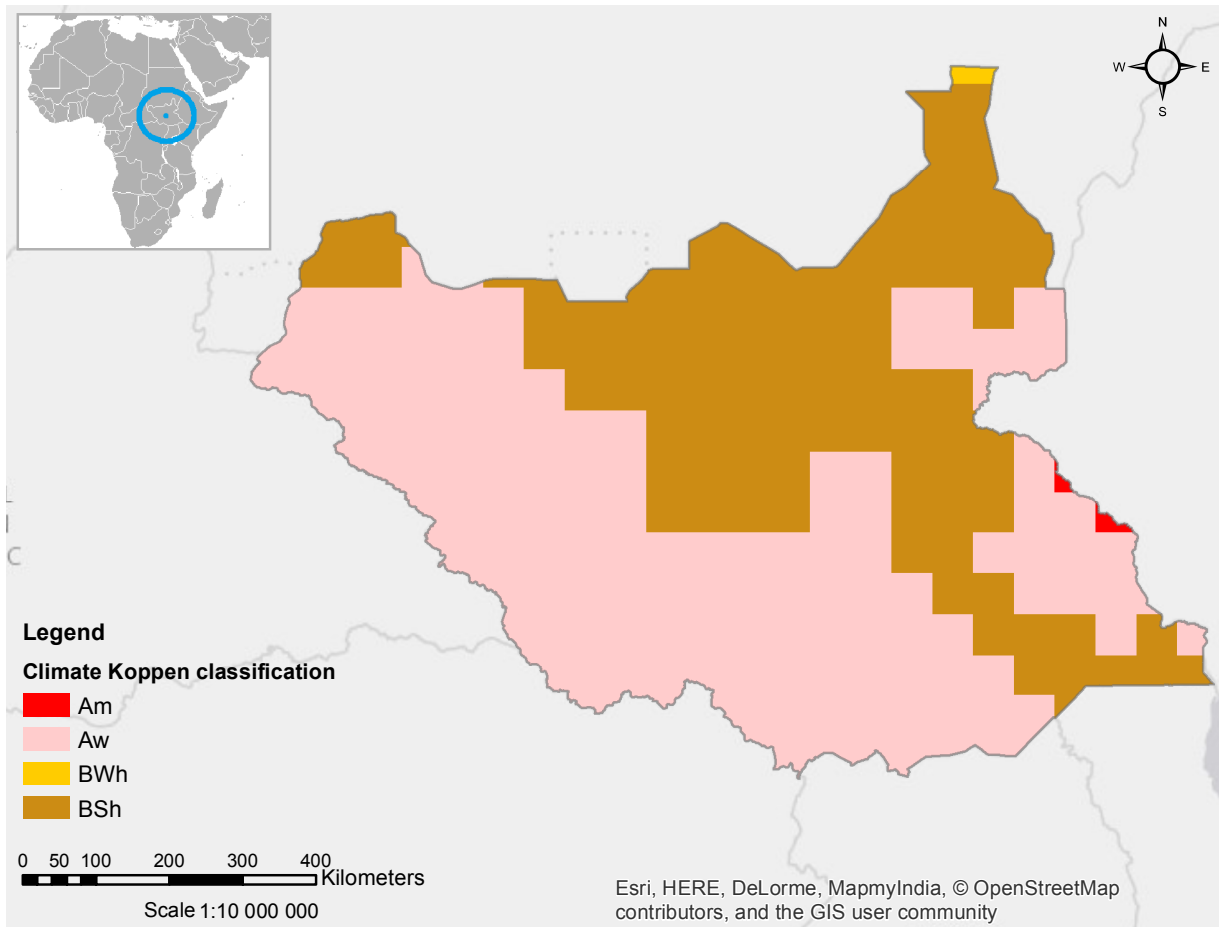


Figure 2.5: Köppen-Geiger classification on the region of South Sudan from observed data between 1976 and 2000. Regular 0.5 degree lat/lon grid, about 56 km at these latitudes (VUVM, 2011).

the census in the southern part was 8,260,490 (SSNBS, 2010). Estimation made by UN (2015) states 12,340,000; while CIA (2015) attests 12,042,910 people in July 2015. SSNBS (2015a) projected for 2015 11,000,000 people.

The nation has the highest population growth rate in the world, registering an annual increment of 4% (CIA, 2015).

The 2008 census data show that the population is very young, with half of it below 30 years old. Life expectancy is very low compared to values in neighboring countries. Population is uneven between the ten states, being Jonglei the most inhabited one (1,443,500 people in 2008) while Western Bahr El Ghazal the least one (358,692 in 2008) (Fig. 2.4 for geo-political references). The 83% of the population lives in rural areas (SSNBS, 2010).

Moreover, distribution and density of the population are affected by refugees movements. South Sudan hosts both external refugees from Sudan, as a consequence to the long War in Darfur, and internal refugees, subsequently to the outbreak of violence in December 2013. At this regard WHO (2015a) reported:

“The humanitarian situation in South Sudan has deteriorated since the outbreak of violence on 15 December 2013. Total of 195,416 persons has been displaced to camps from Bor, Bentiu and Malakal in Jonglei, Unity and Upper Nile states.”

People move and establish in arranged settlements (defined as Internally Displacement Persons IDP) or to PoC - Protection of Civilians sites, as to say, sites where civilians seek protection and refuge at existing United Nations bases when fighting starts (UNMISS, 2015).

Since the beginning of new fights, south-sudanese people are additionally moving abroad seeking

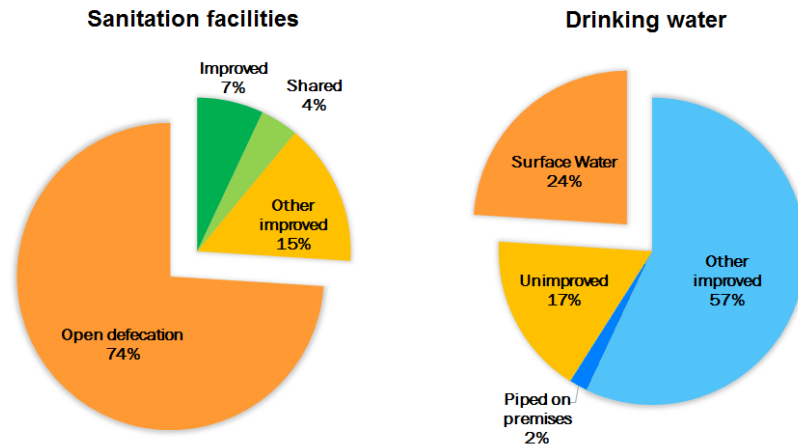


Figure 2.6: Water, sanitation and hygiene conditions in South Sudan. Color scale following UN definitions on WASH. Data from WHO & UNICEF (2015).

for protection: UNHCR (2016), in the last update on June 3, 2016 reports 844,406 displaced persons crossing into Ethiopia, Kenya, Sudan and Uganda. The number of refugees that moved into the nation is 272,261 .

Migrations are affected, besides frequency and intensity of conflicts, by the seasonality of rain, whose direct consequence is on the impossibility to cross the country in the mud, as described previously.

2.3.2 Water and sanitation

According to WHO & UNICEF (2015), the 59% of the population has access to improved sources of drinking water (considering as improved ‘Piped on premises’ and ‘Other improved’, definition by UN, see reference), i.e. people use water that received some kind of treatment. The 24% instead uses surface water (see Fig. 2.6). In urban areas the percentage of people with access to improved systems is 67%, while is 57% in rural areas. Many inhabitants have to walk for more than 30 minutes to collect drinking water (SSNBS, 2012).

As regards sanitation, only the 7% of the population uses improved sanitation facilities. In urban areas, the 16% has access to improved sanitation facilities and the 10% shares them. The 74% of the peoples still practice open defecation. These conditions enhance the risk of water-driven infectious diseases, as cholera, to spread.

Conflicts and social instability worse the situation. WHO (2015a) in its report on December 2013 added:

“Poor water, hygiene and sanitation conditions in the camps for the internally displaced people increases risk of communicable diseases.”

2.4 Cholera epidemics

Cholera epidemics affected the country back in 2006, when the number of cases totaled 19,777; in 2007 were 22,412; in 2008, cases totaled 27,017; and in 2009 cases totaled 48,035 (Ujjiga et al., 2015). In 2012 an outbreak has been avoided, thanks to a preventive mass vaccination campaign decided on a risk assessment for the potential impact of cholera into refugee camps (Porta et al., 2014). As WHO anticipated, the fear of a new outbreak moved the South Sudanese Ministry of Health - SSMoH - to action. As reported by Abubakar et al. (2015) and Azman et al. (2016), at the beginning of 2014 the SSMoH requested the intervention of WHO to vaccinate 163,000 IDPs in six small camps throughout the country using the global oral vaccine stockpile. The six refugee camps

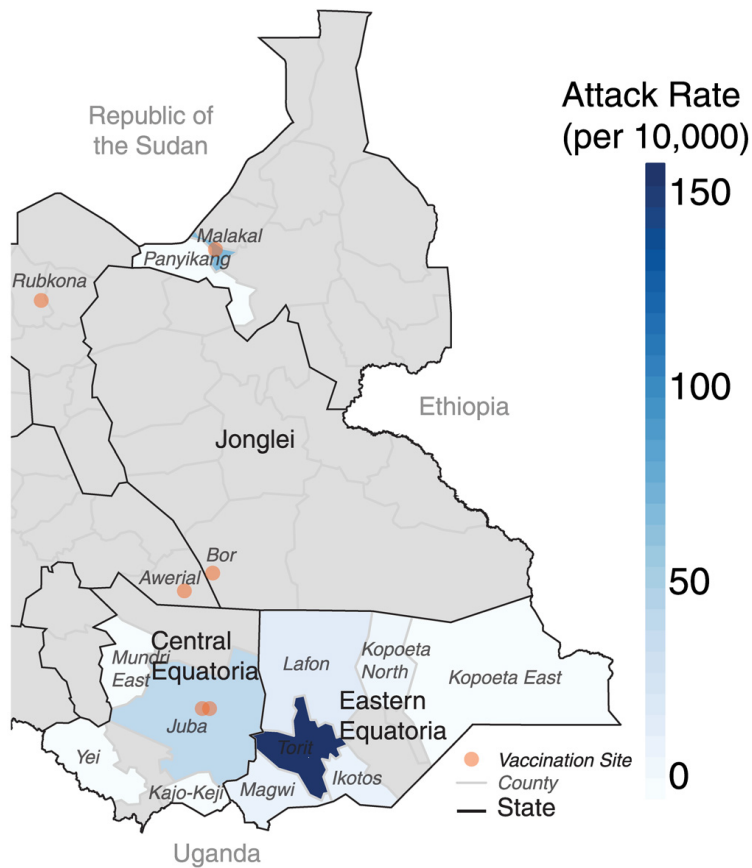


Figure 2.7: County-level attack rates in the 2014 cholera epidemic with respect to the vaccination locations (orange dots). Grey areas represent counties with no suspected cholera cases. Figure from Abubakar et al. (2015).

are located in Awerial, in Lakes state, two sites in Juba, a camp in Rubkona, Unity state, Bor in Jonglei state and Malakal in Upper Nile (Fig.2.7).

A clinic-based cholera surveillance system to record basic patient data and laboratory results has been implemented by SSMoH and WHO. The collected epidemiological data consist in the *cholera suspected cases*, which definition states:

«anyone with acute watery diarrhea diagnosed by a clinician. Suspected cases were considered confirmed if the patient had a culture-positive fecal sample» (Azman et al., 2016).

Our analysis will include all the suspected cases among the health facilities in 2014 and 2015, data available thanks to the Ministry of Health releasing epidemiological records.

2.4.1 Year 2014

Despite the vaccination campaigns whose response varied in space and among the population (Azman et al., 2016), the first case of cholera was confirmed during the vaccination period in the area of the capital Juba on April 23, 2014. The origin of this infection are unknown, although cholera had been reported in the neighboring area of Uganda during previous weeks (Abubakar et al., 2015). In a month, the officials declared a cholera outbreak. In 2014, 6,269 suspected cholera cases were recorded, in which appear 156 deaths. The epidemic last until October 29, 2014. Cases were recorded inside and outside the camps.

As Abubakar et al. (2015) reported, most of the cases occurred outside the camps. The attack rate of the infection (Fig. 2.7), defined as the total number of recorded cases among the population considered, was diverse between areas all over the country due to differences in baseline health care infrastructures. As figure 2.8 shows, during year 2014, the epidemic involved the states of Central

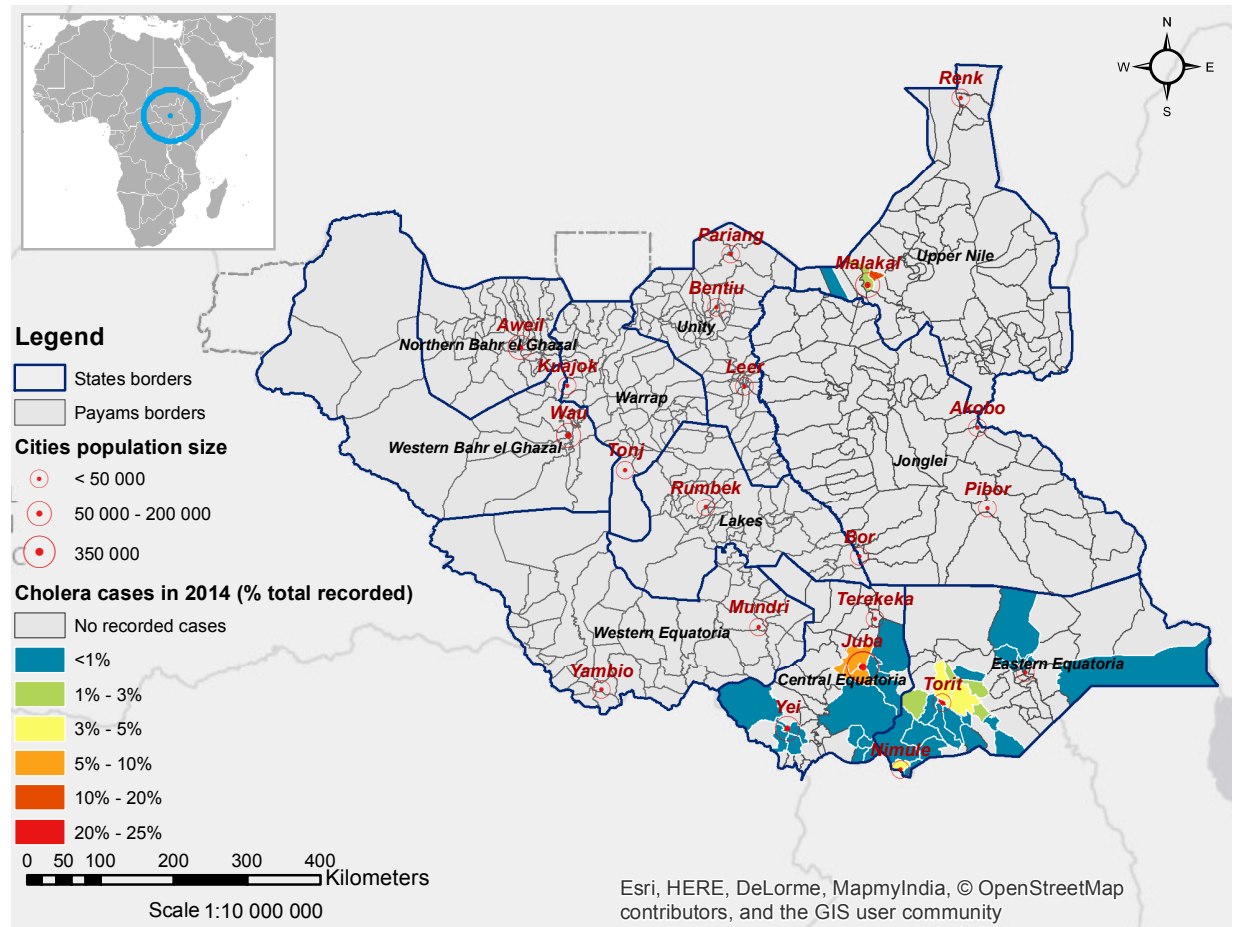


Figure 2.8: Percentage of the total cases occurred in each payam during the epidemic of 2014. The population sizes of the main cities is based on the census data (SSNBS, 2010) and are representative of the population distribution.

Equatoria, Eastern Equatoria and Upper Nile (administrative division Fig. 2.4). In the state of Western Equatoria, only three cases were recorded in the payam near to the city Mundri. As it will be better explained in Chapter 4, these cases do not affect the proposed modeling approach, and will be neglected in the following.

Figures 2.7 and 2.8 show that most of the cases were recorded around the capital area of Juba and in a Payam on the border with Sudan, near Malakal. The infection jumped to Malakal presumably from an infected traveler (Abubakar et al., 2015), over a large area with no confirmed cholera. Juba and Malakal counties were the only two places that experienced cases either within the population targeted for vaccination or the surrounding areas (Abubakar et al., 2015).

2.4.2 Year 2015

The continuous conflicts, displacement of people and other disease outbreaks as measles and tuberculosis, had worsened the sanitation condition, overall between people living in the PoC sites. Although the adoption of further prevention measures (WHO, 2015b), cholera cases were reported by WHO in Eastern Equatoria State (2.4) with 43 cases and three deaths between 11 - 19 February 2015. A new vaccination campaign started, in spite of which, another cholera outbreak had been declared in May 2015, with total number of suspected cases 1,757 including 46 deaths. The epidemic died out on September 24, 2015 (WHO, 2015a). WHO (2015b) supported Oral Cholera Vaccination campaigns in Bentiu and Juba PoCs, targeting more than 100,000 people. Following the reports, other two were planned in Malakal and Juba.

During year 2015, the disease showed up in the two states of Central Equatoria and Jonglei (Fig.

2.4). The regions hit more severely from the epidemic were Bor South, payam of Bor, and Juba.

As Figures 2.8 and 2.9 show, the disease hit the nation differently in places and numbers during the two years; notwithstanding the capital area of Juba, which is also the most populated, was always deeply involved.

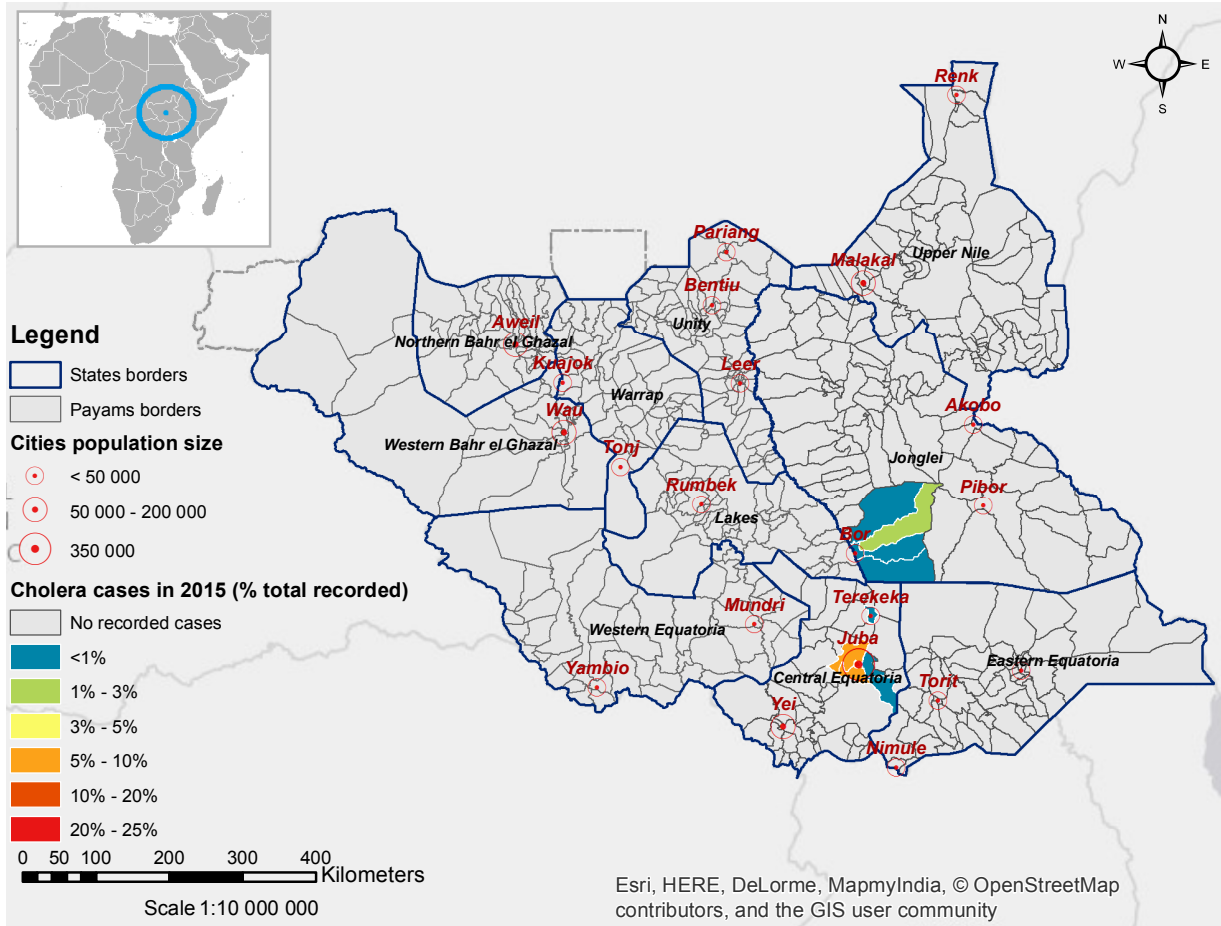


Figure 2.9: Percentage of the total cases occurred in each payam during the epidemic of 2015. The population sizes of the main cities is based on the census data SSNBS (2010) and are representative of the population distribution.

Cholera epidemiological model

Epidemiological models were born to face emergencies arising from lethal diseases and infections. As soon as epidemiological data started to be recorded, the scientific community committed itself to analyze the dynamics of pathogenic diseases, trying to identify the processes that enhance the infection spread and, moreover, to find a feasible mathematical approach to simulate the outbreak. During the last years, the progresses in the computational power have brought to the numerical resolution of mathematical models that are even able to predict epidemics in time and space, and which reliability has been demonstrated for the Haitian cholera epidemics (see e.g. (Andrews and Basu, 2011; Righetto et al., 2011; Bertuzzo et al., 2014; Rinaldo et al., 2014) or for influenza (see e.g., Shaman et al. (2013)) and even HIV/AIDS (see e.g., Cazelles and Chau (1997)).

3.1 Model assumptions

Epidemiological models are based on two main hypotheses (Barabási, 2016):

- *Homogeneous mixing hypothesis* also called *fully mixed* or *mass-action approximation*, according to which each individual has the same probability to get in contact with an infected person. In this way we do not need to know the exact contact network between people;
- *Compartmentalization hypothesis* that classifies each individual according to the state of the disease they are at.

Going into details on *compartmentalization*, during a cholera infectious process it is possible to distinguish three states, or classes, which each individual can be in:

Susceptible S : state in which individuals are in healthy conditions, still not in contact with the pathogen and therefore in risk of infection;

Infected I : state in which individuals contracted the infection and can possibly transmit it;

Recovered R : individuals that for a certain time are immune to the infection and do not contribute to the transmission.

Each pathogen has its own characteristic and by looking at the process of the related disease, we can also define other states:

Immune state in which individuals cannot become infected during a variable period of time after recovering. Measles immunity period is life-long, while cholera immunity response, some months or years, can vary with age of individuals and other factors (Leung et al., 2012).

Asymptomatic and symptomatic states, that differentiate people according to their reaction to the pathogen: individuals getting in contact with it can develop, or not, evident infectious state. Asymptomatic infected do not contribute to the transmission process. Examples are hepatitis of type A and, as already explained in Sect. 1.1 on page 3, cholera;

Removed state that counts for people died due to the disease, possible event in cases of cholera, influenza and measles if not treated at all or in time.

Each state defines a compartment. Individuals can change their state during the infectious process, therefore can move from a compartment to another. At the beginning of an infection, in absence of previous epidemics and vaccination campaigns, all the population is susceptible. When an infected individual enters the system, all the individuals in the susceptible state can contract the illness and follow the path to the infected state, in case of a symptomatic individual or to the recovered state, in case of an asymptomatic individual.

The mathematical approach chosen to simulate the dynamics of the diseases, seen as changes in the state of individuals, hence movements of individuals between compartments, depends on the characteristics of the pathogen, its related disease and environmental factors. All the models are developed on specific requirements of any *base model*, i.e. of a mathematical base structure used to describe the infectious process. The most frequently used base models in epidemiology are *Susceptible - Infected (SI)* model, *Susceptible - Infected - Susceptible (SIS)* model and, *Susceptible - Infected - Recovered (SIR)* model.

In order to understand the modeling approach that has been used in this work, we give a short explanation of the SIR basic model.

3.1.1 SIR model

As Kermack and McKendrick (1927) defined it, a SIR model is the basic model in case of epidemic dynamics that include the recovery process and provide temporary immunity to the recovered individuals, as the case of *V. cholerae* inducted disease. Immunity implies that a recovered individual is not susceptible to the disease for a variable period of time. Immunity also represents a way to limit the spreading of the disease and the number of infected individuals.

Let us define N as the number of individuals in a population or in a community, and t be the time. The state variable $S(t)$, $I(t)$, $R(t)$ represent respectively the number of Susceptible, Infected and Recovered individuals at time t of an infectious process.

The main idea of the *SIR* model is that each individual is a node of the *contract* network. The disease can move from node to node via mechanisms of transmission that are typical of the pathogen considered and that link nodes between them. Each node has k edges and we define β as the rate of transmission, i.e. the number of individuals that contract the infection despite the total number of nodes linked to the infected one (Barabási, 2016).

$$\frac{dS}{dt} = \beta k I(t) [1 - R(t) - I(t)] \quad (3.1)$$

In the same way, the number of people in infected state changes with similar dynamics. The parameter γ in the following equation, accounts for the number of people that gain immunity and recover from the illness in time as a rate of recover:

$$\frac{dI}{dt} = -\gamma I(t) + \beta k I(t) [1 - R(t) - I(t)] \quad (3.2)$$

Always in the same way we can define the differential equation for the recover state as:

$$\frac{dR}{dt} = \gamma I(t) \quad (3.3)$$

The three differential equation here, describe and predict the transition in time of individuals from the healthy state S to the infected I , and the recovered immune state R in a simple contract network in which each node is an individual.

3.2 SIRB Model

Based on the SIR model described in the previous section, the *SIRB* model used in this thesis is built on the previous (Bertuzzo et al., 2008, 2010, 2011) and most recent (Rinaldo et al., 2014; Mari et al., 2015) spatially-explicit epidemiological models for cholera and proposed in Bertuzzo et al. (2012, 2014); Mari et al. (2015) for 2010 Haiti epidemic. In this mathematical framework, the simple contact and contract network of a SIR model made of individuals, is replaced by a network of human communities distributed in the area under study, in which each node represents a community; in this way, the model embeds explicitly the structure of the contract network that enhance the spread of pathogens by reason of human mobility and hydrological connectivity between these. In each community holds the homogeneous mixing hypothesis.

The model is defined as SIRB due to the fact that transmission of cholera can happen, as explained in 1.1 on page 3, via contact with the concentration of the bacteria in the environment. Therefore, together with the dynamic of susceptible, infected and recovered individuals, we need to understand more about the local environmental concentration B of *V. Cholera*. This kind of mathematical approach allows the user to simulate in each node the pathogenic concentration and its variation in time and space; it additionally allows to simulate the decrease of exposure to bacteria as consequence of intervention strategies and population awareness. Moreover, by considering the characteristic of the *V. cholerae* induced disease, the set of differential equations distinguishes the *symptomatic* and *asymptomatic* individuals in the Infected and Recovered states.

Let $S_i(t)$, $I_i(t)$, $R_i(t)$ be the local amount of susceptible, symptomatic infected and recovered individuals and $B_i(t)$ the local concentration of the *V. Cholera* at time t in each node i of the network. Cholera transmission dynamics can be described by the following set of coupled differential equation:

$$\frac{dS_i}{dt} = \mu(H_i - S_i) - F_i(t)S_i + \rho R_i \quad (3.4)$$

$$\frac{dI_i}{dt} = \sigma F_i(t)S_i - (\gamma + \mu + \alpha)I_i \quad (3.5)$$

$$\frac{dR_i}{dt} = (1 - \sigma)F_i(t)S_i + \gamma I_i - (\rho + \mu)R_i \quad (3.6)$$

$$\frac{dB_i}{dt} = -\mu_B B_i + \frac{p}{W_i} [1 + \lambda J_i(t)] I_i - l \left(B_i - \sum_{j=1}^n P_{ij} \frac{W_j}{W_i} B_j \right) \quad (3.7)$$

In which the value

$$F_i(t) = \beta_i(t) \left[(1 - m) \frac{B_i}{K + B_i} + m \sum_{j=1}^n Q_{ij} \frac{B_j}{K + B_j} \right] \quad (3.8)$$

defines the force of the infection. Details on each equation and on the model follow (see Fig. 3.1 for a schematic representation of the links among the different stages.)

Susceptible The dynamic of susceptible people is described by eq. (3.4). The population size in each node i is defined by H_i and it is assumed to be at demographic equilibrium. The human mortality rate is defined by the parameter μ expressed in d^{-1} , hence the product μH_i is a constant recruitment rate. The parameter ρ , measured in d^{-1} , defines the rate at which recovered individuals lose their immunity and therefore are susceptible again. The force of infection $F_i(t)$ defines the rate at which susceptible individuals become infected due to ingestion of contaminated water. In this way, the local abundance of susceptible people changes according to basic dynamic of population, defined by the first term of the equation, and to the dynamic of the compartments I_i and R_i , with modification of the total infected $F_i(t)S_i(t)$ and recovered people from symptomatic and non infected that lose immunity at rate $\rho R_i(t)$.

Through the assumption of demographic equilibrium we can rewrite the equation (3.4) simply as:

$$S_i = H_i - I_i - R_i \quad (3.9)$$

valid for each node i .

Force of the infection The force of infection, eq. (3.8), contains the reason for the infection to pass between individuals and communities, i.e. human mobility and the probability of contact with contaminated water. The fraction $B_i/(K + B_i)$ defines the probability that an individual in node i becomes infected due to exposure to a local concentration B_i of *V. Cholera*. K is named *half-saturation* constant and expresses the concentration of *V. cholerae* in water that yields 50% chance of catching cholera, assuming that the only route for infection is the ingestion of contaminated water from non-treated sources (Codeço, 2001).

Due to human mobility, susceptible individuals can move from their residing node i to a destination node j , where they can be exposed to the local concentration B_j and yield $B_j/(K + B_j)$ probability of get infected in j . The chance for an individual to travel is given by the value of the parameter m assumed, in this formulation, to be node-independent. Therefore the term $(1 - m)$ defines the chance to remain in the native location i and be exposed to the concentration B_i .

The human mobility is modeled through a *gravity model* (Erlander and Stewart, 1990). The *gravity model of migration* is a mathematical formulation in transportation derived from Newton's law of gravity and is used to predict the degree of interaction between two sites. From Newton's third law of mechanics, we can think of bodies as "locations", and masses as "importance". In this context, the gravity model is used to compute the *connection probability* between nodes, defined as the probability that an individual resident in node i reaches j as destination, bringing the risk of infection with him.

The connection probability Q_{ij} is computed through the following formula :

$$Q_{ij} = \frac{H_j e^{-\frac{d_{ij}}{D}}}{\sum_{k \neq i}^n H_k e^{-\frac{d_{ik}}{D}}} \quad (3.10)$$

The "importance", or the attractiveness of each location, is the population size H_i , while the deterrence factor, as in Newton's, depends on the distance d_{ij} between the nodes. It is represented by an exponential kernel dependent on the shape factor D , measured in km .

The formulation of the gravity model states that the more the attractiveness of a place, in this case the population size, the higher would be the probability of choosing that as destination. This probability decreases when the distance among two nodes increases. The shape factor D controls the importance of distance as a deterrence factor: the higher this value, the less distance affect the connection probability.

The parameter $\beta_i(t)$ in eq.(3.8), measured in d^{-1} , represents the maximum exposure rate, as to say the maximum frequency at which individuals are exposed to the local concentration B_i . This value can change in time and space, and specifically, it decreases with the increment of population awareness of cholera transmission risk factors and, with intervention strategies against the disease. We assume the maximum local exposure rate $\beta_i(t)$ to decrease proportionally to the local cumulative attack rate, defined as

$$\frac{C_i}{H_i}$$

where C_i stands for the cumulative reported cases and of course depends on time. We describe the variation in time of $\beta_i(t)$ through the following exponential function:

$$\beta_i(t) = \beta_0 e^{-\frac{C_i}{H_i \psi}} \quad (3.11)$$

in which β_0 is the value of the exposure at the beginning of the epidemic, measured in d^{-1} . The dimensionless parameter ψ represents the rate at which the value of local exposure $\beta_i(t)$ decreases with awareness of population. The mathematical approach in eq.(3.11) assumes that population

awareness of cholera risk is higher in regions hit more severely by the epidemics. In this way, as shown for the Haiti epidemic (De Rochars et al., 2011), it is possible to imitate the health response targeted to the most-at-risk communities, as it was even in South Sudan (Azman et al., 2016) as explained in Sect. 2.4 on page 13. Moreover, in this way it is possible to account for directly possible changes in behavior of individuals, in response to information campaigns.

This formulation of the “force of infection” represents the main engine in the epidemic dynamics for people to move from one state to another.

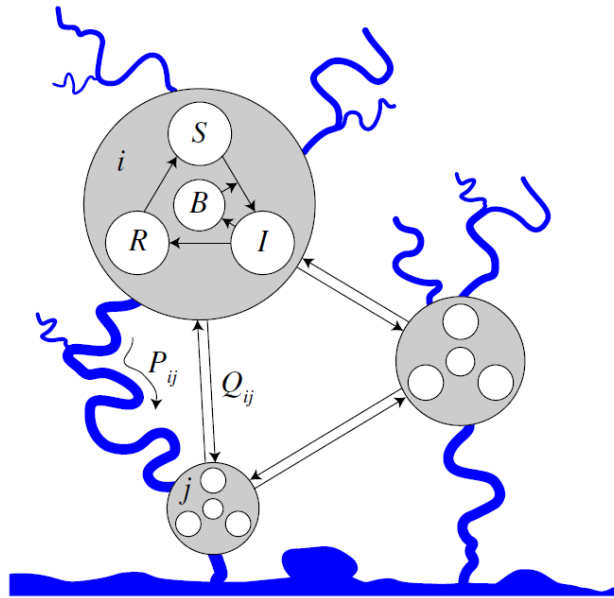


Figure 3.1: Schematic representation of the SIRB model (Bertuzzo et al., 2014). The number of Susceptible, Infected and Recovered, together with the concentration of Bacteria, change within the communities i , here represented by gray circles. The epidemic can move to other communities j via human mobility, with probability Q_{ij} , and via hydrological transport, with chance P_{ij} .

The three classes I, R and B are described as follows.

Infected The equation (3.5) describes dynamic of infected people. Symptomatic and asymptomatic individuals are discerned using the dimensionless parameter σ , representing the fraction of infected individuals that develop symptoms and entering in the symptomatic infected I_i class. The fraction σ depends on the dose of bacteria ingested. For simplicity, we assume this dose to be constant in space. Symptomatic infected people can recover from cholera at a rate γ , measured in d^{-1} , or die due to cholera, at rate α , or due to other causes at rate μ as seen for susceptibles in eq. (3.4). In case of death or recovery, individuals move from this class. The product $\sigma F_i(t) S_i$ defines the number of new symptomatic infected in time, while the second subtractive term removes from the class individuals that died or recovered.

Recovered Recovery state dynamics are described by equation (3.6). The fraction of asymptomatic individuals $(1 - \sigma)$ recovers much more rapidly from the disease, in around one day (Nelson et al., 2009), and their contribution to the *Vibrio cholerae* environmental concentration is lower. In fact, as (Kaper et al., 1995; Nelson et al., 2009) stated, they shed bacteria at a lower rate (1,000 times for asymptomatic against $> 10^4$ for symptomatic) and the distribution of asymptomatic patients does not strongly affect the local quantity of *V. cholerae* that is shed for subsequent transmission. Therefore, it is not needed to consider them in the transmission process. However it is fundamental to account for them into the recovery class, as they develop temporary immunity that can contribute in the process of disrupting outbreaks. Furthermore, they act on the susceptible compartment, eq.(3.4), losing their immunity at a rate ρ or dying at a rate μ , as symptomatic infected do too. The product $(1 - \sigma) F_i(t) S_i$ counts in this class the number of recovered asymptomatic infected in

time; the term $\gamma I_i(t)$ adds the number of new recovered individuals from symptomatic infection in time. The last term removes from this class the recovered individuals that died or lost their immunity.

Environmental concentration Changes in time and space of the environmental concentration of *Vibrio cholerae* are defined by equation (3.7). This concentration is measured in cells per m^3 . This equation accounts for all the factors that affect the local amount of free-living vibrios in the water reservoir, as to say, population dynamics of bacteria, rainfall enhancement effect and hydrologic connectivity that disperses them. In this formulation we assume that there is not a local reservoir of bacteria and that the bacteria is not indigenous, hence the concentration is directly affected by the new-born infection. Regarding population dynamics of bacteria, it is assumed that the death rate of *V. cholerae* in the environment exceeds the birth rate. This excess appears in eq.(3.7) as the net mortality rate μ_β , expressed in d^{-1} , that reduces the local concentration B_i in time.

Symptomatic infected individuals, as they are supposed to be non-mobile, contribute exclusively to the local abundance of bacteria at a rate defined as p/W_i , where p is the rate at which one person excretes bacteria, that reach and contaminate the local reservoir of volume W_i . p is measured in cells per day per person. W_i is measured in m^3 . This volume is assumed to be proportional to the population size H_i , as to say $W_i=cH_i$ as in Rinaldo et al. (2014). The constant value c is the water consumption per capita, measured in m^3 per person. In addition, rainfall induced runoff increases this local abundance due to washout of open-air defecation sites and to overflow of latrines (Rinaldo et al., 2014). The structure of the model accounts for these phenomena via the coefficient λ , measured in $d\ mm^{-1}$. The contamination rate p is therefore increased by additive terms via λ and the rainfall intensity $J_i(t)$ (Righetto et al., 2011; Rinaldo et al., 2014).

The hydrologic dispersal parameter l , measured in d^{-1} , represents the rate at which the pathogen can travel from node i to node j with probability P_{ij} , decreasing the local abundance B_i . P_{ij} takes unitary value in cases in which j is the unique downstream node between the neighborhood of i , and zero otherwise. The summation term

$$\sum_{j=1}^n P_{ij} \frac{W_j}{W_i} B_j \quad (3.12)$$

is the hydrologic transportation, that, similarly to the mobility probability seen in the force of infection (3.8), defines the probability that the bacteria move from the reservoir of volume W_i in the node i having local concentration B_i , to the reservoir of volume W_j in j .

3.3 Model parameters and calibration

The just-described mathematical framework wants to simulate the behavior of the four state variables $S_i(t)$, $I_i(t)$, $R_i(t)$ and $B_i(t)$ in each node of the network in the most possible realistic way.

Whatever, approaches of this kind require a lot of assumptions to reduce the natural complexity of environmental processes, and most of the times these are not even sufficient to allow to estimate via analytic methods the values of the variables (Baratti, 2014; Vrugt, 2016). Therefore, errors and uncertainties lie in all the process of modeling: these lie in measurements of the environmental process, in the mathematical approach chosen, in forcing and, as we are going to see, parameters. All models are characterized by *parameters*, as to say, numerical values bringing information about the environmental mechanisms under study. We call *calibration* the processes by which we define parameters values for an optimal performance of the model, granting the proposed mathematical structure to reproduce as best the observed real system. Parameters can assume a unique value during the time of simulations, or change during this period. Many research studies have been dedicated in estimating epidemiological and hydraulic parameters, thus some of the model parameters

can be found in literature. However, most of the parameters are problem dependent and require calibration.

Various calibration method exists: parameters can be evaluated through experimental methods, as for the estimation of "dispersion coefficients" in an aquifer (Di Molfetta and Sethi, 2012), or using numerical methods, as the ones used in this thesis for epidemic modeling.

Table 3.1 resumes the parameters in the SIRB model in order of appearance in the equations (3.4),(3.5),(3.6),(3.7),(3.8),(3.10),(3.11) and recalls their meaning, together with method of evaluation required.

Table 3.1: Parameters of the model

Parameters	Units	Description	Evaluation
μ	d^{-1}	Human mortality rate	Literature
ρ	d^{-1}	Loss of immunity rate	Calibration
β_0	d^{-1}	Exposure rate at the beginning of the epidemic	Calibration
ψ	–	Rate of decrease of the exposure $\beta_i(t)$	Calibration
m	–	Probability of travel, node independent	Calibration
D	km	Shape factor of the exponential kernel in gravity model	Calibration
K	d^{-1}	Half saturation constant	Calibration
σ	–	Fraction of symptomatic infected	Calibration
γ	d^{-1}	Recovery rate	Literature
α	d^{-1}	Human mortality rate due to cholera	Literature
μ_β	d^{-1}	Bacterial net mortality rate	Calibration
p/W_i	d^{-1}	Rate of excreting bacteria per each symptomatic infected, contaminating the water volume W_i	Calibration
l	d^{-1}	Hydrological dispersion	Calibration
λ	$d mm^{-1}$	Rainfall enhancement effect	Calibration

As the table 3.1 shows, most of the parameters should be calibrated. The human mortality rate μ , can be easily found in statistics of the country and census. The recovery rate γ and the human mortality rate due to cholera α , can be evaluated using epidemiological records.

We can reduce the number of parameter to estimate by introducing the *dimensionless bacterial concentration*

$$B_i^* = \frac{B_i}{K}$$

where K , we recall, is the half-saturation constant from eq.(3.8). This new quantity allows to group three model parameters, as to say:

- p , the rate of excreting bacteria by one infected individual;
- c , the volume per capita of water reservoir W_i in which the bacteria sheds;
- K , the half saturation constant;

in a unique ratio defined as

$$\theta = \frac{p}{cK} \quad (3.13)$$

The ratio θ has an interesting meaning: it resumes all the parameters related to water, contamination and sanitation: an higher value of θ , means that the rate of excreting bacteria is higher, and its consequential water pollution worse. We can use this parameter to understand the sanitation conditions and the resulting contamination of the environment.

Moreover, to simplify the implementation of the algorithm, we define k as the reciprocal of the parameter ψ :

$$k = \frac{1}{\psi} \quad (3.14)$$

in which ψ , we recall from eq.(3.11), is the rate of decrease of the local exposure $\beta_i(t)$ due to population awareness.

Table 3.2: Reduced parameters of the model

Parameters	Units	Description	Evaluation
μ	d^{-1}	Human mortality rate	Literature
ρ	d^{-1}	Loss of immunity rate	Calibration
β_0	d^{-1}	Exposure rate at the beginning of the epidemic	Calibration
k	–	Decrease of the exposure $\beta_i(t)$	Calibration
m	–	Probability of travel, node independent	Calibration
D	km	Shape factor of the exponential kernel	Calibration
θ	d^{-1}	Sanitation conditions	Calibration
σ	–	Fraction of symptomatic infected	Calibration
γ	d^{-1}	Recovery rate	Literature
α	d^{-1}	Human mortality rate due to cholera	Literature
μ_β	d^{-1}	Bacteria mortality rate	Calibration
l	d^{-1}	Hydrological dispersion	Calibration
λ	$d\ mm^{-1}$	Rainfall enhancement effect	Calibration

Table 3.2 shows the final reduced set of parameters; ten parameters have to be calibrated.

The evaluation of the parameters via numerical methods can be both *deterministic* or *probabilistic*. To define parameters in a deterministic way implies to seek and find unique values for parameters that fit well the observation data. These values represent a “local optimum” in the domains of definition, meaning that can exist other parameter combinations with an equivalent fit. Moreover, due to the intrinsic and epistemic errors that characterizes hydrological models and the observation data, a unique solution is not representative of these uncertainties and there is no reason to believe that only one set of parameters is true (Beven and Binley, 1992).

Therefore, a probabilistic approach should be preferred, where all the possible parameters combinations and values in the domains that retrieve a satisfactory fit are considered. This probabilistic approach aims at the estimation of the posterior probability density function (*pdf*) of the parameters, that helps in optimizing the performance of the model.

In order to get information about these pdfs, *statistical inference* is used. This means that we deduce properties of an underlying distribution by exploiting the available observation data (Upton and Cook, 2014), the epidemiological model, and the prior distribution of the parameters. Therefore, it is necessary to start from some hypothesis on the pdfs and test them with data.

There are two theory in statistics for inference (Ewens and Grant, 2005): *classical* or *frequentist* methodology and the *Bayesian* approach. We will briefly give some details on the Bayesian approach in next section in order to understand the calibration method that has been used.

3.3.1 The Bayesian approach

The objective of the Bayesian approach is to compute the probability density function of the parameters conditioned to the available information, i.e., the observed data (Ewens and Grant, 2005). This is called *posterior* pdf. Bayes rule rewrites the posterior pdf as the normalized product of the likelihood function (measuring the fit of the model with the data) and the starting hypothetical parameter pdf named as *prior*.

We can clarify this idea thanks to an example (Ross, 2010). Let us take the context of a criminal investigation. There is the 60% of chance *a priori* that a certain suspect is guilty. Acquiring a *new* piece of evidence, the inspector in charge gets to know that the criminal has a certain characteristic

C , that is also shared with the 20% of the population. How does the probability that the suspect is guilty change with this new information? Or in other terms, which is the *posterior* probability that the suspect is guilty given the *new* piece of evidence?

Let G define the event that the suspect is guilty. At the beginning, the prior probability of the event $P(G)$ is 0.6. Therefore, G^c is the event that the suspect is innocent, whose prior probability is $P(G^c) = 0.4$. Let C be the event that he possesses the characteristic of the criminal.

We define the probability of posses the characteristic of the criminal, being guilty, as the conditional probability $P(C | G)$, and it has the unitary value, since we know thanks to the new information, that the real guilty has this characteristic. We define the probability of posses the characteristic of the criminal, being innocent, as the conditional probability $P(C | G^c)$, equal to the percentage of the population that has this characteristic and that is not suspected.

We can define the *posterior* probability $P(G | C)$ by using Bayes theorem:

$$P(A | B) = \frac{P(A)P(B | A)}{P(B)} \quad (3.15)$$

that applied to our example gives:

$$\begin{aligned} P(G | C) &= \frac{P(GC)}{P(C)} = \frac{P(G)P(C | G)}{P(G)P(C | G) + P(G^c)P(C | G^c)} \\ &= \frac{(0.6)(1)}{(0.6)(1) + (0.4)(0.2)} = 0.8824 \end{aligned}$$

The example shows that, using the Bayesian theorem in eq.(3.15), the chance for the suspect to be guilty increases from 0.6 to 0.88 thanks to the acquisition of new information.

Similarly to the example, we can apply the Bayesian theorem for the posterior pdfs of the parameter of the model. Let Θ be the set of parameters of the model, in our case:

$$\Theta = \{\theta, l, m, D, \lambda, \beta_0, \mu_\beta, \rho, \sigma, k\}$$

We are interested in finding the posterior distribution of the parameters $P(\Theta | Y_{obs})$ to optimize the model. The variable Y_{obs} is the vector of the system observations which are related to the model outputs and, thus, to the parameters. In our case, Y_{obs} is a matrix that contains the recorded suspected cholera cases in time and space. Similarly to the example, using the Bayes theorem eq. (3.15) on conditional probabilities, we can define the posterior as:

$$P(\Theta | Y_{obs}) \propto P(\Theta)\mathcal{L}(\Theta | Y_{obs}) \quad (3.16)$$

in which $P(\Theta)$ is the prior distribution of the set Θ . The term $\mathcal{L}(\Theta | Y_{obs})$ is called *Likelihood function*. The likelihood is defined as the probability of the observed outcomes dependently by the values of the parameters, so that:

$$\mathcal{L}(\Theta | Y_{obs}) = P(Y_{obs} | \Theta)$$

It is important to highlight that the likelihood does not express a distribution of probability yet a probability, dependent on the parameters values. In other words, it gives a measure of the goodness of both the calibration method and the model. Thanks to the likelihood function in Bayesian formalism, the posterior distribution of the parameters of the model can be derived by conditioning the spatio-temporal behavior of the model on measurements of the observed system response (Vrugt, 2016).

Probabilistic approaches as the Bayesian one, are preferred because of their ability to handle parameter, state variable and model output uncertainties (Vrugt, 2016). However, the solution of Bayesian approaches is not an easy task and in most of the cases an analytical solution does not exist. This is the reason why numerical methods are wide-spreading. Most methods are based on Monte Carlo methods and Markov Chain processes, as *Iterative Simulations* (Gelman and Rubin,

1992), the *Differential Evolution Markov Chain* DE-MC (ter Braak, 2006) and the *Differential Evolution Adaptive Metropolis* - DREAM method (Vrugt et al., 2012). These methods, once assumed the shape of the prior and the likelihood function (Beven and Binley, 1992; Vrugt, 2016), sample possible parameter realizations from the posterior distribution by simulating the response of the model and optimizing the likelihood function in the Bayesian problem.

During the first tries and analysis, the DREAM method was used for this work to explore the parameter space and to evaluate the posterior distribution adopting the *DREAM_{ZS}* variant of the algorithm, as in (Bertuzzo et al., 2014) (for further details (Vrugt, 2016)). In our test case, this approach did not succeeded to accurately fit the dynamics of this case study.

Another typology of calibration methods are based on *Data Assimilation (DA)*. The main idea of this technique is to include real system observations into the model, in order to correct immediately its response and quantifying simulation uncertainties (Pasetto, 2013). DA technique can be extended to infer the distribution of the model parameters in a dynamical way. This is useful when the parameter distribution can change in time: DA sequentially, i.e. at each time step, track the parameters using the collected data (Pasetto et al., 2016). The technique of the *Ensemble Kalman Filter*, here used to calibrate the spatially explicit SIRB model, belongs to this class. Section 3.3.2 goes into details of this approach as applied to our cholera model.

3.3.2 Ensemble Kalman Filter

The Ensemble Kalman Filter, or *EnKF* was first proposed by Evensen (1994) as an improvement of the so-called Kalman Filter, or *KF*, (Kalman, 1960), with the aim of applying the algorithm to non-linear systems and to reduce the computational costs. The Kalman Filter (*KF*) method, in fact, solves the Bayesian problem and finds the posterior pdfs of the state variables in linear problems. Assuming all the pdfs to be Gaussian distributed, KF analytically computes the mean values and the variances of the state variables, since the method provides formulas for advancing them at each time step, when real observations are incorporated into the model. One possibility to overcome the linearity assumption consists in estimating the mean and the variances linearizing the equations and computing the Jacobian matrix at each time step, as performed in the Extended Kalman Filter (*EKF*). It is though evident that the cost of the computation of the Jacobian is high.

EnKF solves the Bayesian problem using a Monte Carlo method, a simple computational algorithm that uses repeated random sampling to approximate the probability distribution of the variables. For the advantages that it brings, EnKF finds large use in hydrological modeling (see e.g., (Camporese et al., 2009)) and epidemic modeling (see e.g., (Gupta et al., 2015)).

In the following, we explain how EnKF applies to our cholera model.

Let us define \mathbf{x}_k , resuming the output of our model at each time step k (Pasetto et al., 2016), where k is the epidemiological week (from Sunday to Saturday), as:

$$\mathbf{x}_k = \{(I_i, R_i, B_i, C_i), \text{ with } i = 1, \dots, n\}$$

in which I_i is the number of new infected in each node i , R_i the number of recovered, B_i bacteria concentration per m^3 and C_i the cumulative number of weekly infected in the node.

The mathematical framework that gives as output \mathbf{x}_k can be written as:

$$\mathbf{x}_k = \mathcal{F}(\mathbf{x}_{k-1}, \Theta, J(t), t_{k-1}, t_k) \quad (3.17)$$

in which $\mathbf{x}_k \in \mathbb{R}^{4n}$, being n the number of nodes considered; $J(t)$ is the daily rainfall, input of the model and \mathcal{F} is the non-linear operator that solves the system of equations (3.4) - (3.7) from time t_{k-1} to t_k , i.e. from one week to another.

We can describe the relationship between the weekly recorded cases $\mathbf{y}_k \in \mathbb{R}^m$, aggregated in a number of domains m , and the state system \mathbf{x}_k using the following equation:

$$\mathbf{y}_k = \mathbf{H}_k \mathbf{x}_k + \xi_k \quad (3.18)$$

where \mathbf{H}_k is the so-called *observation function* relating the weekly real observed cases to the weekly simulated ones. The role of the observation function is to upscale the results of the simulation in each node $i = 1, \dots, n$ to the spatial level at which the recorded cases have been aggregated, therefore $\mathbf{H}_k \in \mathbb{R}^{m \times n}$. The value $\mathbf{H}_k \mathbf{x}_k$ and \mathbf{y}_k would coincide whether the simulations and the observations were errors-free. The vector $\xi_k \in \mathbb{R}^m$ represents the measurements error, whose components are modeled as independent Gaussian random variables with mean equal to zero and standard deviation σ_ξ , i.e.:

$$\xi_k \sim \mathcal{N}(0, R_k), \quad i = 1, \dots, n \quad (3.19)$$

being R the covariance matrix of the measurements errors, that due to the hypothesis on independent errors, is a diagonal matrix filled with $\sigma_{\xi,k}^2$.

At each new observation acquisition, using the Bayes formula eq.(3.15), we can rewrite the posterior distribution p^a of the state as:

$$p^a(\mathbf{x}_k | \mathbf{y}_1, \dots, \mathbf{y}_k) = c p^f(\mathbf{x}_k | \mathbf{y}_1, \dots, \mathbf{y}_{k-1}) \mathcal{L}(\mathbf{y}_k | \mathbf{x}_k) \quad (3.20)$$

similarly to what we have stated for the parameters in equation (3.16). This step is define as *analysis step* or *update*. p^f represents the forecast pdf at time t_k , that was computed using the previous assimilation $p^a(\mathbf{x}_{k-1}, \Theta_{k-1} | \mathbf{y}_1, \dots, \mathbf{y}_{k-1})$ at which were acquired the data \mathbf{y}_{k-1} . In other words, p^f represents the response of the model at each time step before the new acquired observation \mathbf{y}_k at t_k changes the pdf to p^a .

Using the EnKF method, p^f at time k for the states \mathbf{x}_k is approximated by the ensemble of N random samples taken from the initial distribution, hence:

$$p_k^f(x) \sim [\mathbf{x}_1^f, \dots, \mathbf{x}_N^f]$$

and the update of the states happens for each realization $j \in N$ using the following equation:

$$\mathbf{x}_k^{a,j} = \mathbf{x}_k^{f,j} + \mathbf{K}_k^{f,j} (\mathbf{y}_k^j - \mathbf{H}_k \mathbf{x}_k^{f,j}) \quad (3.21)$$

in which the operator $\mathbf{K}_k^{f,j}$ is called "Kalman Gain" and contains the observation function H_k , the covariance matrix of the measurements error R_k and the covariance matrix P_k of the ensemble (for further details see e.g. (Kalman, 1960; Mandel, 2009)):

$$\mathbf{K}_k^f = P_k H_k^T (H_k P_k H_k^T + R_k)^{-1}$$

The vector \mathbf{y}_k^j , using (3.18), $\mathbf{y}_k^j = \mathbf{y}_k + \xi_k^j$ represents the random perturbations of the observed measurements \mathbf{y}_k , introduced to correctly estimate the variance of the updated variables.

Whether we are interested in computing the update of the parameters Θ , together with the states, the method allows to treat them as state variables, and therefore to change their forecast pdfs. In this case the update is computed using the "state augmentation" as:

$$\begin{pmatrix} \mathbf{x}_k^{a,j} \\ \Theta_k^{a,j} \end{pmatrix} = \begin{pmatrix} \mathbf{x}_k^{f,j} \\ \Theta_k^{f,j} \end{pmatrix} + \mathbf{K}_k^{f,j} (\mathbf{y}_k^j - \mathbf{H}_k \mathbf{x}_k^{f,j}) \quad (3.22)$$

similarly to what we have stated through eq. (3.21).

This process can be schematically seen through Fig. 3.2. On step (1), an environmental process as a cholera epidemic, blue line, and its measurements, dots, are represented. On step (2), the mathematical model tries to mimic the real phenomena. Uncertainties, in pink, define a confidence interval for the model results, that with time becomes larger, and the mean value of the ensemble, in red, detaches from the real mechanism, leading to wrong evaluations. On step (3), DA techniques, as the Kalman Filter and EnKF, at each time step correct the model evaluations, updating state variables forecast. Uncertainties reduce in time, and the mean value approaches the observed phenomenon.

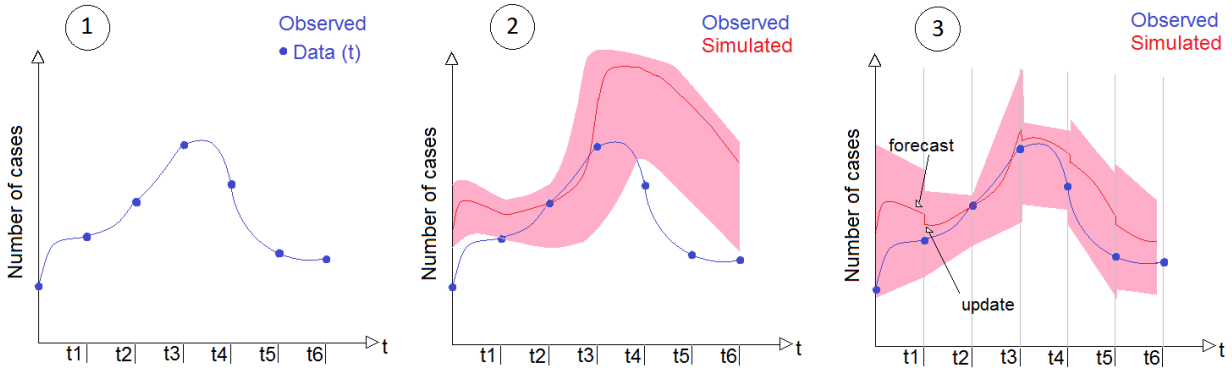


Figure 3.2: Schematic representation of the DA technique. For more details see Sect.3.3.2.

As Pasetto et al. (2016) reported, one disadvantage of EnKF is the so-called filter “inbreeding”: parameter distribution rapidly converges toward one value, underestimating uncertainties. In this work, we have tried to overcome this problem due to the high uncertainty associated with epidemiological records, whose variance is unknown. As we have seen, the analysis step is obtained by the Kalman gain of the ensemble, containing information on errors variance and correlations between the observations and the simulated states. We control convergence using the Kalman gain: we gradually increase the measurement error variance σ_{ξ}^a until the parameter variances $\sigma_{\Theta_{\xi}^a}$ are higher than a desired tolerance. On each repetition i , we set a value $c_1^i > 1$ to increase the measurement error. The update is accepted if $\sigma_{\Theta_{\xi}^a} > c_2 \sigma_{\Theta_{\xi}^f}$, as to say the ratio between the parameter variances forecast and the parameter variances of the analysis step, is greater than a value c_2^i defined between zero and one.

In this way we can control how the parameter variances decrease in time, avoiding the rapid reduction of the probability space explored by the ensemble. Moreover, we avoid drastic change in parameters values in one analysis step.

Model setup and epidemiological data

The modeling approach described in Chapter 3, together with DA calibration technique, need in order to be performed, specific inputs.

The epidemiological records, containing daily records of suspected cholera infected individuals, are required to perform the Data Assimilation, accumulating cholera cases during each week. Further details on the temporal and spatial behavior of the disease given in the records were useful to define the network in which the model performs. As explained earlier, the nodes of the network are representative of distributed communities and, therefore, information about the population distribution and size are required to define them. These requirements are the same as the gravity model of mobility, in which, we recall, the attractiveness of the nodes is represented by their population size. Moreover, rainfall measurements during the period of analysis in the area of study are required to perform SIRB. Last, but not least, initial conditions have to be chosen in order to solve the state variables $I_i(t), R_i(t), B_i(t), C_i(t)$ in each community.

Data were processed creating appropriate MATLAB scripts and using and creating spatial references on GIS.

Further details follow.

4.1 Epidemiological records

Epidemiological records of both years 2014 and 2015 were provided by the SSMoH. Records contain data regarding the date of onset of the symptoms, the date of arrival at the health facility and the provenience of the patients. All the cases were reordered and timed using the date of onset of the symptoms. Georeference of the cases at the level of the Payam was possible using the information on provenience, and overlapping data of the shapefiles, provided by the SSMoH, SSNBS and the WHO, and other spatial information obtained by OpenStreetMap (2015). This step was the most delicate one.

4.2 Framework

Analyzing the hydrography (Fig. 2.3), the topography (Fig. 2.2) and the spatial distribution of the disease during the two years, we decided not to consider hydrological connectivity between communities (which is present in SIRB through the parameter l) since there is not a clear hydrographic connection between the nodes that recorded cholera. Therefore, in order to define the spatial domain for the simulations, we used the distribution of recorded suspected cases. In both years, as we showed in Sect. 2.4 on page 13, the right part of the country has been affected by the disease. The number of cases and the places in which the infection appeared are the reasons why we delineate the model within the borders of the states Central Equatoria, Eastern Equatoria, Jonglei and Upper Nile (for geo-political reference please see figs. 2.4 on page 11). As anticipated, we chose to neglect the three cases that appeared in the state Western Equatoria. From a mathematical point of view, the structure of the model does not allow for zeroes infected in the nodes, and a certain response, even

if small, is always expected all over the network. Therefore, to include these cases and the node in which these were recorded in our domain is a completely arbitrary choice, that would not strongly affect the output, yet it would have increased the computational cost due to a higher number of nodes.

To define the communities distribution, we used the administrative division of the country. The population in each node consists in the inhabitants of the *Payams*. To optimize the performance of the model, we modified the spatial information regarding this geo-political division. The mathematical structure, in fact, gains stability when the spaces in which we define the communities have homogeneous extensions. This means that we should prefer division in areas having, more or less, the same size. As Fig. 2.4 on page 11 shows, payams sizes are very irregular and for most inhabited zones, the number of divisions is higher and irregularity greater. Especially in the capital area, Juba, this geo-political structure creates confusion and, to the purpose of this work, is not necessary. Based on (USAID, 2005; OpenStreetMap, 2015) and the information provided by the Souther Sudanese government, we decided to merge together in a unique Payam the small payams named Muniki and Kator, located in less than 10km around the city center of Juba and that can be considered as big districts of the capital. The same kind of incorporation has been done for Malakal, whose administration is actually subdivided in Central, Eastern, Northern and Southern Malakal. Fig. 4.1 shows the modifications for the case of Juba. We limited our modifications to most populated areas to not upset the administrative division.

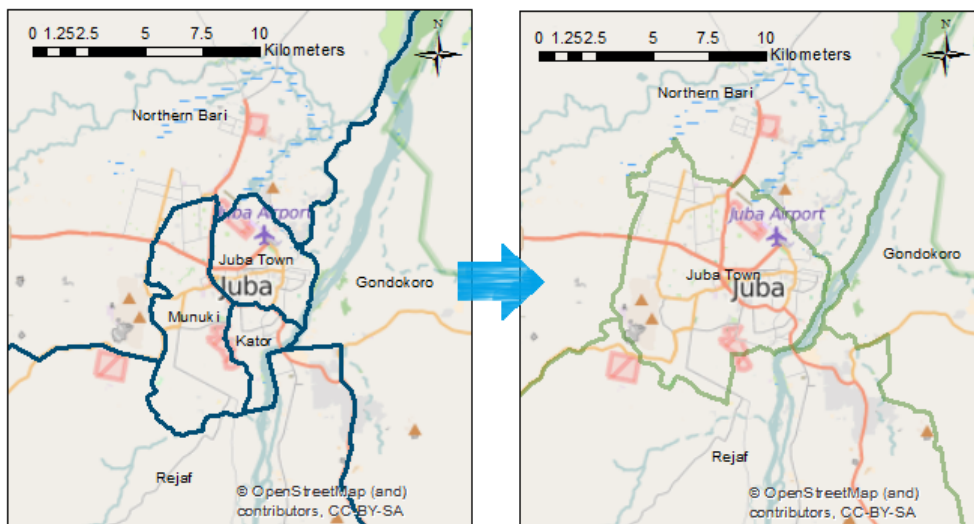


Figure 4.1: Modifications on the geo-political assessment of Juba to optimize the model. Names of the Payams are given.

In the domain of this work, a total of 236 Payams, hence nodes, are considered. Nodes position is computed using the population distribution, as it will be described in sect. 4.3. The model simulates the epidemics in all the nodes. The calibration, that will be discussed in the following sections, runs at the spatial level of the Counties in which cholera cases were recorded. In total, 10 Counties were severely affected by the disease between the two years: Juba, Yei, Kajo-Keji, Torit, Magwi, Ikotos, Lopa, Kapoeta North, Bor South and Malakal. The output of the model will be shown, for comparison with the real observed cases, in these areas.

Fig. 4.2 redefines the Region Of Interest - ROI with which we worked.

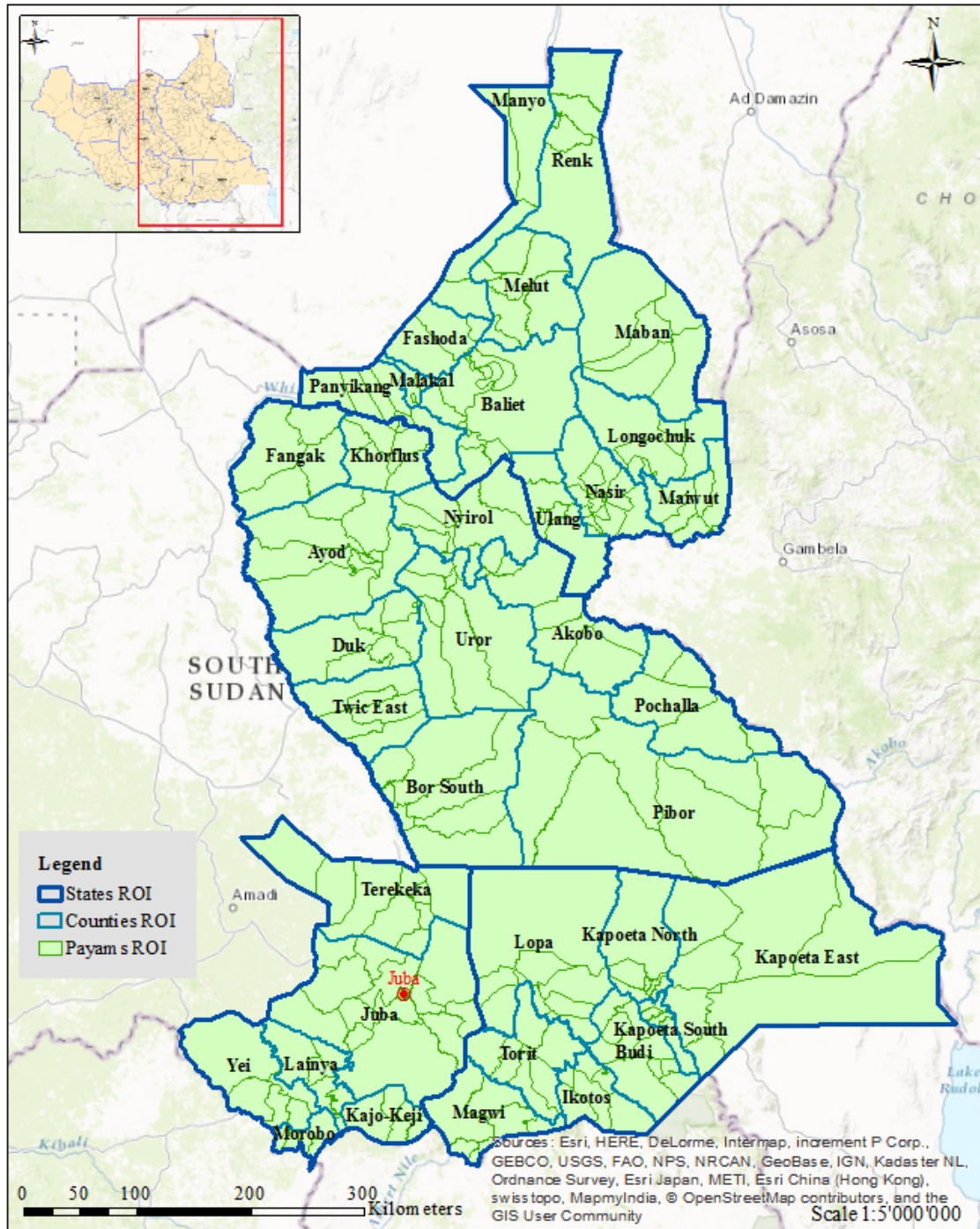


Figure 4.2: Map of the spatial domain of the model. We defined a Region Of Interest - ROI to run the simulations. Each payam, whose borders are define by thin green lines, consists in a node in our network. Results will be shown at the level of the Counties, borders in light blue lines, whose names are reported in the map. State division is highlighted in dark blue.

4.3 Centroids

The position of the nodes in the spatial domain is computed using the population distribution in each payam. We define as 'centroid' the point in which falls the center of the area of the Payam weighted on the population distribution in the same area. The concept is similar to the one of the "center of mass", where the masses are replaced by the number of inhabitant in each cell of the image.

For the population distribution we used the map provided by WorldPop (2013), in which each pixel value represents the number of people per grid, estimated using remotely sensed map. The raster image has spatial resolution equal to 0.000833333 decimal degrees, approximately 100m at the equator. The evaluation is based on land covers and remote sensing. Chosen between the four maps available, the version that we propose estimates the number of people per grid square, with national totals adjusted to match UN population division estimates and it is updated at 2013 (for further details <http://esa.un.org/wpp/> and reference).

In order to reduce the computational cost related to the number of cell treated in the algorithm, we re-sized the original raster seen in Fig. 4.3, enlarging the cell size. Each cell of the new raster contains the information of 16 cells of the original one. The new raster for the population distribution has spatial resolution equal to 0.0033332 decimal degree, approximately 370m at the equator (Fig. 4.4).

First, the algorithm aims to calculate the total population inside the areas of a single Payam. From the shapefiles provided, we create a raster image of the Payam division having resolution 0.0033332 decimal degree. Each Payam is identified by an "ID number" from 1 to 263: these values fill the cells of the raster, locating the position of the payams.

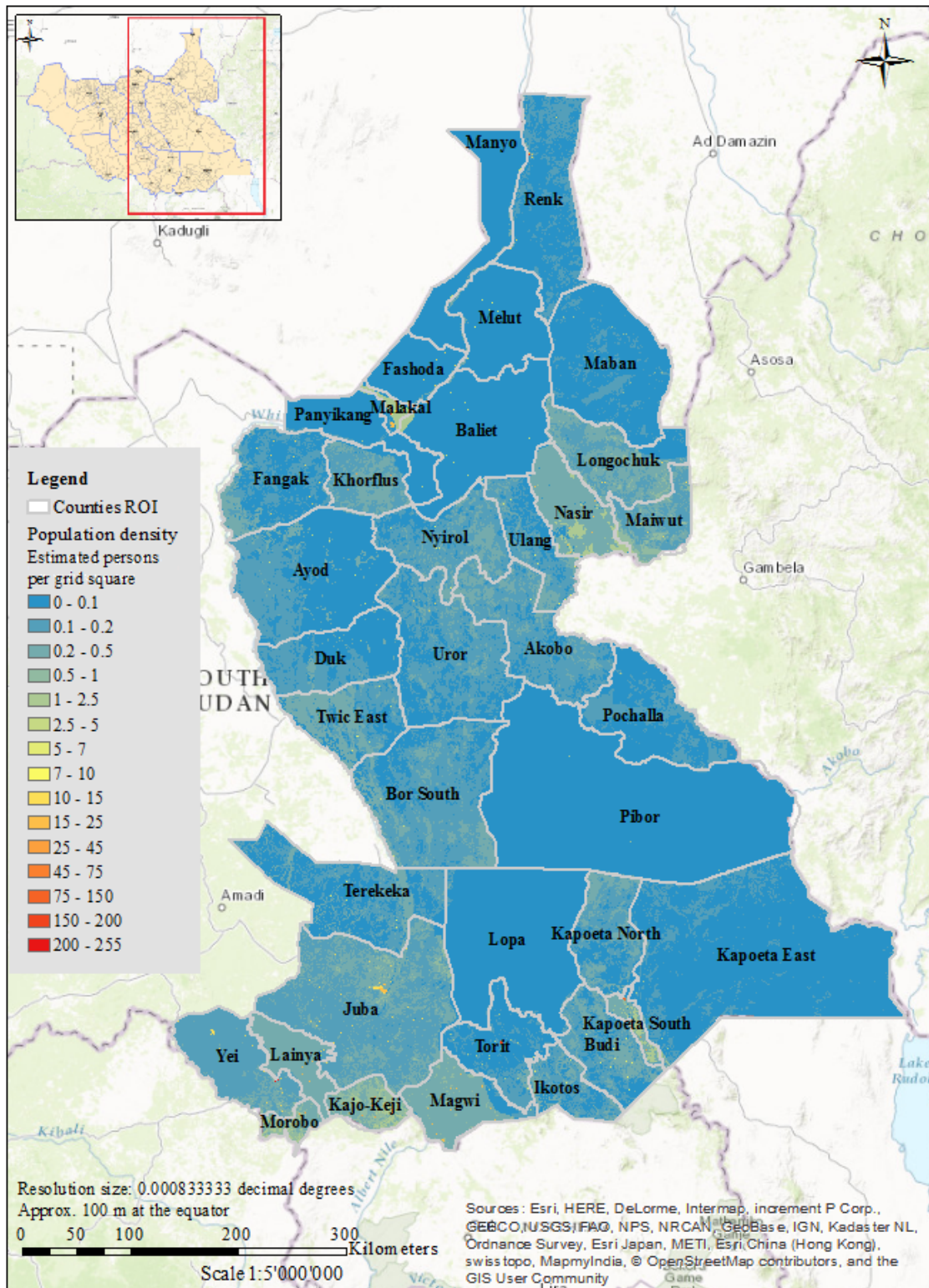


Figure 4.3: Estimated numbers of people per grid square, with national totals adjusted to match UN population division estimates. Cell size 0.000833333 decimal degrees, approximately 100m at the equator. We highlight the administrative division at the level of Counties. Source WorldPop (2013).

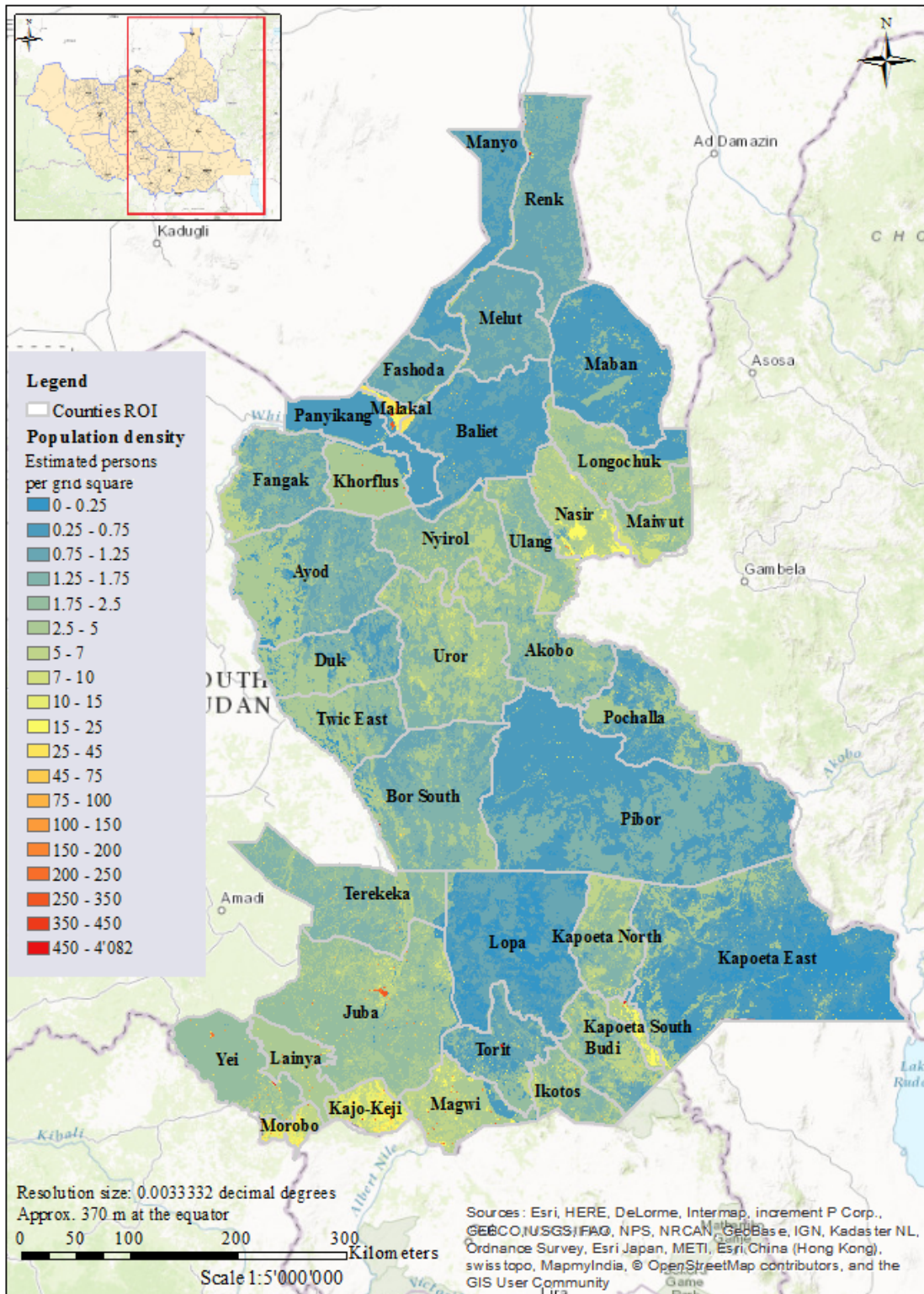


Figure 4.4: Estimated numbers of people per grid square, re-sized to compute the centroids. Cell size 0.0033332 decimal degrees, approximately 370m at the equator. We highlight the administrative division at the level of Counties. The map shows that the country in the domain of study has really low population density, exceptions are the big cities as Juba, and the County Malakal.

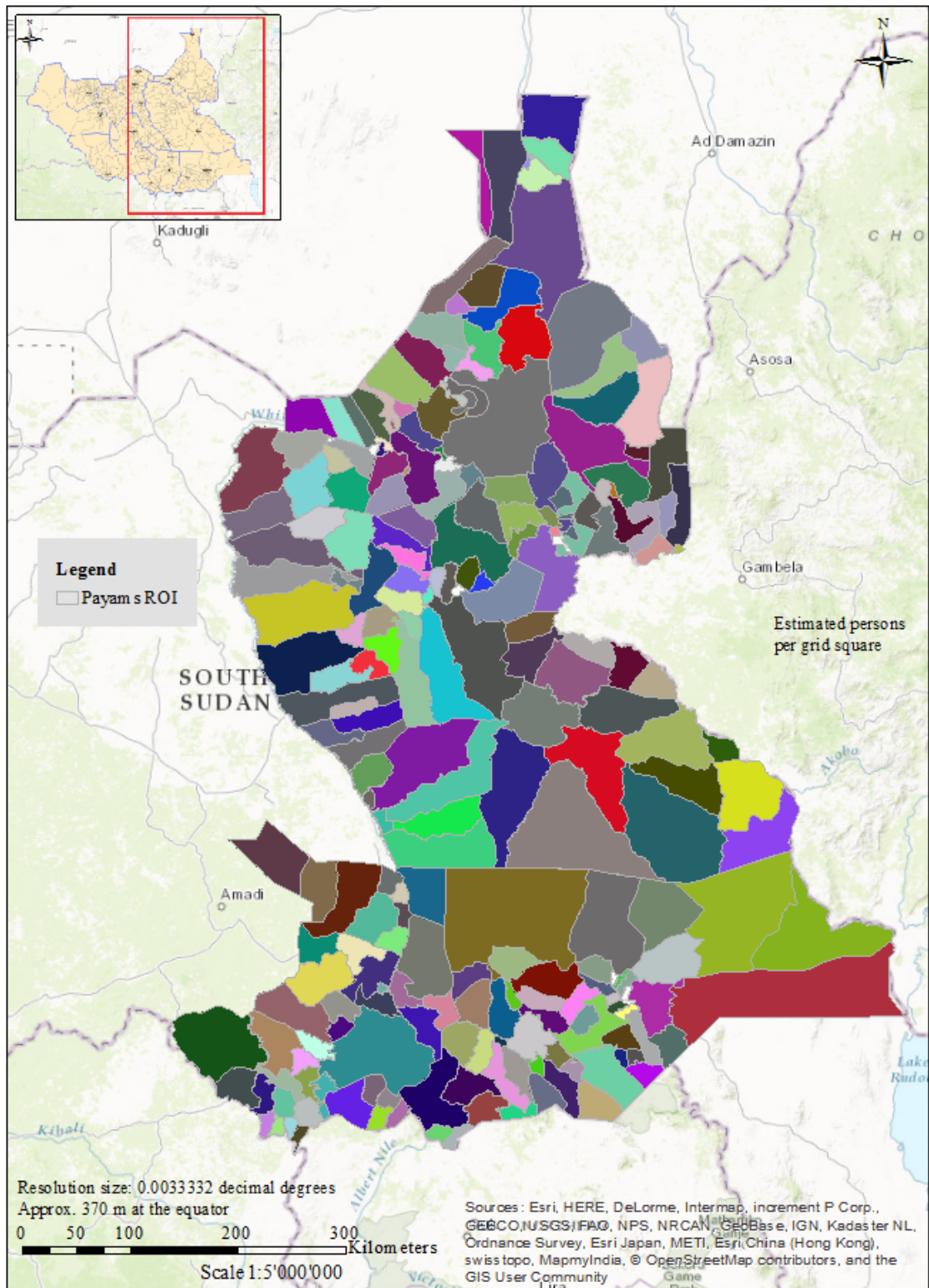


Figure 4.5: Raster image of the division in Payam, created to compute the centroids. Cell size 0.0033332 decimal degrees, approximately 370m at the equator. We highlight the administrative division at the level of Payam: each one is represented using a different color.

Both raster images are delimited in longitude and latitude ($29^{\circ} - 36^{\circ}E$; $3^{\circ} - 12^{\circ}$), having the same number of cells. The computation scans all the pixels located in this grid, from left to right and from the bottom to the top, comparing the ID numbers with values in the cells of the Payam raster image. When one ID number is found in the image, the position of the cell is stored and used in the Population raster image, to evaluate the total population in the area. Fig. 4.6 shows the grid through which the raster images are scanned.

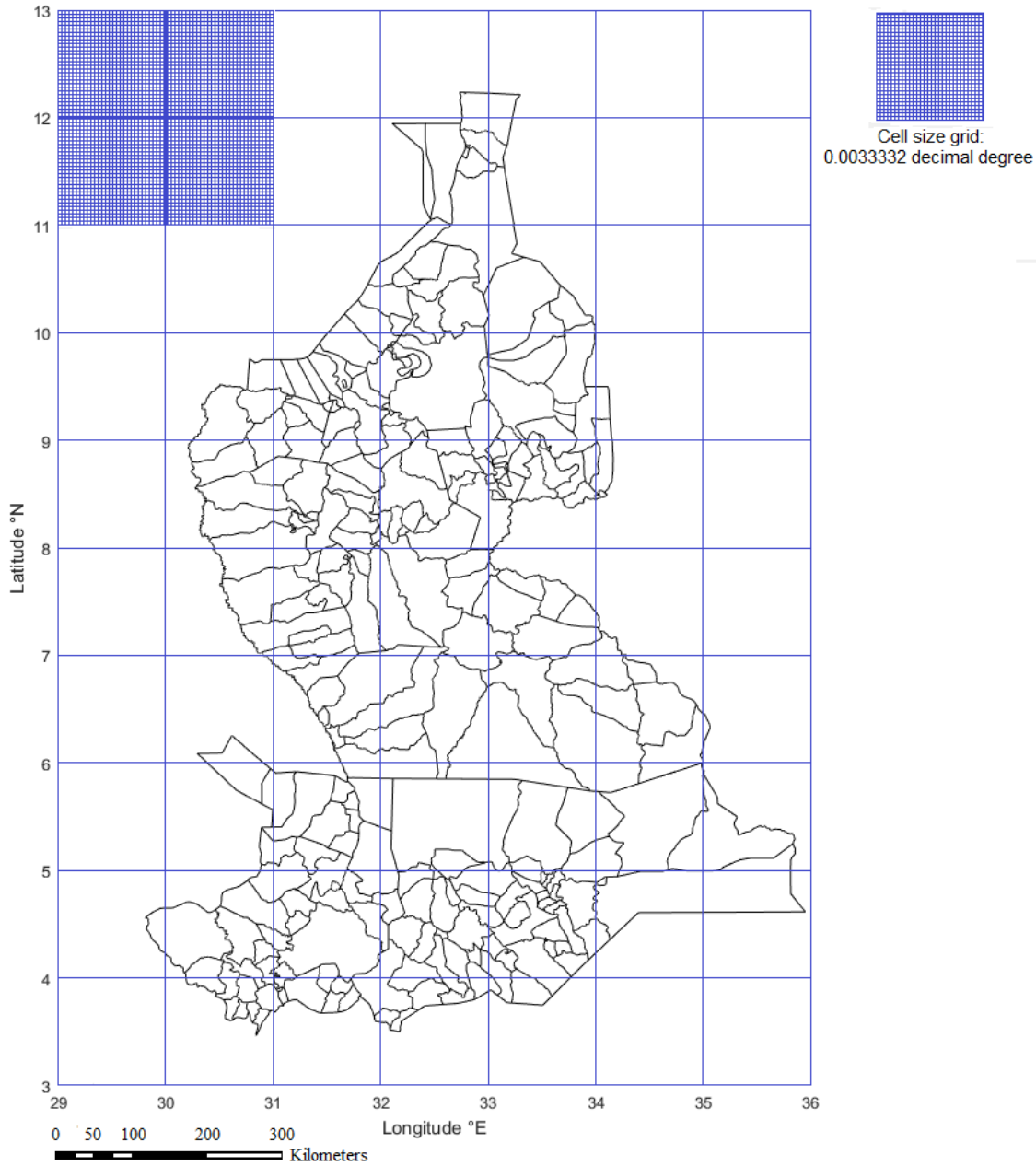


Figure 4.6: Grid in the algorithm that scans raster images of the Payams and of the population distribution to compute the centroids.

The centroid of each area is the result of the weighted position of each cell size in the grid considered. Due to the irregularity of the shape of the payams, in some cases the centroid did not fall into its belonging area. We forced these points to stay into the borders of the Payam in analysis, using a build-in function of MATLAB. Fig. 4.7 on the facing page shows the results of this algorithm, i.e. the position of the nodes in latitude and longitude coordinates.

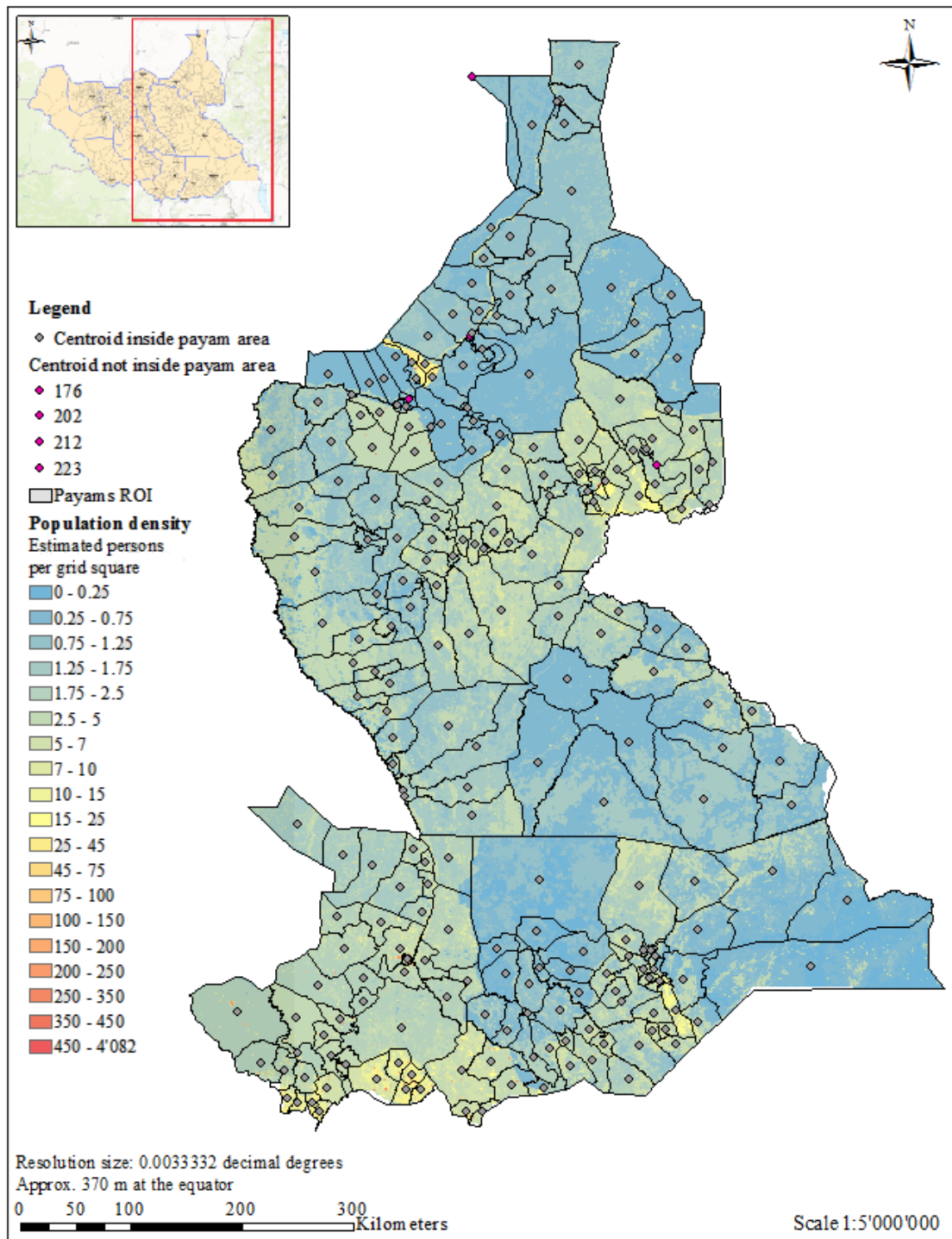


Figure 4.7: Position of the nodes weighted on the population distribution. 'Not inside' points are highlighted in purple.

4.4 Population

The map offered by WorldPop (2013) is a useful source of information for population distribution. Although computing the total estimated number of people in each payam we realized that these values do not match the numbers of the 2008 last census (SSNBS, 2010) and the rate of population growth provided by CIA (2015). In fact, as the website reports, population maps are updated to newest versions when improved census or other input data become available. Due to the unstable political conditions discussed in Chapter 2, new certain information are not available. Reasonable

population values for each payam, therefore each node, were found in official projections provided by (SSNBS, 2015c,b).

These projections match the growth rate stated by the CIA (2015): comparing the data of the 2008 census with the projections for the year 2015, the average growth rate computed as:

$$\frac{H_i(2015) - H_i(2008)}{H_i(2008)}$$

results approximately +0.3%, that approaches the values of the annual growth rate of 4% in 7 years. These values appear in the model as H_i in each node i .

4.5 Distances

In order to derive the mobility of individuals around the network using the gravity model (eq. (3.10)), we compute distances d_{ij} between the centroids using the *haversine formula* (for further information see Inman (2010)). The equation has importance in navigation, as it is useful to compute distances between two points on a sphere using longitudes and latitudes. For any two points on a sphere, the haversine of the central angle between them is given by:

$$\text{hav}\left(\frac{d}{R}\right) = \text{hav}(\varphi_2 - \varphi_1) + \cos(\varphi_1) \cos(\varphi_2) \text{hav}(\lambda_2 - \lambda_1) \quad (4.1)$$

in which *hav* is the *haversine function* defined as:

$$\text{hav}(\theta) = \sin^2\left(\frac{\theta}{2}\right) = \frac{1 - \cos\theta}{2}$$

where θ is any angle and

- d is the distance between the two points along a great circle of the sphere, i.e. d is the spherical distance in which we are interested;
- R is the radius of the sphere;
- φ_1, φ_2 are the latitude values of the points expressed in radians;
- λ_1, λ_2 are the longitude values of the points expressed in radians.

Solving for d , equation (4.1) becomes:

$$d = 2R \arcsin \sqrt{\sin^2\left(\frac{\varphi_2 - \varphi_1}{2}\right) + \cos(\varphi_1) \cos(\varphi_2) \sin^2\left(\frac{\lambda_2 - \lambda_1}{2}\right)} \quad (4.2)$$

that can be easily be compacted (4.3) through the $\arctan 2$ with two elements and defining the value a :

$$a = \sin^2\left(\frac{\varphi_2 - \varphi_1}{2}\right) + \cos(\varphi_1) \cos(\varphi_2) \sin^2\left(\frac{\lambda_2 - \lambda_1}{2}\right)$$

$$d = 2R \arctan 2\left(\sqrt{a}, \sqrt{1-a}\right) \quad (4.3)$$

The formula applies to our model using as points on the sphere the position of the nodes in our network and their coordinates. R is the radius of the earth, whose value used is $R = 6371km$.

4.6 Rainfall data

Rainfall data were downloaded from the Climate Data Library (IRI/LDEO, 2016). Information provided regard the daily estimated precipitation, expressed in $mm d^{-1}$, evaluated by the NOAA - National Oceanic and Atmospheric Administration - in the African continent. In order to analyze both years, we took the data during the period January 1, 2014 - December 31, 2015 within the range ($29.5^\circ - 36^\circ E$; $3^\circ - 12.5^\circ N$). The spatial resolution of the data is $0.1^\circ N$, approximately 10 km at the equator. The format in which data are provided is a table containing a vector of the time T , time step of a day, and a matrix $X \times Y$, where X is the longitude and Y is the latitude, in which compare the values of daily precipitation in that coordinates.

Fig. 4.8 shows the rainfall estimation during the first day of analysis in our region of interest, data processed using MATLAB 2015.

To each single node of the network we assign the mean daily rainfall fallen in the area of the Payam, evaluating the position in each cell similarly to what was conducted to compute the total population in the area. In order to solve this algorithm we create a raster image of the payam

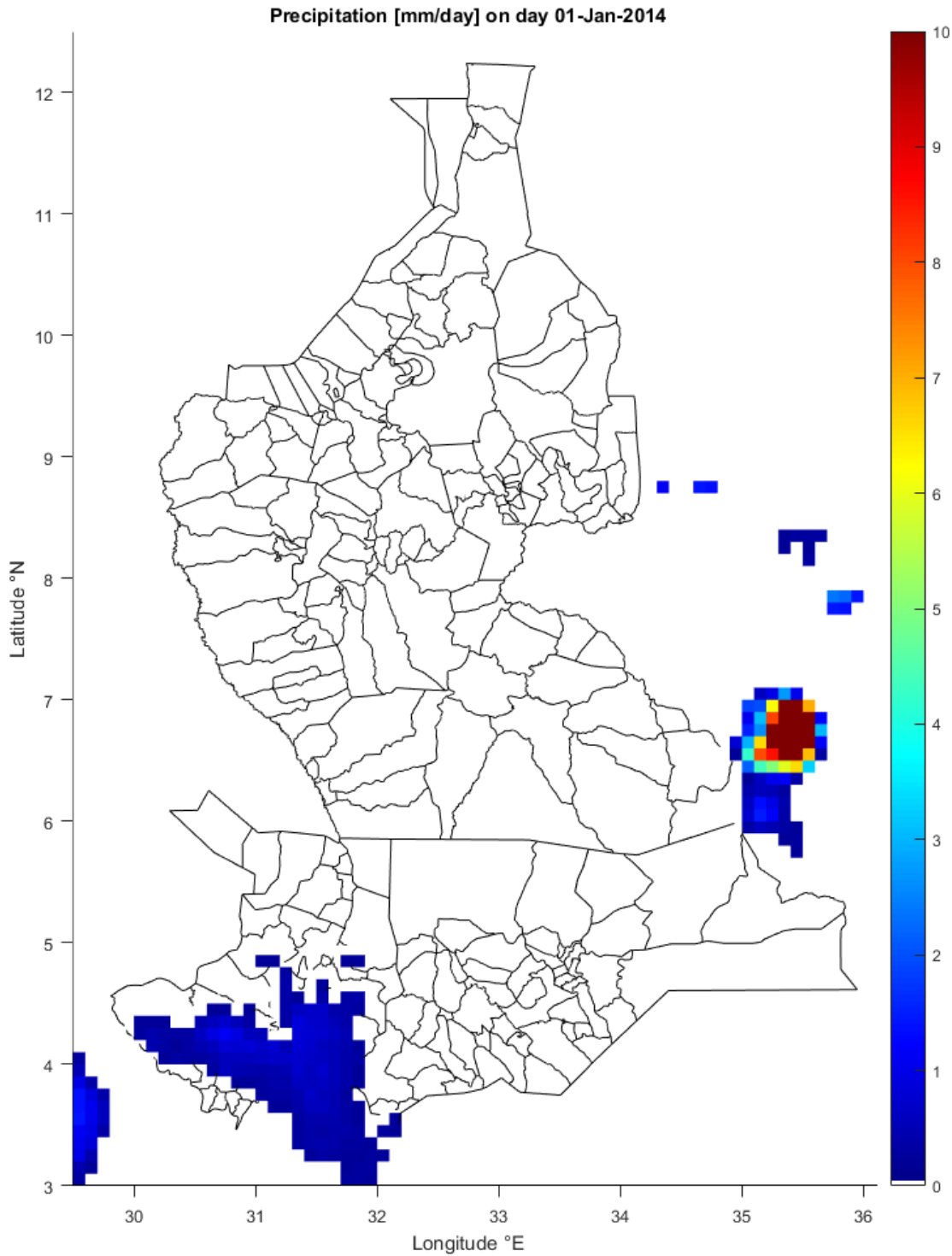


Figure 4.8: Rainfall estimation during the first day of analysis in our spatial domain, January 1st, 2014

administration having the same spatial resolution of the rainfall data, i.e. 0.1 decimal degree. Fig. 4.9 on the next page shows the new raster image for payams representation.

As the map shows and as one can notice comparing this map with the previous raster image in Fig. 4.5, to increase the cell size compromises the resolution of the image, and borders of the areas are less detailed. Moreover, it is possible that the cell size is bigger than the dimension of the payams and that, in these cases, these are included in nearby bigger payams. Fig. 4.10 focuses in a specific area of the vector, on the left, and raster image, on the right, of the Payam representation. Circles highlight areas characterized by various small regions. Not all of these regions are represented in the raster image on the right, yet are included in other regions.

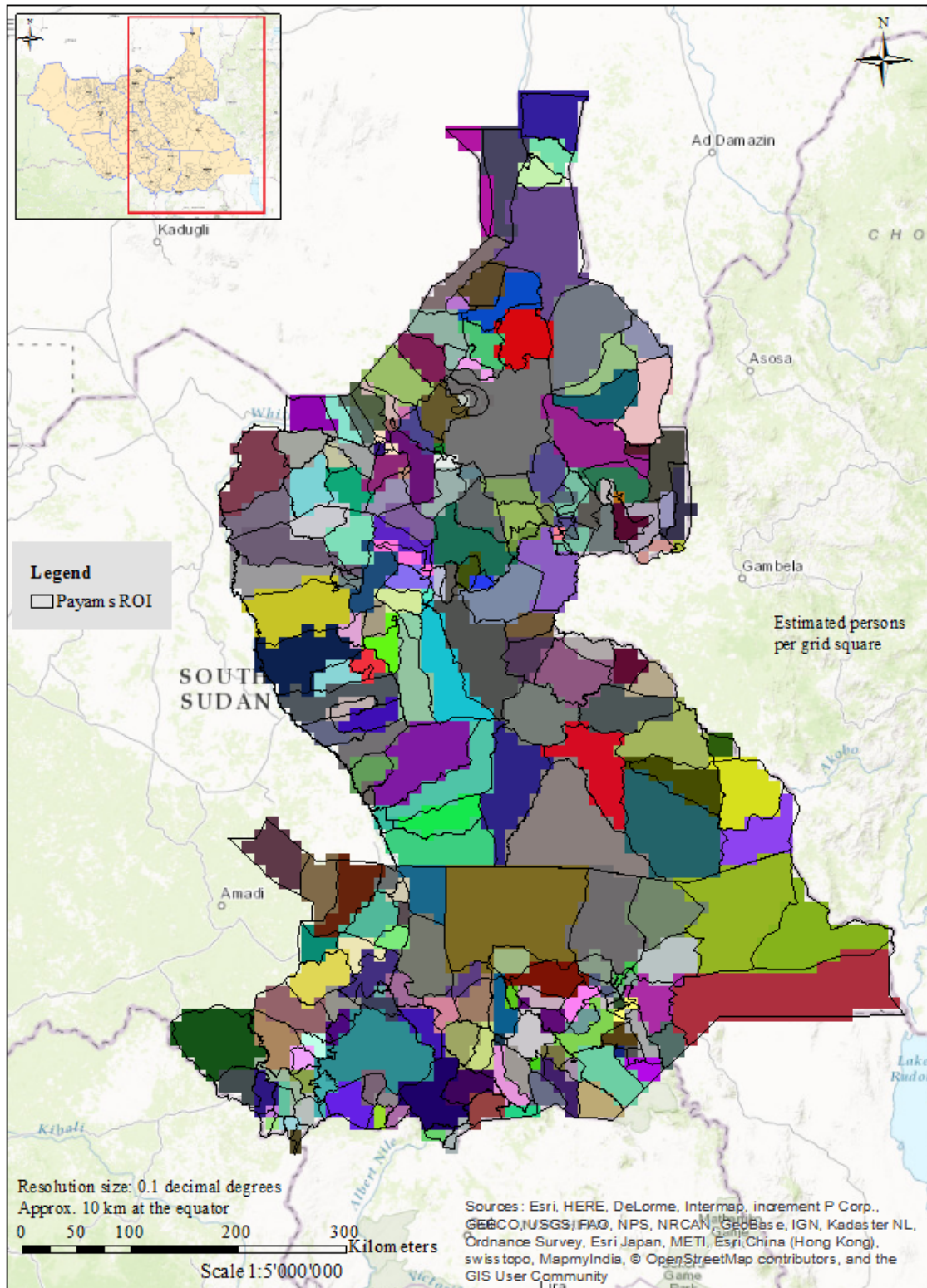


Figure 4.9: Raster image of the division in Payam, created to compute the mean values of rain in each community. Cell size 0.1 decimal degrees, approximately 10 km at the equator. We highlight the administrative division at the level of Payam. The color bar is the same used in fig. 4.5 on page 35 for comparison.

To avoid wrong evaluation, we compare the values of the pixels in the raster image with the ID numbers. Whether some ID did not appear in the raster, the mean daily rain in the area could not be computed. In this case we assign to this payam, hence node, the daily rainfall data interpolated in

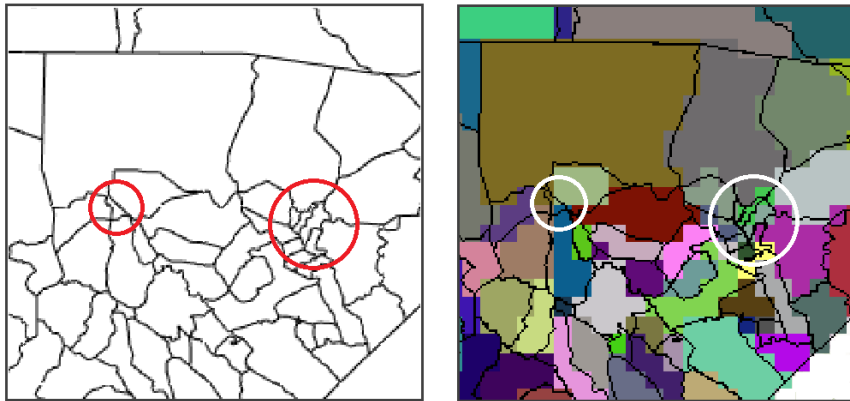


Figure 4.10: Comparison between the Payam vector image and its raster image, focusing on a specific area

the coordinates of the corresponding centroid. For this step, we used the 2D interpolation function available in MATLAB.

4.7 Adapting the model

The analysis on the context and on the epidemiological records let us develop an appropriate mathematical approach for this particular case study.

For the reason explained in Sect. 3.2 on page 19, we consider the population in each node to be at demographic equilibrium. Therefore the equation for the susceptible class in each node i is eq.(3.9).

Since we are neglecting the hydrological transport of the bacteria, the parameter l that stands for this phenomenon will be set to the constant value zero in all the simulations. The relative eq.(3.7) for the environmental concentration of bacteria in this approach becomes:

$$\frac{dB_i}{dt} = -\mu_B B_i + \frac{p}{W_i} [1 + \lambda J_i(t)] I_i \quad (4.4)$$

We recall that, the value p/W_i is replaced by the parameter on water and sanitation θ (see Sect. 3.3 on page 22).

Therefore, calibration is required for the following nine parameters,

$$\Theta = \{\theta, m, D, \lambda, \beta_0, \mu_\beta, \rho, \sigma, k\}.$$

while l is kept to constant null value.

The parameters μ , γ and α , respectively human mortality, rate of recovery and mortality due to cholera, can be estimated from literature (see Sect. 3.3 on page 22). Table 4.1 shows the assigned values. The mortality rate is taken from the statistic provided by CIA (2015). For the recovery rate, we use the value as in Haiti model (Rinaldo et al., 2014), value that is comparable with the duration of the symptoms arise from the epidemiological records. For what concerns the mortality rate due to cholera, this is computed using the epidemiological records of 2014 as follows:

$$\alpha = \frac{\text{Recorded deaths 2014}}{\text{Tot cases 2014} * \text{2014 epidemic duration period}}$$

We decide to use the value α computed from 2014 into 2015 simulations, since the magnitude of this number for 2015 epidemic is the same.

4.8 Calibration set-up

The requirements of the calibration are the size of the ensemble N and the values of the constants c_1 and c_2 to control the inbreeding problem, as seen in Sect. 3.3.2 on page 26. Based on preliminary

Table 4.1: Fixed parameters

Parameters	Units	Value	Evaluation
μ	d^{-1}	$2.25 * 10^{-05}$	CIA (2015)
γ	d^{-1}	0.2	Rinaldo et al. (2014)
α	d^{-1}	$1.145 * 10^{-04}$	From epidemiological data 2014

sensitivity analyses, we have seen that stable results are obtained with $N = 3000$, $c_1 = 5$, and $c_2 = 0.8$.

Outliers, i.e. updated values of the parameters outside the prior, are forced to their prior boundaries using a 'reflection technique', that projects, as a mirror on the borders, these values within the boundaries.

The time step of the simulations is weekly. We use the "epidemiological week", whose starting day is Sunday. Weekly output are therefore given on Saturdays. This works for both observed and simulated state variables.

For each realization during DA, the update of the state variables is accepted whether the following condition is accepted:

$$S_i = H_i - I_i - R_i > 0$$

as to say, it is not possible to have more susceptible than the population in the i -th node.

As anticipated in Sect.4.2, the calibration runs at the spatial level of 10 Counties. This implies that the observation function \mathbf{H} in eq.(3.18), transfers the cumulative weekly cases C_i simulated in each node i , i.e in each Payam, to the Counties, in which we define the observation points. Therefore in our case, the dimension of \mathbf{H} , the vector of weekly recorded cases \mathbf{y}_k , and the vector of the measurements error ξ_k are $\mathbf{H} \in \mathbb{R}^{10 \times 236}$, $\mathbf{y}_k \in \mathbb{R}^{10}$, $\xi_k \in \mathbb{R}^{10}$.

The goodness of each realization is computed using the Root Mean Squared Errors (RMSE). Per each realization j the errors at each time k are defined as:

$$Err = \mathbf{H}\mathbf{x}_k^j - \mathbf{y}_k^j \quad (4.5)$$

Therefore the RMSE is:

$$RMSE = \sqrt{\frac{\sum_{j=1}^N (\mathbf{H}\mathbf{x}_k^j - \mathbf{y}_k^j)^2}{N}} \quad (4.6)$$

that can be mediated both in time and on number of realization. To compare simulations, we will use a single value RMSE, mediated first on realizations, and in time afterwards.

4.9 Initial conditions and time of the simulations

In order to perform simulations and calibration, initial conditions - IC and time of the simulations have to be set for both the two years of investigation. We apply the initial conditions to the first day of simulation ($t = 0$), that changes in the two years. The susceptible at time $t = 0$ are given by the equilibrium between the population, the initial symptomatic infected and the recovered:

$$S(i) = H_i - I_i(0) - R_i(0)$$

where

$$R_i(0) = (1 - \sigma)I_i(0)$$

We assume $B_i(0)$ to be in equilibrium with the local number of infected individuals, therefore:

$$B_i^*(0) = \frac{\theta I_i(0)}{H_i \mu \beta}$$

Details on the initial conditions for both years follows.

2014 epidemic The 2014 epidemic started on April 23, 2014 and last until October 29, 2014. We assign as initial conditions the cumulated recorded cases until May 17, 2014. During this month, cases were recorded in the capital Juba and in four adjacent Payams. All these nodes belong to the County of Juba. Simulation last until the last day of the epidemic. we apply the initial conditions to the first day that is simulated, as to say May 18,2015. The simulation starts from a total number of infected equal to 168.

2015 epidemic The 2015 epidemic started on May 18, 2015 and last until September 23, 2015. We assign as initial conditions the cumulated recorded cases until June 20, 2015. As 2014 epidemic, during 2015 one first cases were recorded in the capital Juba and in nearest payams, so that all nodes belong to Juba County. We apply the initial conditions to the first day simulated, June 21, 2015. The simulation starts from a total number of infected equal to 172. Simulation last until the last day of the epidemic.

Table 4.2 resumes what just stated.

Table 4.2: Initial conditions and times

Year	IC Period	Simulated	County IC	Nodes IC	Cum. IC	Cases
2014	23/04/2014	- 18/05/2014	- 1; Juba County	4; 7; 9; 235; 236	169	
	17/05/2014	29/10/2014				
2015	18/05/2015	- 20/06/2015	- 1; Juba County	7; 9; 235; 236	172	
	20/06/2015	26/09/2015				

4.10 Pseudo-code

We would like to give an idea on how EnKF and SIRB model work together via the simple pseudo-code that follows.

```

1 %
2 % Pseudo Code for EnKF and SIRB model.
3 % Given for year 2014, updating both states and parameters
4 % We show the initialization of the model and the first step of the DA method,
5 % avoiding loops for the time in which the simulation runs and the Number of the
6 % realization used.
7 %
8
9 % ===== INPUT DATA ===== %
10 % load the input files
11 J = load rain; % rainfall data in each node, mean or interpolation
12 Pop = load population; % population size in each node
13 Obs = load weekly cases; % recorded cases in each node
14 Centr = load centroid; % position of the centroids and ID number
15 dij = load distances; % distances between nodes
16 H = load upscale matrix; % matrix to upscale from payams to counties:
17 % objective function
18 nodes = 236; % number of nodes
19
20 Input = [J, Pop, Obs, Centr, dij, H, nodes];
21
22 % ===== TIMING ===== %
23 % definition of the time of the simulation
24 start_time = 18/05/2014;
25 end_time = 29/10/2014;
26
27 % definition of the time of the model in day
28 time = start_time :1: end_time;
29 % definition of the time of the model in weeks
30 week time = start_time: 7 :end_time;
31
32 % ===== INITIALIZE ===== %
33 % definition of the parameters: l is null l=0;
34 pars = [theta, m, D, lambda, beta0, muB, rho, sigma, K];
35 % for all the parameters: Domain in which the parameter can change
36 p_range = [low_bound : up_bound];
37
38 % Initializing the EnKF
39 N = 3000; % size of the ensemble
40 c1 = 5; % constant to increase the measurements errors
41 c2 = 0.8; % constant to accept the update
42
43 % Initialize the parameter ensemble:
44 % definition of the random sampling in the ranges for each realization
45 pars = rand(p_range, Nre);
46
47 % definition of the IC for year 2014
48 I0 = cumsum(Obs(23/04/2014:17/05/2014)); % Infected at time t=0
49 R0 = (1-sigma)/(sigma*I0); % Recovered at time t=0
50 S0 = H0 - I0 - R0; % Susceptible at time t=0
51 B0 = (theta*I0)/(H0*muB); % Concentration at time t=0
52 nodesIC = find(I0 ≠ 0); % nodes of IC
53 nodesIC = H*nodesIC; % upscale to counties
54 % using obj function
55 IC = [I0,R0,S0,B0,nodesIC];
56
57 % ===== STATE EVALUATION ===== %
58 % simulation to forecast the states at the k-th week and solve the SIRB model

```

```

59 a = H*exp(-dij/D);           %mobility nominator
60 % term for mobility denominator dj
61 % need to remove the zero distance on the diagonal
62 b = a*(1-eye(263));
63 Qij = a/sum(b);             %mobility probability from node i to node j
64
65 % exposure rate
66 beta = beta0*exp(-cumsum(Obs(1:=t)))
67
68 %----- SIRB FUNCTION -----%
69 % function containing the differential equations of the SIRB to solve
70 % t contains the time, y the actual state of the system
71 % from which we solve dy per each day k+1
72 function dy=sirb(t,y,par);
73     % Susceptibles at k+1
74     S = H - I - R;
75     % force of infection
76     F = ((B*(1-m))/(1+B)+m)*S*beta;
77     % solve for the infected dy(1) = I(k+1)
78     dy(1) = (1-sigma)*F - (gamma+mu+rho)*I;
79     % solve for the recovered dy(2) = R(k+1)
80     dy(2) = (1-sigma)*F + gamma*I - (mu+rho)*R;
81     % solve for the concentration dy(3) = B(k+1)
82     dy(3) = -mu*B + (theta/H)*(1+lambda*R)*((1-m)*(Qij)*I);
83     % solve for the cumcases dy(4) = cumcases(k+1)
84     dy(4) = sigma*F;
85 %-----%
86 % solve the differential equations at daily time step. states contain the daily ...
87     model
88 % response in each node: as to say I,R,B,cumulative I for each realization Nre
89 [t,States] = ode45(@sirb, time, IC, par, options);
90
91 % evaluate the weekly cases using a function @dafun that repeats the SIRB weekly
92 %the value sim_cases is what we defined as Hx, cumulative number of infected in ...
93     the week
94 [sim_cases, y] = feval(@dafun,par,Inputs,states);
95
96 % ===== DA + EnKF ===== %
97 % we want to update both the states and the parameters of the system
98 % using the state augmentation
99 % We control the inbreeding, 10 times trial to update the states
100
101 trial = 0;
102 for i=1:10
103     trial = trial + 1;
104     old_pars = par;
105     old_states = y;
106
107     Prior = [old_pars,old_states];
108
109     % variance of the prior needed to control the inbreeding
110     var_prior = var (Prior);
111
112     % define a value for the simulated cases standard deviation
113     % variation coefficient
114     CV = 0.1;
115     sim_std = c1*CV;
116
117     % formula for the kalman gain K = P*H^T*(H*P*H^T + R)^-1
118     % we decompose the value P, covariance matrix of the ensemble as 1/N-1*(X*X^T)
119     % in which X contains the deviation from the mean of the states
120     % and define as Y the product H*X
121     mean_prior = mean(Prior);
122     % deviation from the mean values
123     X = Prior - mean_prior;

```

```

122
123     % The value  $Y*Y^T=(H*X*X^T*H^T)/N-1$  is simply the covariance matrix of the ...
           response of the model
124     mean_sim_cases = mean(sim_cases);
125     % deviation from the mean per each obs
126     dev_sim = sim_cases - mean_sim_cases;
127     YYT = 1/(N-1) * dev_sim*dev_sim';
128     % add the value R, diagonal matrix of the errors, that completes the term ...
           (H*P*H^T + R)
129     YYT_R = YYT + diag (sim_std.^2);
130
131     % complete the terms of the kalman gain
132     XY = 1/(N-1) * X * dev_sim;
133     K= YYT_R \ XY;
134
135     % compute normally distributed error, supposed to be independent, ...
           associated to the simulations
136     pert = sim_cases + randn;
137     % store the generated added error that we associate to the measurements ...
           s.t. err = (yk - Hxk)
138     err= pert - sim_cases;
139
140     % Update proposed
141     [Update_prop] = Prior+K*err;
142
143     % compute the variance of the update to control the inbreeding
144     var_up = var (Update);
145
146     ratio = sqrt (var_up/var_prior);
147
148     if ratio < c2
149         if trial < 10
150             Update = Prior;
151         else
152             Update = Update_prop;
153         end
154     end
155 end
156
157 % back to the steps of the model and the data assimilation
158
159 Update(1) = States;
160 Update(2) = pars;
161
162 [t,States] = ode45(@sirb, time, States, pars, options);

```

Results and discussion

The input data and the set-up seen in the previous chapter are used to run calibration and simulations. Our aim would be to find constant values in time for the parameters, adequate to perform the cholera model in both years. Therefore, we start in our analysis from the first year of the epidemic, the most critical, seeking for these values. This allows to understand whether the dynamics of the infection were similar among the two years.

As mentioned before, Sect.3.3, during first attempts the DREAM method was used to evaluate the parameters. With the aim of reducing the discussion, we do not show these results as they were not satisfactory. We show the results obtained using DA technique, EnKF. In order to understand the response of the model, we started to perform simulations using the same prior pdfs of the Haiti model (Bertuzzo et al., 2014; Mari et al., 2012). These let us understood that appropriate ranges for this case study were required.

For all the simulations, we show the simulated epidemiological curve compared to the weekly observations, the cumulative simulated and the observed cases, the simulated curves in all the ten counties of our interest and the changes in the parameter evaluation.

5.1 Prior definition

5.1.1 First attempts for year 2014

The first simulations that we performed, starting from 2014, had as prior pdfs the ones used to calibrate the model for the Haiti cholera events, shown in table 5.1 (Bertuzzo et al., 2014). The hydrological dispersion l is set to zero, as we described earlier. The parameter θ , containing all

Table 5.1: Range of the parameter prior distribution from Haiti case study

Parameters	Units	Prior
θ	d^{-1}	[0.01 - 10]
l	d^{-1}	[0 - 0]
m	—	[0.0001 - 1]
D	km	[1 - 300]
λ	$d mm^{-1}$	[0.01 - 10]
β_0	d^{-1}	[0.01 - 10]
μ_β	d^{-1}	[0.01 - 1]
ρ	d^{-1}	[0.0005 - 0.02]
σ	—	[0.03 - 0.2]
k	d^{-1}	[1 - 1000]

the information related to water, contamination and sanitation (eq. (3.13)), represents the rate for shedding excreta and water contamination rate, and it can vary between 0.1 days and 100 days. The node-independent probability of travel m , changes between the unitary value and zero. The range definition for shape factor D of the gravity model, is based on analysis of the distances considered as reachable in the Haitian territory. λ , that defines the aggravating effect of the rain, has a large domain, as the initial exposure rate to bacteria β_0 and as the other parameters values showed in the table.

As figure 5.1 shows, using this prior, the model overestimates the number of cases recorded in our spatial domain. We compare the results of two simulations: one using the state augmentation, i.e. both update of states and parameters (blue palette), to which we will refer to as "Simulation M1" for simplicity; the other using constant values for the parameters (magenta palette), that we will call "Simulation M2". Mean values of the ensemble are represented by the lines, credible interval of 90% - or uncertainties - by the shadows. The black dots represent the weekly recorded cases.

At the beginning, as it is possible to see from the cumulative curves in Fig. 5.2, and from the response of the model at the County - level in Fig. 5.3, the model starts immediately to overrate the actual process. At the first step of the data assimilation, the update of both states and parameters tries to reduce the mean and the uncertainties, but there are still some wrong values that do not allow a good performance of the model. In the case in which the values for the parameters are constant, the corrections at each time step very slightly reduce the uncertainties, whose magnitudes are higher than the observations and than the results of Simulation M1.

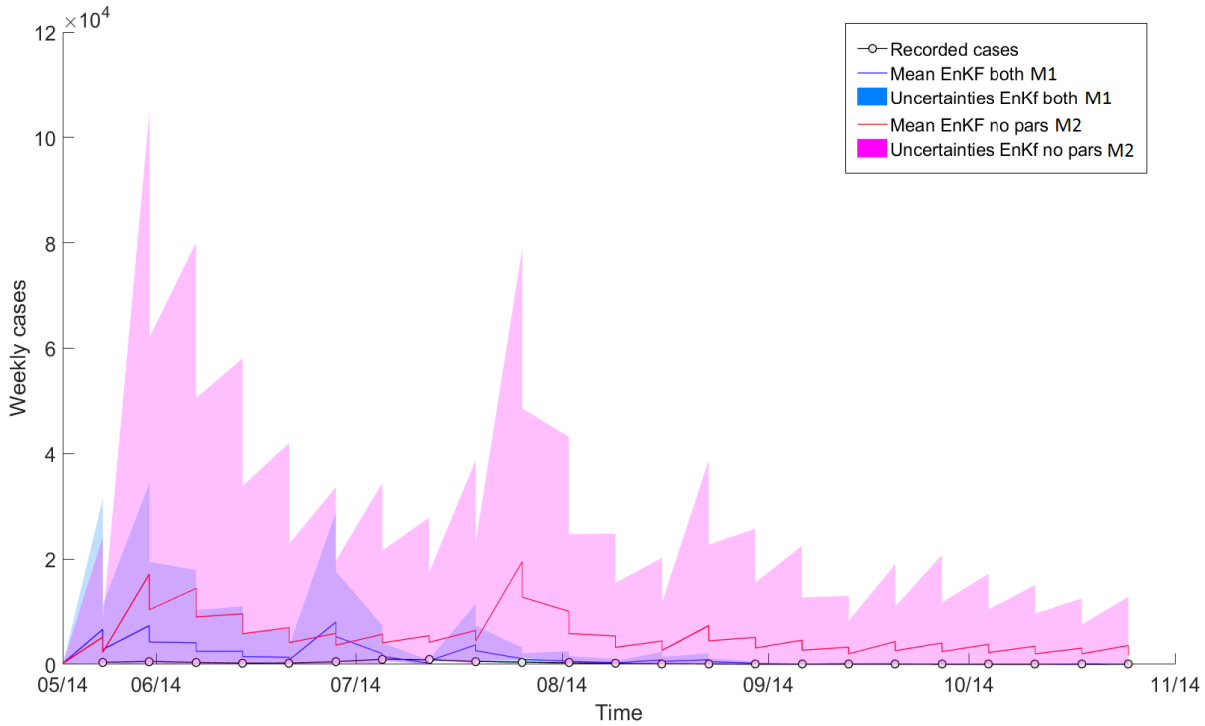


Figure 5.1: First scenario for year 2014 using the prior pdfs for the Haitian case study. Epidemiological curve in our domain. The model overrates the process whether the parameters pdfs are updated or not. In the last case, uncertainties are higher.

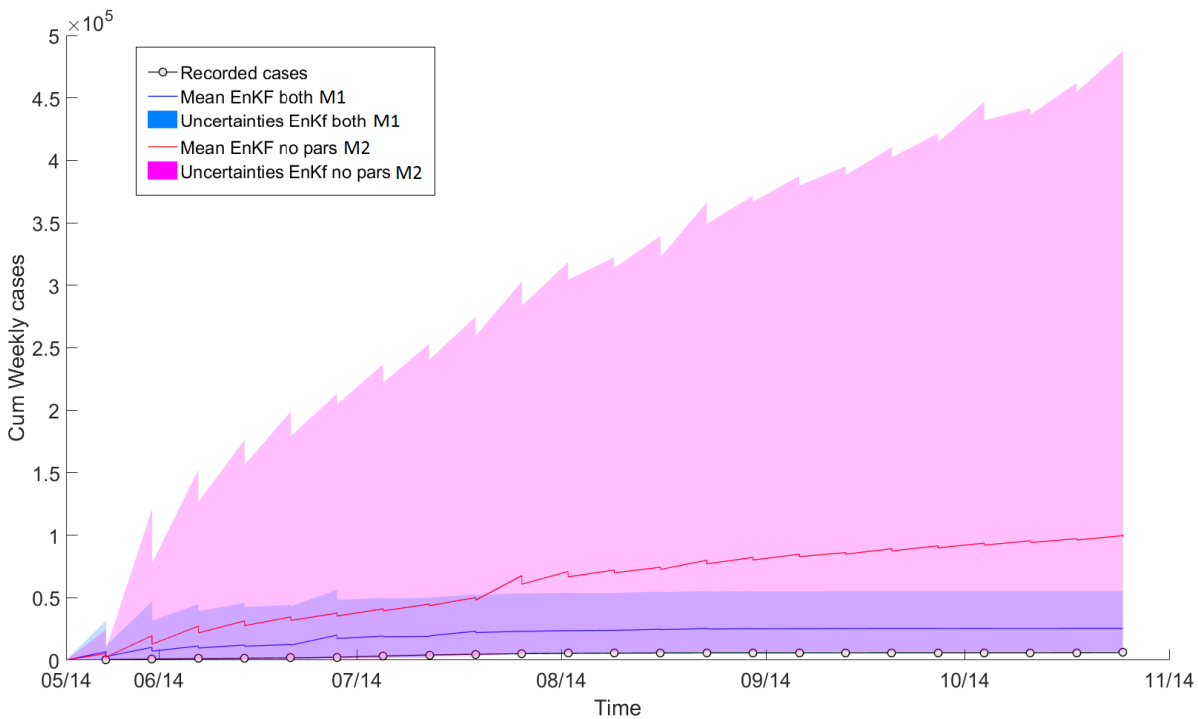


Figure 5.2: First scenario for year 2014 using the prior pdfs for the Haitian case study. Cumulative curve of weekly cases. The model overrates the process whether the parameters pdfs are updated or not. In the last case, relative uncertainties are higher.

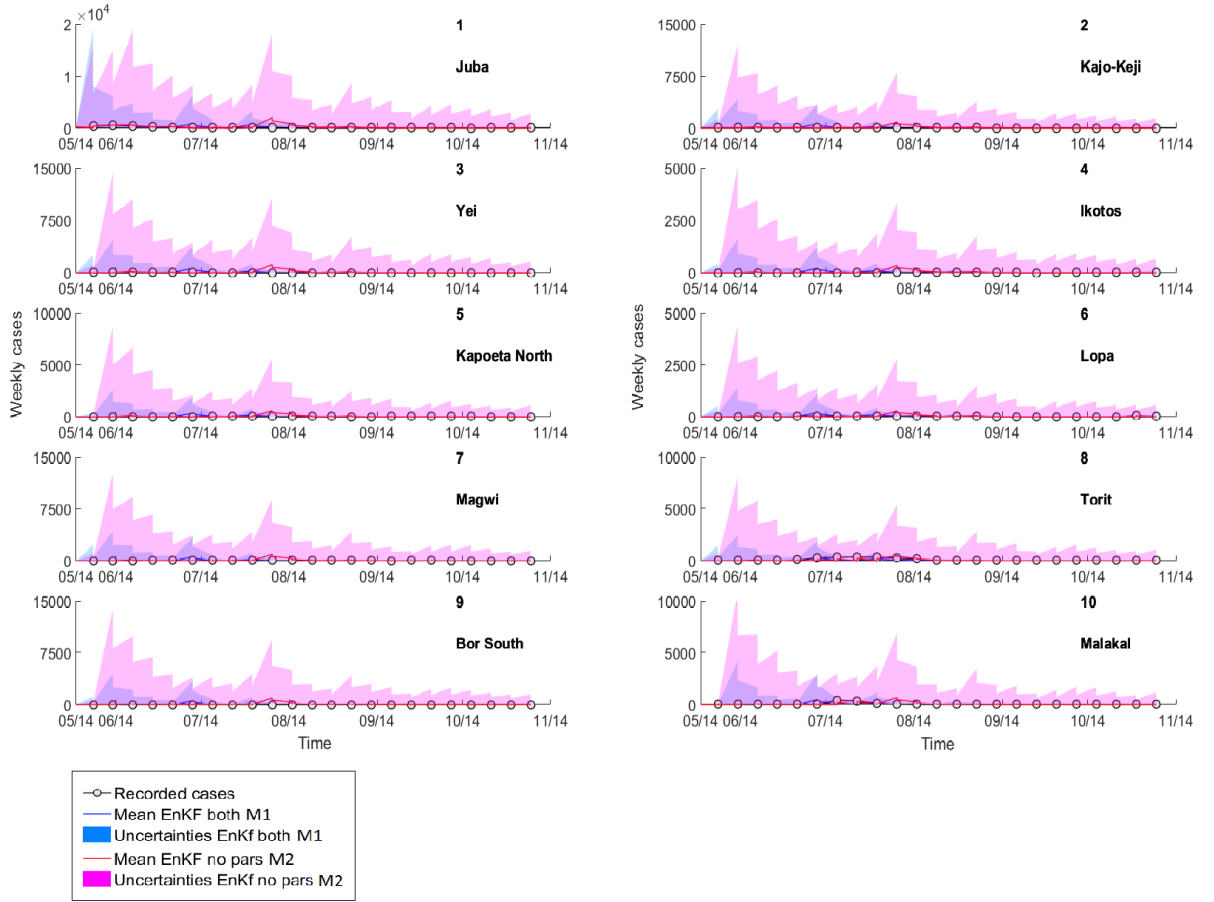


Figure 5.3: First scenario for year 2014 using the prior pdfs for the Haitian case study. Epidemiological curves in the Counties in which cholera was recorded. Magnitudes of the uncertainties are high and the mean values are far away from the real observed phenomena.

In order to correct this evaluation, we have tried to figure out which were the parameters that mostly affected the model, focusing on the values chosen by the algorithm on the first four weeks of simulations. Figure 5.4 shows the behavior of the parameter in time.

The trends in this figure made us understand that the wrong response maybe possibly due to high values of the parameters and their combinations.

Focusing on Simulation M1, parameters values change a lot during the update, restricting their prior values and moving away from the bounds. The combined parameter θ , from the prior whose maximum value is $10 d^{-1}$, reduces from a starting maximum value of almost $7 d^{-1}$ associated to the uncertainties, to a maximum value of $2 d^{-1}$ at the end of the simulation. Regarding the probability of travel m , the maximum value for uncertainties reduces from 0.9 to 0.3. The shape factor D do not detach too much from the prior distribution. On the opposite, the coefficient λ for the rainfall enhancement effect, reduces its maximum value to $2 d mm^{-1}$, against its prior $10 d mm^{-1}$. The same trend has the exposure rate β_0 that, by the time the data assimilation helps in decreasing the uncertainties, assess to a maximum value of $2 d^{-1}$. The same happens with the mortality rate of bacteria μ_β , assessing to approximately $0.4 d^{-1}$; the fraction σ of symptomatic infected, slightly restricts its prior range, having as upper bound the value $0.15 d^{-1}$. The same happens for loss of immunity rate ρ , whose upper bound value reduces to $0.015 d^{-1}$. The maximum value awareness parameter k instead, settles during the data assimilation to 200.

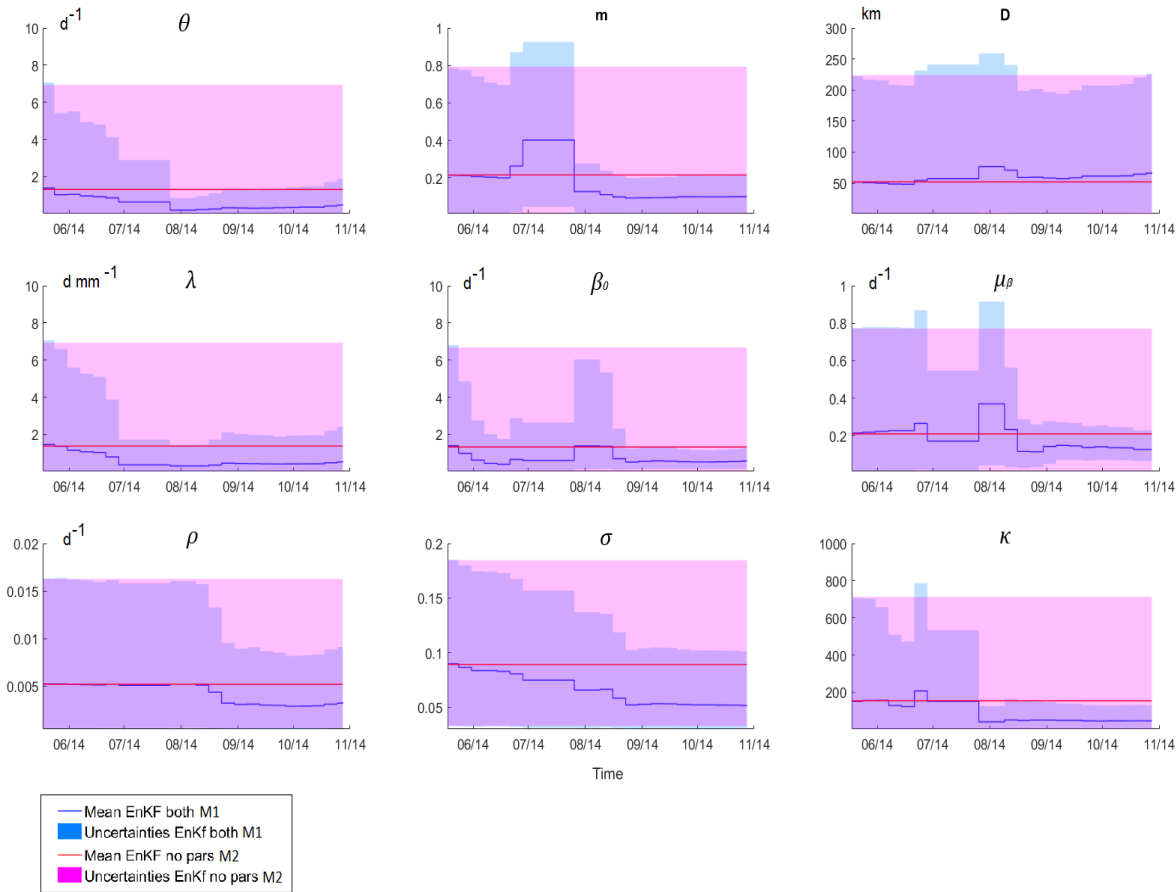


Figure 5.4: First scenario for year 2014 using the prior pdfs for the Haitian case study. Parameters values change in time for Simulation M1, while remains constant during Simulation M2.

5.1.2 Prior for South Sudan

Based on the trends of the parameters during the Data Assimilation conducted using the prior of Haiti, we have tried to restrict the prior ranges with the aim of reducing the uncertainties of the model at the beginning of the simulations. Focusing on the first four weeks in various scenarios, we have found new prior ranges that can work well for this case study (table 5.2) and that were used to perform the EnKF and SIRB model for both years and whose results will follow.

As the table shows, we redesigned both upper and lower bounds. We have seen that too high values of the parameters lead to overrate of the infected in our network. From the trials done to reduce the uncertainties, we understood that too low values instead, drift the model to underrate them. Comparing this table with the one seen before, 5.1, the values than adapt to South Sudan case are lower that the one used for the Haiti model. The Haitian cholera events were more severe than the ones in this case study. Weekly recorded cases in that country reached numbers as 3×10^4 . It is though reasonable to have, e.g., high values of θ , indicator of the worsening of the sanitation condition, and β_0 , indicator of the amount of bacteria daily shed. The epidemics we are dealing with, for what we know, did not show similar attack rate.

Table 5.2: Range of the parameter prior distribution for South Sudan case study

Parameters	Units	Prior
θ	d^{-1}	[0.1 - 0.5]
l	d^{-1}	[0 - 0]
m	–	[0.1 - 0.35]
D	km	[50 - 250]
λ	$d\ mm^{-1}$	[0.2 - 0.8]
β_0	d^{-1}	[0.2 - 0.5]
μ_β	d^{-1}	[0.02 - 0.07]
ρ	d^{-1}	[0.0015 - 0.015]
σ	–	[0.05 - 0.15]
k	d^{-1}	[100 - 450]

5.2 Year 2014

We compare the responses of different simulations performed using the new prior. We used the Ensemble Kalman Filter algorithm twice, similarly to what has been done testing the prior of Haiti case study: once updating in one case both states and parameters using the state augmentation (blue palette in the figures), subsequently updating only the states and using constant values of the parameters in time (magenta palette in the figures). For simplicity, as before, we will refer to these two respectively as "Simulation M1" and "Simulation M2". Moreover, we tested this new prior in an "Open Loop" simulation, that performs the SIRB model without Data Assimilation and uses random values for the parameter into the defined ranges.

Simulations using EnKF

The model shows an overall good agreement with the data. As Fig.5.5 shows, the mean of the ensemble of both simulations approaches the real behavior of the epidemic in our domain of study. Uncertainties, that for simulations M2 are higher than the other one, decrease in time. The peak of the epidemic, that was recorded during the second week of July 2014, is shifted of one week by the model in both simulations, but its magnitude is almost captured.

It is interesting to see through the cumulative response in Fig. 5.6, that the model offers a good approximation of the real curve, that at the end of simulations is found in between the results of Simulation M1 and M2. As the figure shows, the confidence interval when parameters pdfs are not updated is larger.

At the level of the Counties and in both simulations, as shown in Fig. 5.7, our mathematical framework is able to reproduce almost perfectly the dynamic of the epidemic in Juba, one of the County hit more severely by the infection and where it begun. Actually, the two simulations in here almost have the same mean and confidence interval. The response of the simulations is not as perfect in the other counties. In terms of numbers, the mean and the variances are not so distant from the real number of cases recorded, and the magnitude of the simulated and real phenomena are comparable, overall for what concerns simulation M1. Some overestimation are present in the Counties of Kajo-Keji, Yei, Ikotos. As we said, a certain response is always expected in all the nodes of the network: therefore we can justify the output of the model in Bor South County, in which simulated cases are present even though there were no recorded cases in 2014 year. Regarding Torit and Malakal, it is very difficult to peak this two events, despite the mean values of simulation M2 approximate better the real values of weekly recorded cases. Further details on these behaviors will be given in Sect. 5.4 on page 62.

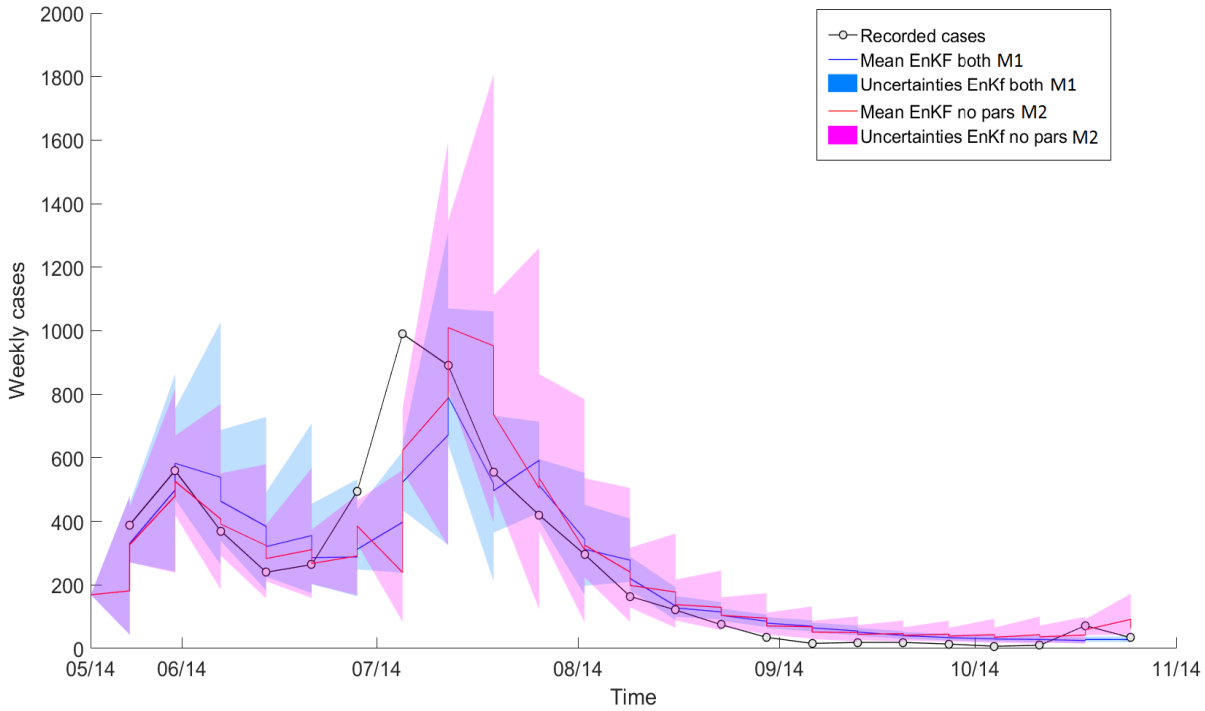


Figure 5.5: Results for 2014 using the new prior in EnKF procedures. Epidemiological curve in our domain. Mean values of both simulations approach the real observations.

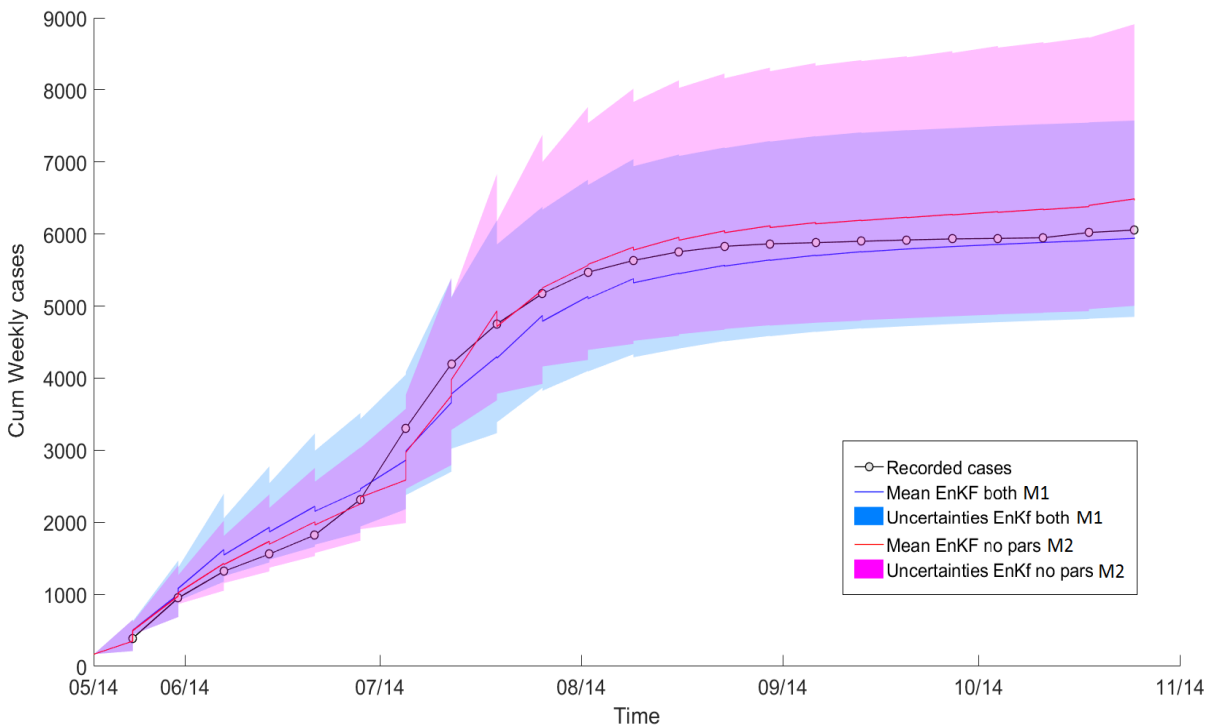


Figure 5.6: Results for 2014 using the new prior in EnKF procedures. Cumulative curve of weekly cases. The three curves of EnKF calibration procedure and the observation almost overlap.

Fig.5.8 shows how parameters change during the Data Assimilation and the values assumed whether constant. Focusing on the trends of time-dependent parameters, Simulation M1, it is possible to see that even though the credible intervals restrict in time, the variability of these

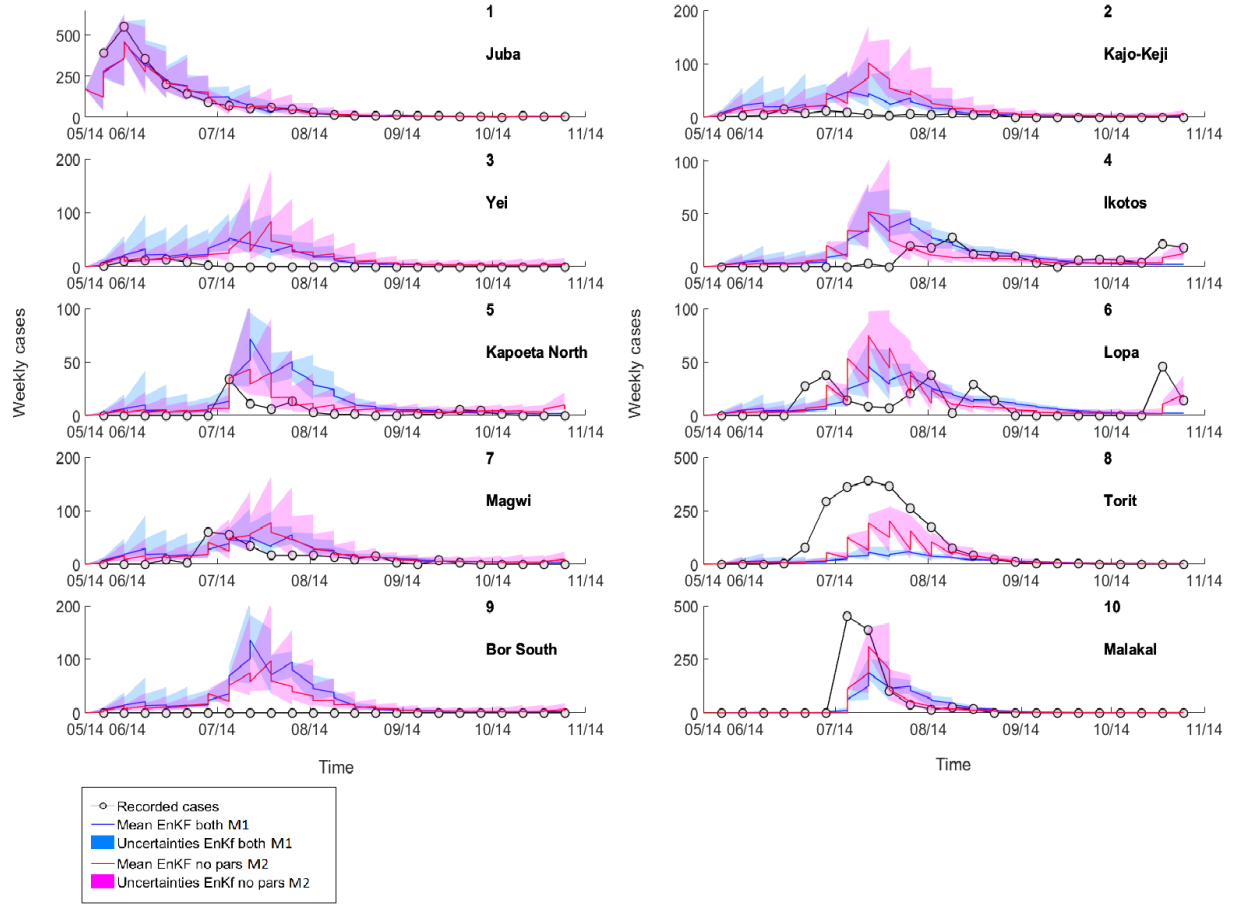


Figure 5.7: Results for 2014 using the new prior in EnKF procedures. Epidemiological curves in the Counties in which cholera was recorded. The simulations offer a good representation of the dynamic of the epidemic, overall in Juba.

makes difficult to find constant values that can fit the model. We can read this figure recalling the equations of the model (3.4) - (3.7) and the meaning of the parameters. As the epidemic decreases in time, after the peak of the simulation at the end of July 2014, the mean value of θ , indicator of the sanitation conditions, drastically decreases from $0.26 d^{-1}$ to $0.17 d^{-1}$, possibly mimicking some kind of strategies that acted to reduce the risk of infection. From the point of view of the phenomena described, at the beginning the simulation is reproducing a rate of contamination equal to $1/4$ days, value that changes to $1/6$ days after the peak. Complementary, the simulated mortality rate of the bacteria μ_β , increases in time toward its upper bound in order to reduce the bacteria concentration in the water, hence the risk of the disease, with the effect of reducing the number of simulated cases in time, approaching the real infected. The lifetime values of bacteria that the model is using during the simulations are comparable to the values stated by clinical observations (e.g. (Kaper et al., 1995; Nelson et al., 2009) of few months. In our case, lifetime of bacteria is about one month ($\mu_\beta = 0.04 d^{-1}$). The exposure rate β_0 slightly increases after the simulated peak. Hence the interval between ingestion of contaminated food or water changes from 3 days to 2 days ($\beta_0 = 0.03 - 0.4 d^{-1}$). Following this trend, k , the inverse of the parameters ψ that controls the decrease of the exposure rate β , decreases, meaning that the awareness of the population as regards the illness increases. It is interesting to see that the loss of immunity rate ρ settles to a quasi-constant average value of $0.009 d^{-1}$, i.e. on average people that recovered from the disease lose their immunity after 112 days. We can assume this value to be valid: in fact, our rate takes into account both symptomatic and asymptomatic infected that, as various authors showed (see e.g. (Koelle et al., 2005; King et al., 2008)), have different immunity duration, with symptomatic infected

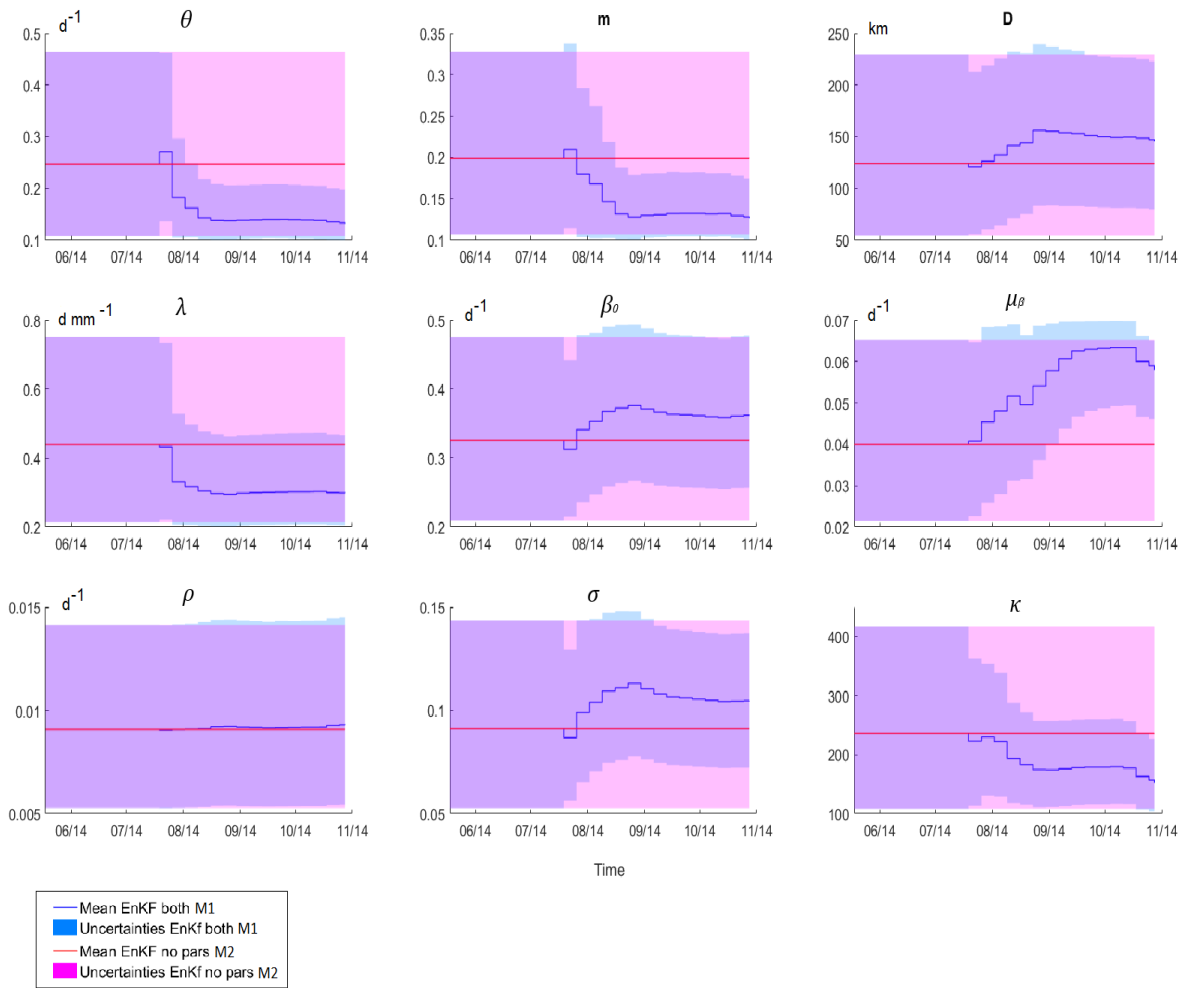


Figure 5.8: Results for 2014 using the new prior in EnKF procedures. Parameters values change in time for Simulation M1, while remain constant during Simulation B.

gaining on average multi-year immunity, while asymptomatic ones few months or less. Regarding the fraction of symptomatic infected σ , it shows similar trend to the global epidemiological curve that is simulated. The effect of rainfalls, whose coefficient is λ , reduces in time following the seasonality of rain and the global trend of the epidemic. Looking at the mobility indicators, m and D , the first one slowly shifts to lower values after the peak in July, while D does not show big changes during the period of analysis, stating that distances do not affect in time movements of people. Further discussion on the role of these two will follow.

For what concerns the constant values, these coincides with the values of the parameters at the beginning of Simulation M1. Again, in this simulation the confidence is higher.

Simulation using Open Loop

In order to test the validity of the prior, we performed an "Open Loop" simulation, in which the output of the model is given using randomly sampled parameters, without any kind of correction of state variables.

As the Fig. 5.9 show, the confidence interval of the model contains the real curve, meaning that the prior that we have chosen fit the model and the dynamic to mimic, yet the mean does not approach the observations. This let us understand that Data Assimilation is required for a good behavior of the model and correct the state variables.

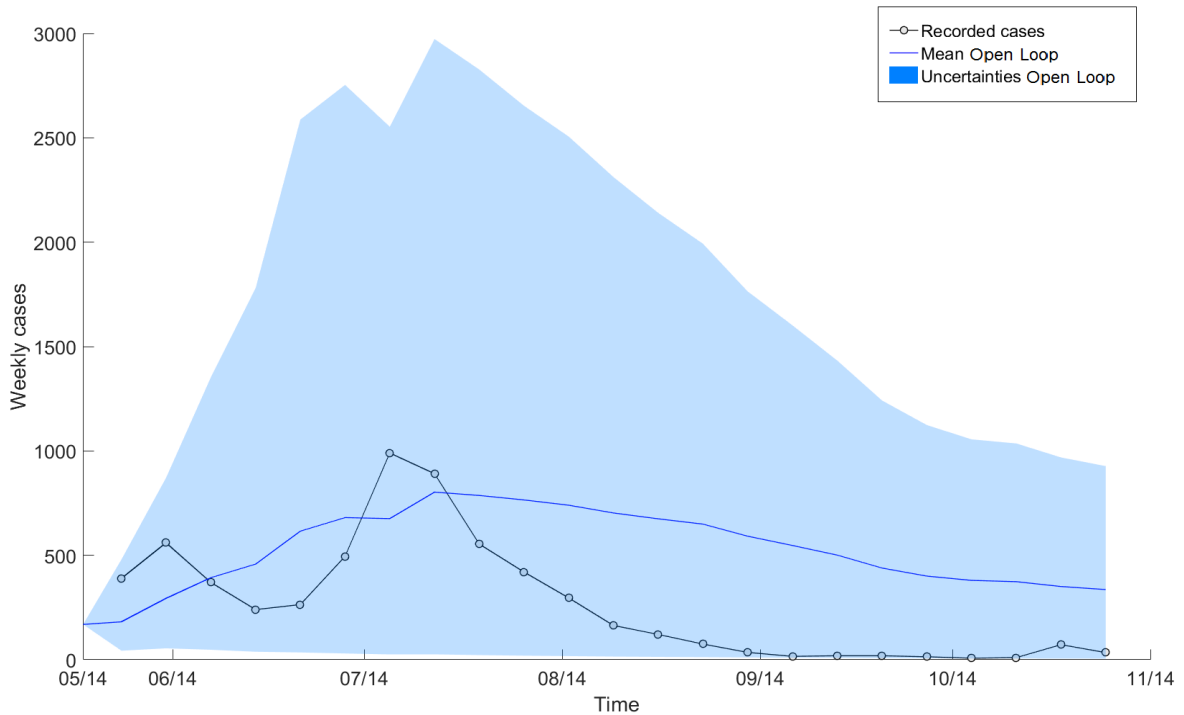


Figure 5.9: Results for 2014 using the new prior in Open Loop simulation. We use random sampling of the parameters to perform the model without DA. Observations fall into the confidence interval, yet the mean does not approach them.

We can compare the goodness of the simulations just described using the Root Mean Squared Errors of the four (see Sect. 4.8 on page 42). As the table 5.3 shows, using the new prior adapted for this case study, we definitely reduce the mean and the maximum RMSE with respect to the simulations performed using the prior for Haiti. This means that we are reducing the errors associated to the output of the model, approaching the real observations. As expected from the figures, the mean RMSE for the Open Loop is higher than the ones for the simulations in which the Data Assimilation technique has been developed. Among these two, the one in which parameters are kept constant, has a lower mean RMSE, therefore preferable. Maximum values of RMSE among these two are practically the same.

Table 5.3: RMSE comparison for simulations of year 2014

Simulation	Mean RMSE	Max RMSE
EnKF: parameters update; prior Haiti	175.6385	1.1570e+03
EnKF: no parameters update; prior Haiti	633.5467	2.2280e+03
EnKF: parameters update; new prior	39.0639	177.2061
EnKF: no parameters update; new prior	33.9874	177.9327
Open Loop: new prior	80.5312	199.6132

5.3 Year 2015

Seen that the prior used in the Haiti case study was not successful in our domain, we chose to directly perform simulations using the new prior, whose results are quite good for the previous year. As before we performed EnKF twice and an Open Loop simulation to test the prior. We will use the definition "Simulation M1", "Simulation M2" to distinguish among the two EnKF procedures.

As Fig. 5.10 shows, the model tends to overrate the global number of cases in our spatial domain. At the beginning of the simulations, as the uncertainties show, DA corrects the state variables, and updates the parameters in one case, reducing the simulated number of infected. Even though the trends are similar, the confidence interval for the simulation M2 when parameters are constant in time, is larger.

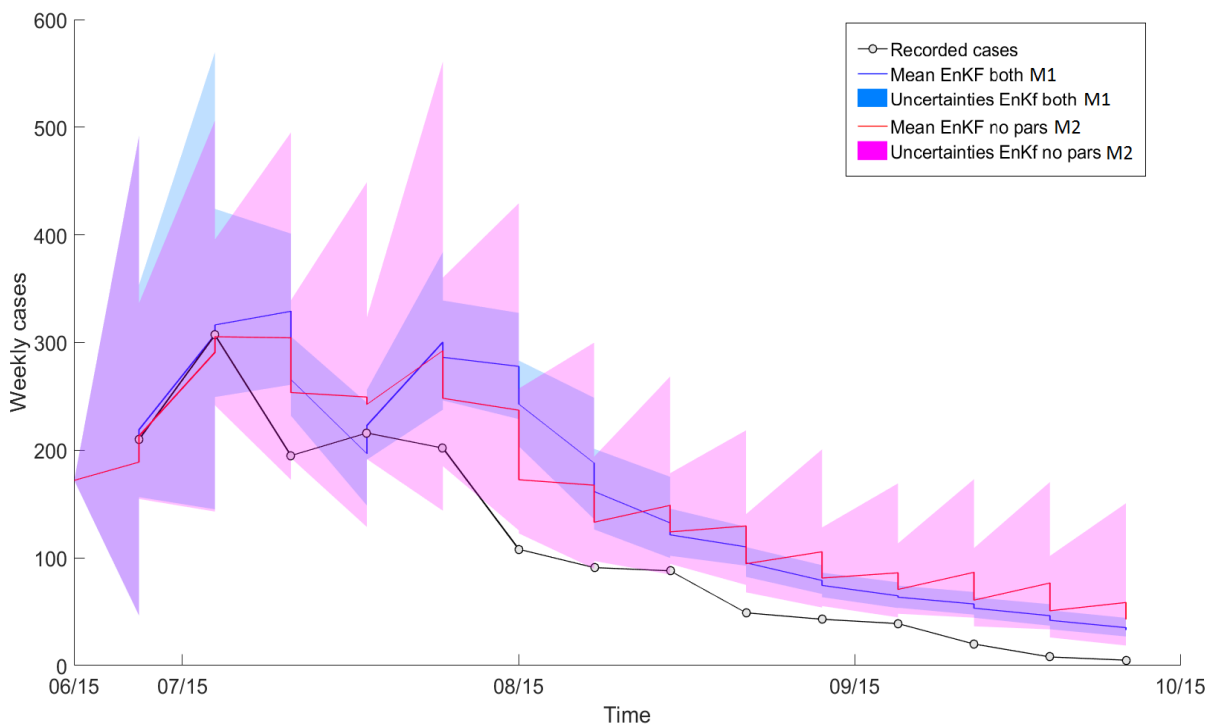


Figure 5.10: Results for 2015 using the new prior in EnKF procedure Epidemiological curve in our domain. Trends of the mean values are similar to the real observed phenomena, yet overestimation is present.

The cumulative curves confirm the overestimation of the model in both simulations.

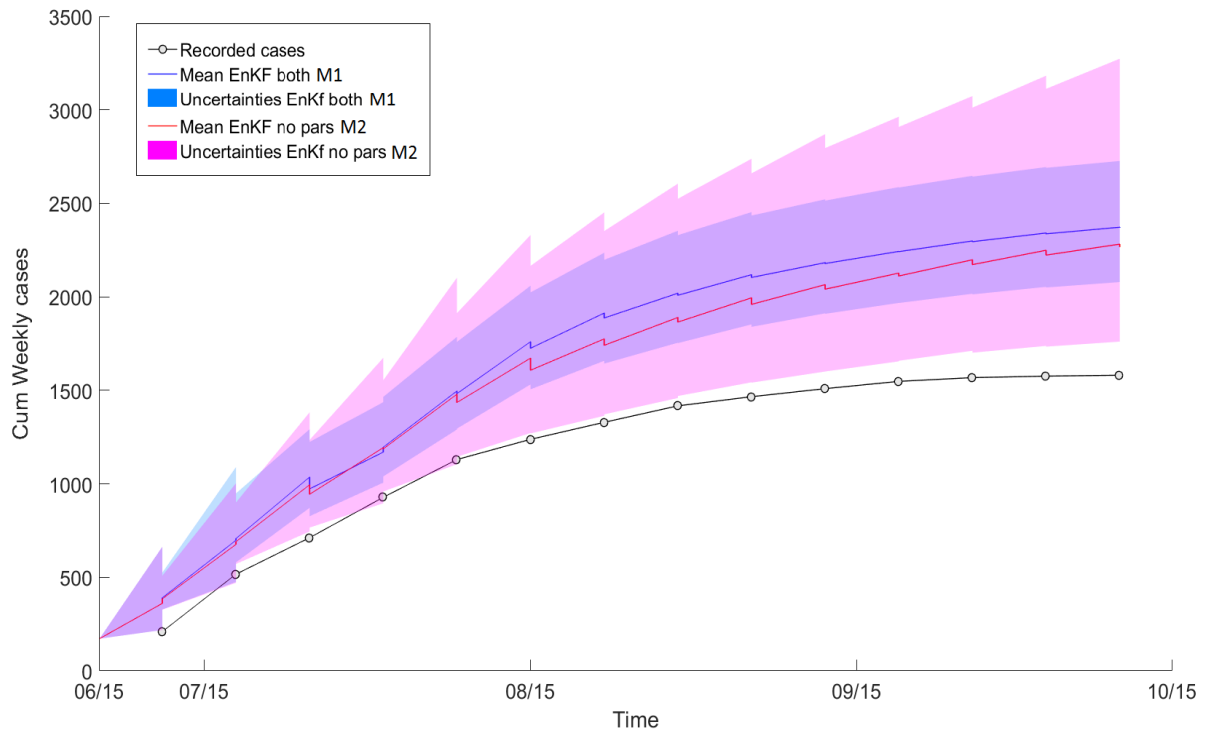


Figure 5.11: Results for 2015 using the new prior in EnKF procedures. Cumulative curve of weekly cases. The curves of the EnKF calibration procedure detach each other towards the end of the simulations, yet the observed cumulative curve stays below them

At the level of the County the model captures, almost perfectly, timing and magnitude of the epidemic in Juba, whether parameters are kept constant or subject to update. As we have stated in the previous lines, the mathematical approach used does not allow for zeroes. Therefore, as we can see from Fig. 5.12, the model is simulating cases in the other Counties in which there were no recorded cases, even if the magnitude of these numbers is low. We can consider this as an explication to the global overestimation seen in the epidemiological curve in our domain for 2015 (Figs 5.10 - ??). There are no great differences between the two EnKF simulations, that are quite the same all over the Counties. The response in Bor South, whose peak is difficult to capture, needs some further details that will be given in Sect. 5.4.

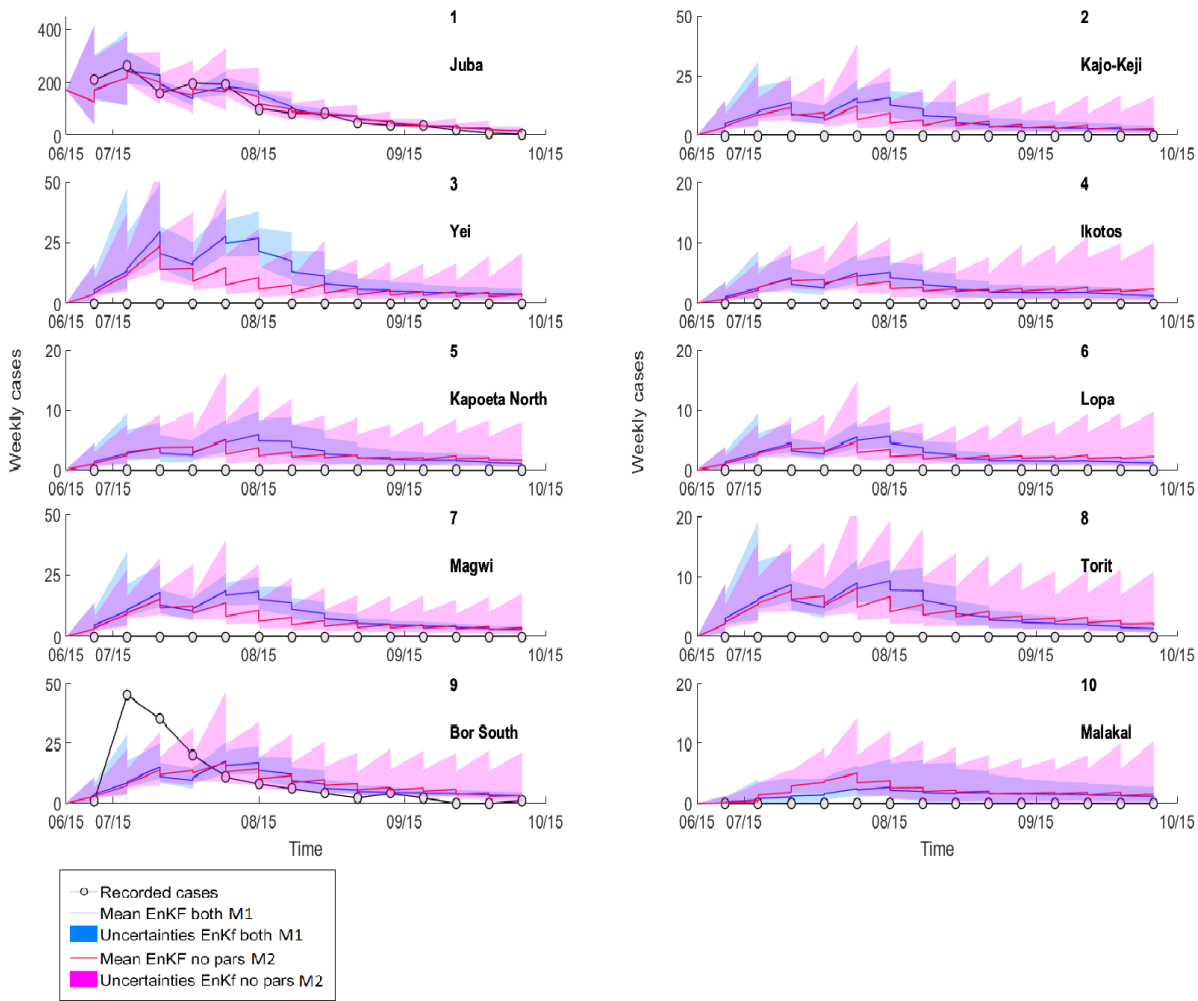


Figure 5.12: Results for 2015 using the new prior in EnKF procedures. Epidemiological curves in the Counties in which cholera was recorded. The simulations offer a good representation of the dynamic of the epidemic in Juba, and a relative low response in cholera-free Counties.

As regards the parameters, focusing on Simulation M1, their variability and uncertainties are higher compared to the trends seen during 2014 simulations. θ , for the sanitation condition and the contamination rate, firstly decreases to a lower frequency 1/7 day, while at the end of the simulation it becomes 1/5 days. Despite the worsening of the sanitation condition through the parameter θ , for consistency of the simulation with the data, the awareness of the population regarding the risk of contracting the illness increases. This is represented by the parameter k , whose value rapidly decreases towards its lower bound 100. Complementary, the mortality rate of bacteria μ_β , subsequently to some oscillations, increases from $0.04 d^{-1}$ to $0.06 d^{-1}$ at the end of the simulation; the initial exposure rate, β_0 whose starting value is 1/3 days, changes to 1/4 days, leading to a lower possibility of contract the infection via ingestion of contaminated food and water. The influence of the rain reduces through the coefficient λ , whose values change from $0.4 d^m m^{-1}$ to $0.3 d m m^{-1}$. Again, the mean value of the loss of immunity rate ρ assesses around $0.009 d^{-1}$, while σ defining the fraction of symptomatic infected follows the reduction of infected, and reduces, after the peak of the epidemic in July, to the mean value 0.07, i.e. the 7% of the people that get in touch with the bacteria showed symptoms. For what concerns the mobility parameters, m decreases in time from 0.2 to 0.12, trying to contain the spatial spreading of the epidemic and let the simulation to be consistent with the data. This behavior of the model is confirmed by the shape factor of mobility D that increases in time, giving more importance to distances as deterrence factors for mobility.

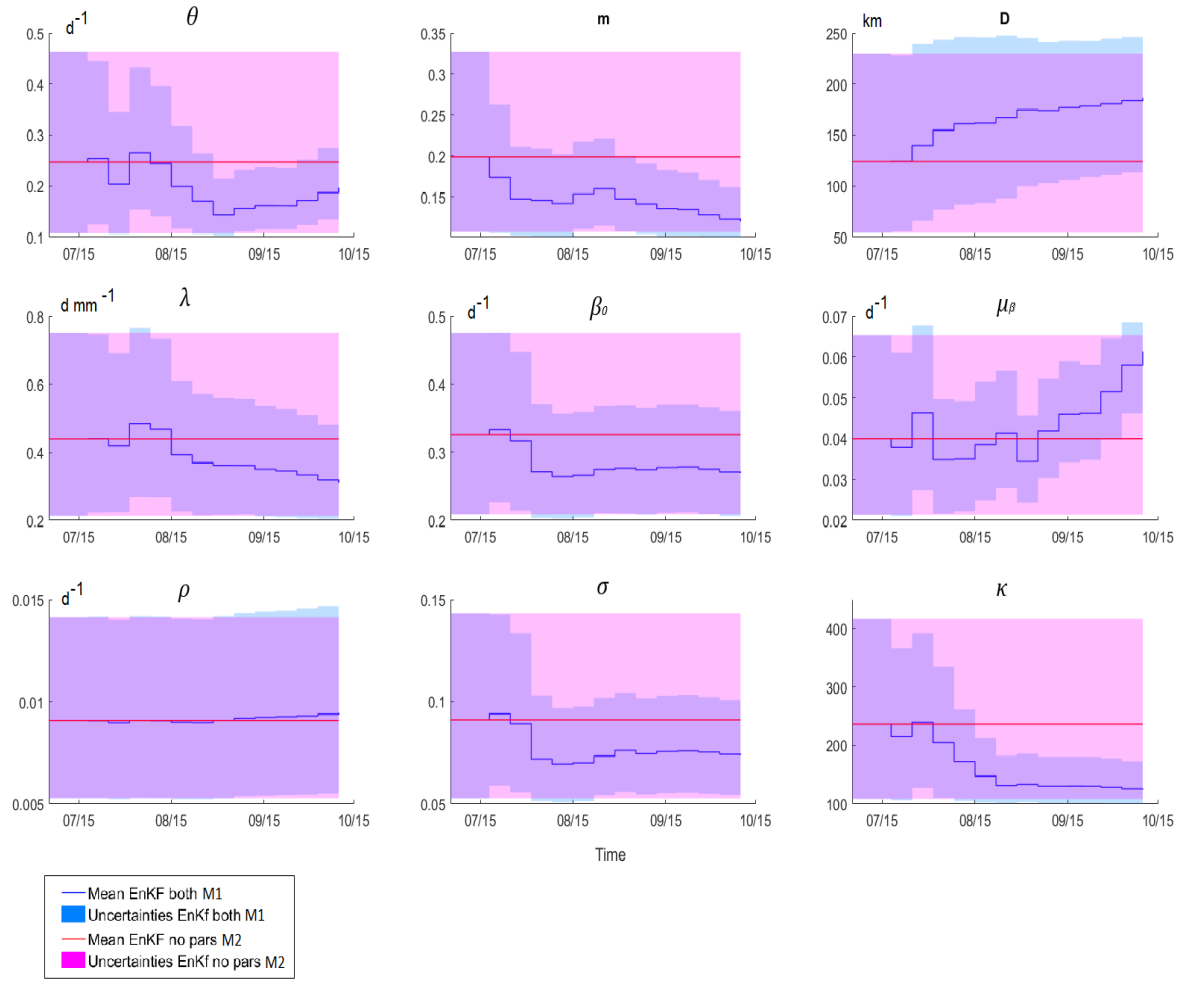


Figure 5.13: Results for 2015 using the new prior in EnKF procedures. Parameters values change in time for Simulation A, while remain constant during Simulation B.

To what concerns the constant values, these coincides with the values of the parameters at the beginning of Simulation M1. Again, in this case, the confidence interval is higher.

Open Loop

Similarly to what we have stated for 2014, the Open Loop in Fig. 5.14 for year 2015 let us understand that, even though the confidence interval of the simulation contains the curve, DA is required for a good agreement of the model with the data.

What stated is confirmed by the RMSE computation, Table 5.4. The Open Loop again results non adequate for this case study. For what concerns EnKF, values of the mean RMSE of the two simulations are really near, and whether is needed to choose, we would prefer the simulations in which parameters are subjected to update in order to reduce the uncertainties, that as we saw, are higher in case of non-update of parameters pdfs.

Table 5.4: RMSE comparison for simulations of year 2015

Simulation	Mean RMSE	Max RMSE
EnKF: parameters update; new prior	11.8527	34.8859
EnKF: no parameters update; new prior	12.1196	34.8859
Open Loop: new prior	64.7669	89.0379

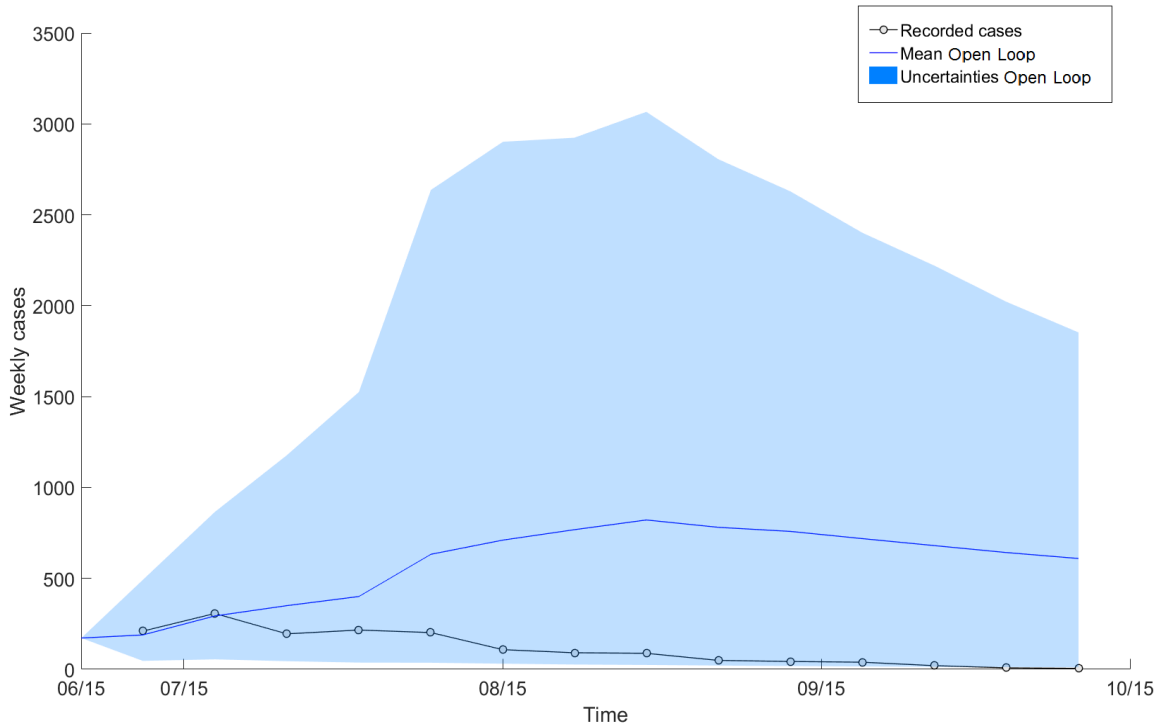


Figure 5.14: Results for 2015 using the new prior in Open Loop simulation. We use random sampling of the parameters to perform the model without the DA. Observations are into the confidence interval, yet the mean do not approaches them.

5.4 Discussion

The SIRB model, together with the calibration technique EnKF, shows an overall good agreement with the cholera cases recorded in the spatial domain under study. The results that we have previously described are sufficiently satisfactory on the global scale (Figs 5.5 - 5.10), yet looking at the spatial level of the Counties, the model has some difficulties to capture the actual trend of the epidemics (see Figs 5.7 - 5.12), with the exception of Juba, whose dynamics are perfectly represented by all the simulations performed.

Focusing on year 2014 at the level of the Counties (Fig. 5.7 on page 55), the simulated epidemiological curves deviate from the real ones especially in Malakal and Torit, in which the model does not reproduce correctly times and numbers of the infection. Looking at the spatial distribution of the recorded cases in 2014, Fig. 2.8, the infection seems to be not spatially correlated, and the possibilities that single travelers moved the epidemic away from its origin site, as for Malakal in 2014, could be high. The same works for the following year, when cases were recorded only in Juba and Bor in 2015 (Fig.2.9). Therefore, one possible reason for this behavior of the model can be found in the mobility. As Ujjiga et al. (2015) identified through their study, travel to cholera outbreak areas is considered as a risk factor. Moreover, previous studies regarding cholera outbreak in Southern Sudan showed that the risk was associated with being a visitor to Juba (CDC, 2009). As we said in Chapter 2, the country is subject to important migratory fluxes that are not that easy to simulate via a simple gravity model. These fluxes move people towards the capital, in which are present PoCs sites, and to other places. In fact, the epidemic started in Juba, far away from Malakal, and that can be reached by flight connections that were not considered in this work. In our mathematical framework it is difficult to simulate cases in more distant areas, as e.g. Malakal, without spreading the infection all over the nodes between these two, as happens for example in Bor South County during 2014 simulations, located in between Juba and Malakal. The gravity model, whose response is shown in Fig. 5.15, let the disease spread more severely in places that are more connected between each other. As the figure shows, Malakal is not directly connected to Juba

and the model is favoring the nodes in Yei and Kajo-Keji County, since the modeled probability of moving towards these is higher. As regards 2015 epidemics, the all zeroes observed data in the counties around Juba that the model uses to corrects the states of the system, try to contain the response in these places and affect the simulation in Bor South, despite this one is well connected to Juba through the mobility model.

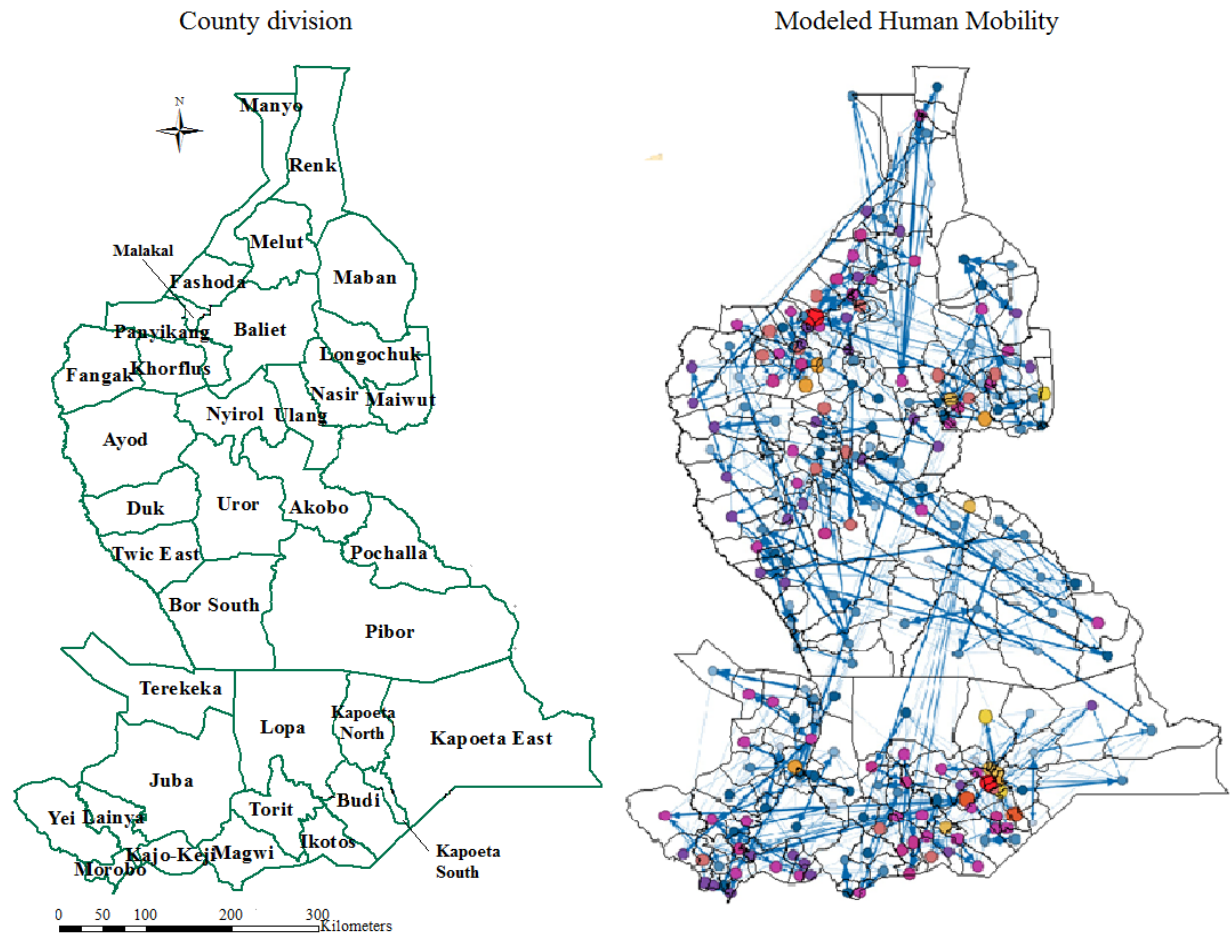


Figure 5.15: Response of the gravity model. From each node i , the thickness of the arrow is proportional to the probability $P > 0.01$ of choosing the node j as destination. The color and magnitude of the nodes is proportional to the number of connections for each node. As nodes are representative of the Payams, the underlying figures highlights the administrative areas. For comparison, the County division used for the calibration is represented on the left.

Furthermore, the migrants fluxes and camps establishment change the distribution of the inhabitants in the areas considered, affecting the position of the nodes in a loop that involves the gravity model.

Last, one should include among the possible reasons for the misfitting between the simulation and the observed data, the biased case reporting or identification. Our analysis includes in fact, all the suspected cases that were recorded among the health facilities. During 2014, when the infection moved from Juba to Malakal, there were no confirmed cases in Jonglei. We should think about the possibility that the bacteria affected displaced people in this state that lived outside the vaccinated PoC camps (Abubakar et al., 2015). Hence, there are reasons to believe that there is some lack of information regarding cases distributed in diverse areas. This hypothesis can be supported by the three cases recorded in Western Equatoria and that were not included in this analysis (see Sect. 2.4): there is no assurance that no other infected were present in that area, considering the fact that, for what we know, no vaccination campaign took place over there. To support this hypothesis, different studies show that education and age can influence people in going to health care infrastructure. As

an example, Luby et al. (2004) reported in their studies, children are less likely to consult a health care practitioner for symptoms of diarrhoeal diseases as cholera.

Conclusions

Improving global access to water, sanitation and hygiene is a critical step to reducing Africa's cholera burden. Vaccinations campaigns are helping people all over the continent and their validity is tested everyday more (e.g. (Luquero et al., 2014; Abubakar et al., 2015)), unfortunately a lot of people still do not have access to them. We argue that epidemiological model can help in understand risk factors and dynamics of transmission and even more, forecast possible new events. Therefore we would like to make the point on our work, suggesting future possibilities and further studies that can help in treating cholera, especially in South Sudan, where the unstable social conditions have lead to another cholera outbreak at the moment of writing this manuscript.

The mathematical model that we proposed was adapted to analyze and to represent the epidemics that affected South Sudan in 2014 and 2015. This deterministic mathematical approach is not exempt from limitations and uncertainties, yet we would like to highlight its potentiality.

The use of DA technique for the calibration of the parameters is an interesting choice that can be supported by its advantages. First, it allows to accelerate the calibration procedure reducing the computational cost compared with other calibration method (e.g. DREAM) (Pasetto et al., 2016). Second, the method admits the parameters to change in time, sequentially updating their values via incorporation of new observations. Looking at their physical meaning, this is preferable in cholera modeling. The exposure rate β_0 , the population awareness on cholera risk factors k and the sanitation conditions θ can actually improve during the time of the disease, acting on the transmission routes and changing the probability of contracting the infection. Especially in this case study, as shown by the results in the previous chapter, the dynamic of the epidemics are better retrieved using the state augmentation technique (see Sect. 3.3.2). In fact, the confidence intervals in all the simulations M2, in which parameters were kept constant, were larger than the ones in simulations M1, in which uncertainties reduced in time. Of course, in this procedure the basic point was to find appropriate domains of variability, resulted definitely smaller than the Haitian prior pdfs first used.

Despite the difficult context and the lack of information that favored the uncertainties, the SIRB model was able to retrieve the trends of the epidemics during both years, capturing numbers and timing. The best agreement with the data was showed for the global curves and for Juba during both years, having the model able to reproduce the epidemiological curves almost perfectly.

As regards the response in the other counties, we already discussed about possible reasons and limitations for what concerns the model for human mobility, which is not able to reproduce the migratory fluxes all over the spatial framework considered. For further understanding of the epidemics, one possibility to go over this problematic can be the incorporation of mobile phone data to understand the role of mass gathering in spreading the infection, as Finger et al. (2016) in the last formulation of the SIRB model. In fact, mobile phone data sets are an important new source of information about the dynamics of populations overall in Africa and provide an opportunity to measure human mobility directly for entire populations (Wesolowski et al., 2015). By the way, according to SSNBS (2012), only the 15% of the Southern Sudanese population posses a phone, and further investigations would be needed to understand whether these data are reliable or have

changed.

Another methodology would be, whether data are available, to adapt and modify the gravity model. On one hand, we could include into the formulation an indicator for the "safety" of the site. In literature, example of the validity of socio-political indicators in modeling mobility to understand spread of disease can be found, as Li et al. (2011) studied for Influenza. On another hand, we could introduce meta-population dynamics to better understand spatial heterogeneity of the disease, as in Xia et al. (2004).

Looking at the limitation of the model, one should include the strong assumptions used to simplify the mathematical framework. As we described in Chapter 3, we consider the population to be at demographic equilibrium. This assumption deletes further stochasticity of host demography, yet it is not realistic in our context. In fact, the high growth rate in the country (see Sect. 2.3.1) should be considered when modeling the year 2015, yet this would required certain data on population size and distribution.

Other assumption that can compromise the results of our approach is the hypothesis of non pre-existing immunity. We are not considering in fact the vaccination campaigns that took place at the beginning of 2014 and during the period in study. Therefore, all the population is considered all the time as susceptible and in risk of contracting the disease. The same works for 2015, in which we are not considering neither the vaccinations, nor the previous year epidemic that create immunity in both symptomatic and asymptomatic infected. Hence, we would like to explore the response of the model introducing either as initial condition during calibration procedure, or as a new equation in the epidemiological model, the recovered individuals that gained immunity and the individuals that in each node obtained immunity through vaccinations. Moreover, as Azman et al. (2016) reported, cholera showed both inside and outside the camp. In order to understand the transmission routes, additional information could be acquired by the conduction of surveys and questionnaires among refugees, together with environmental assessments, to evaluate the use of safe drinking water, personal food and hygiene and the use of improved sanitation facilities. These could be useful tools for understanding risk of disease, as showed by Ujjiga et al. (2015); Swerdlow et al. (1997); Cummings et al. (2012). Moreover, surveys can be helpful in modeling the mobility and understand as well how movements are affected by the rain season, that as we discussed in this work, impede connections between the cities and that we did not took into account.

Finally, another possibility would be to focus on the role of Juba, trying to understand whether there are some phenomenon that enhance the risk of infection in the capital, associated to the risk of spreading the infection allover the Country.

We hope with our work to be helpful and that new and more precise information will be soon available to improve it.

Bibliography

- Abubakar, A., Azman, A. S., Rumunu, J., Ciglenecki, I., Helderma, T., West, H., Lessler, J., Sack, D. A., Martin, S., Perea, W., Legros, D., and Luquero, F. J. (2015). The first use of the global oral cholera vaccine emergency stockpile: Lessons from south sudan. *PLoS Medicine*. doi:10.1371/journal.pmed.1001901.
- Andrews, J. and Basu, S. (2011). Transmission dynamics and control of cholera in Haiti: an epidemic model. *Lancet*, 377:1248–1255. doi:10.1016/S0140-6736(11)60273-0.
- Azman, A., Rumunu, J., Abubakar, A., West, H., Ciglenecki, I., and Helderma, T. e. a. (2016). Population-Level Effect of Cholera Vaccine on Displaced Populations, South Sudan, 2014. *Emerg Infect Dis.*, 22(6). doi:10.3201/eid2206.151592.
- Barabási, A.-L. (2016). *Network science*. Cambridge university press.
- Baratti, E. (2014). *Stima dei parametri di modelli idrologici mediante ottimizzazione dell'utilità*. PhD thesis, Alma Mater Studiorum - Università di Bologna.
- BBC (2016). <http://www.bbc.com/news/world/africa>. News update available online.
- Bertuzzo, E., Azaele, S., Maritan, A., Gatto, M., Rodriguez-Iturbe, I., and Rinaldo, A. (2008). On the space-time evolution of a cholera epidemic. *Water Resources Research*, 44. doi:10.1029/2007WR006211.
- Bertuzzo, E., Casagrandi, R., Gatto, M., Rodriguez-Iturbe, I., and Rinaldo, A. (2010). On spatially explicit models of cholera epidemics. *Interface*, 7(43):321–33. doi:10.1098/rsif.2009.0204.
- Bertuzzo, E., Finger, F., Mari, L., Gatto, M., and Rinaldo, A. (2014). On the probability of extinction of the Haiti cholera epidemic. *Stoch Environ Res Risk Assess*, pages 1–13. doi:10.1007/s00477-014-0906-3.
- Bertuzzo, E., Mari, L., Righetto, L., Casagrandi, R., Gatto, M., Rodriguez-Iturbe, I., and Rinaldo, A. (2012). *An epidemic model for the future progression of the current Haiti cholera epidemic*, volume 14. Provided by the SAO/NASA Astrophysics Data System.
- Bertuzzo, E., Mari, L., Righetto, L., Gatto, M., Casagrandi, R., Blokesch, M., Rodriguez-Iturbe, I., and Rinaldo, A. (2011). Prediction of the spatial evolution and effects of control measures for the unfolding haiti cholera outbreak. *Geophysical Research Letters*, 38(6). doi:10.1029/2011GL046823.
- Beven, K. and Binley, A. (1992). The future of distributed models: Model calibration and uncertainty prediction. *Hydrological Processes*, 6:279 – 298. doi:10.1002/hyp.3360060305.
- Bhattacharya, S., Black, R., Bourgeois, L., Clemens, J., Cravioto, A., Deen, J. L., Dougan, G., Glass, R., Grais, R. F., and Greco, M. e. a. (2009). Public health. The cholera crisis in Africa. *Science*, 324(5929):885. doi:10.1126/science.1173890.
- Camporese, M., Paniconi, C., Putti, M., and Salandin, P. (2009). Ensemble Kalman filter data assimilation for a process-based catchment scale model of surface and subsurface flow. *Water Resources Research*, 45. doi:10.1029/2008WR007031.
- Capasso, V. and Paveri-Fontana, S. L. (1979). A mathematical model for the 1973 cholera epidemic in the European Mediterranean region. *Revue d'épidémiologie et de santé publique*, 27(2):121–32.

- Cazelles, B. and Chau, N. (1997). Using the Kalman filter and dynamic models to assess the changing HIV/AIDS epidemic. *Elsevier - Mathematical Biosciences*, 140:131 – 154. doi:10.1038/ncomms3837.
- CDC (2009). Morbidity and Mortality Weekly Report: Cholera Outbreak in Southern Sudan 2007-2009. Technical report, Centers for Disease Control and Prevention. Available online; accessed on March 2016.
- CIA (2015). South Sudan. Central Intelligence Agency. Available online; accessed on March 2016.
- Codeço, C. T. (2001). Endemic and epidemic dynamics of cholera: the role of the aquatic reservoir. *BMC infectious diseases*, 1:1.
- Collins, R. (2015). South Sudan. <http://www.britannica.com/place/South-Sudan>. Available online; accessed on April 2016.
- Colwell, R. R. (1996). Global climate and infectious disease: the cholera paradigm. *Science*, 274(5295):2025–31.
- Cummings, M. J., Wamala, J. F., Eyura, M., Malimbo, M., Omeke, M. E., Mayer, D., and Lukwago, L. (2012). A cholera outbreak among semi-nomadic pastoralists in northeastern Uganda: epidemiology and interventions. *Epidemiology and Infection*, 140(08):1376–1385. doi:10.1017/S0950268811001956.
- De Rochars, V., Tipret, J., Patrick, M., Jacobson, L., Barbour, K., Berendes, D., Bensyl, D., Frazier, C., D., J., Archer, R., Roels, T., Tappero, J., and Handzel, T. (2011). Knowledge, attitudes, and practices related to treatment and prevention of cholera, haiti, 2010. *Emerging Infectious Diseases*, 17(11).
- Di Molfetta, A. and Sethi, R. (2012). *Ingegneria degli acquiferi*. Springer Science & Business Media. doi:10.1007/978-88-470-1851-8 11.
- Erlander, S. and Stewart, N. F. (1990). *The gravity model in transportation analysis : theory and extensions*. VSP.
- Evensen, G. (1994). Sequential data assimilation with a nonlinear quasi-geostrophic model using monte carlo methods to forecast error statistics. *Journal of Geophysical Research*, 99:10143 – 10162. doi:10.1029/94JC00572.
- Ewens, W. and Grant, G. (2005). *Statistical Methods in Bioinformatics: An Introduction*. Springer Science+Business Media, Inc., 2 edition.
- Finger, F., Genolet, T., Mari, L., de Magny, G. C., Manga, N. M., Rinaldo, A., and Bertuzzo, E. (2016). Mobile phone data highlights the role of mass gatherings in the spreading of cholera outbreaks. *Proceedings of the National Academy of Sciences*, 113(23):6421–6426. doi:10.1073/pnas.1522305113.
- Finger, F., Knox, A., Bertuzzo, E., Mari, L., Bompangue, D., Gatto, M., Rodriguez-Iturbe, I., and Rinaldo, A. (2014). Cholera in the lake kivu region (drc): Integrating remote sensing and spatially explicit epidemiological modeling. *Water Resources Research*, 50(7):5624–5637. doi:10.1002/2014WR015521.
- Gelman, A. and Rubin, D. B. (1992). Inference from Iterative Simulation Using Multiple Sequences. *Statistical Science*, 7(4):457–472. doi:10.1214/ss/1177011136.
- Global Security (2016). South Sudan. www.globalsecurity.org. Available online; accessed on 15-May-2016.

-
- Grawert, E. (2010). *After the Comprehensive Peace Agreement in Sudan*. Boydell & Brewer. isbn:1847010229, 9781847010223.
- Gupta, H., Verma, K., and Sharma, P. (2015). Using Data Assimilation Technique and Epidemic Model to Predict TB Epidemic. *International Journal of Computer Applications*, 128(9):5. doi:10.5120/ijca2015906625.
- Harris, J. B., LaRocque, R. C., Qadri, F., Ryan, E. T., Calderwood, S. B., and Morris, J. (2012). Cholera. *The Lancet*, 379(9835):2466–2476. doi:10.1016/S0140-6736(12)60436-X.
- Inman, J. (2010). *Navigation and Nautical Astronomy for the Use of British Seamen (1849)*. Kessinger Publishing, LLC.
- IRI/LDEO (2016). <http://iridl.ldeo.columbia.edu/>. Climate Data Library. Available online; accessed on 7-April-2016.
- Kalman, R. (1960). A New Approach to Linear Filtering and Prediction Problems. *Journal of Basic Engineering*, 88:35 – 45.
- Kaper, J. B., Morris, J. G., and Levine, M. M. (1995). Cholera. *Clinical microbiology reviews*, 8(1):48–86.
- Kelly, M. (2016). Quick facts: What you need to know about the South Sudan crisis. *Mercy Corps*. Available online, accessed on 19-May-2016.
- Kermack, W. O. and McKendrick, A. G. (1927). *A Contribution to the Mathematical Theory of Epidemics*, volume 115. doi:10.1098/rspa.1927.0118.
- King, A., Ionides, E., Pascual, M., and Bouma, M. (2008). Inapparent infections and cholera dynamics. *Nature*, 454:877–880. doi:10.1038/nature07084.
- Koelle, K., Rodó, X., Pascual, M., Yunus, M., and Mostafa, G. (2005). Refractory periods and climate forcing in cholera dynamics. *Nature*, 436(7051):696–700. doi:10.1038/nature03820.
- Leung, D., Chowdhury, F., Calderwood, S., Qadri, F., and Ryan, E. (2012). Immune responses to cholera in children. *Expert Review of Anti-infective Therapy*, 4(10):435 – 444. doi:10.1586/eri.12.23.
- Li, X., Tian, H., Lai, D., and Zhang, Z. (2011). Validation of the Gravity Model in Predicting the Global Spread of Influenza. *Int J Environ Res Public Health*, (8):3134–3143. doi:10.3390/ijerph8083134.
- Lipp, E. K., Huq, A., and Colwell, R. R. (2002). Effects of Global Climate on Infectious Disease: the Cholera Model. *Clinic Microbiology Reviews*, 15(4):757–770. doi:10.1128/CMR.15.4.757–770.2002.
- Luby, S., Agboatwalla, M., Painter, J., Altaf, A., Billhimer, W., and Hoekstra, R. (2004). Effect of intensive handwashing promotion on childhood diarrhea in high-risk communities in Pakistan. *Journal of the American Medical Association*, 29(1):2547–2554.
- Luquero, F. J., Grout, L., Ciglenecki, I., Sakoba, K., Traore, B., Heile, M., Diallo, A. A., Itama, C., Page, A., Quilici, M., M. A., Eiros, J., Serafini, M., Legros, D., and Grais, R. F. (2014). Use of *Vibrio cholerae* vaccine in an Outbreak in Guinea. *New England Journal of Medicine*, 370(22):2111–2120. doi:10.1056/NEJMoa1312680.
- Mandel, J. (2009). A Brief Tutorial on the Ensemble Kalman Filter. Available online under the GNU Free Documentation License.
- Mari, L., Bertuzzo, E., Finger, F., Casagrandi, R., Gatto, M., and Rinaldo, A. (2015). On the predictive ability of mechanistic models for the Haitian cholera epidemic. *J. R. Soc. Interface*, 12.
-

- Mari, L., Bertuzzo, E., Righetto, L., Casagrandi, R., Gatto, M., Rodriguez-Iturbe, I., and Rinaldo, A. (2012). Modelling cholera epidemics: the role of waterways, human mobility and sanitation. *J. R. Soc. Interface*, 9:376–388.
- Mekalanos J. and Lehman A. (2012). Confronting Cholera. www.hms.harvard.edu/news/confronting-cholera. Available online; accessed on 30-June-2016.
- Miller, C. J., Feachem, R. G., and Drasar, B. S. (1985). Cholera epidemiology in developed and developing countries: new thoughts on transmission, seasonality, and control. *Lancet*, 1(8423):261–2.
- Nelson, E. J., Harris, J. B., Glenn Morris, J., Calderwood, S. B., and Camilli, A. (2009). Cholera transmission: the host, pathogen and bacteriophage dynamic. *Nature Reviews Microbiology*, 7(10):693–702. doi:10.1038/nrmicro2204.
- OpenStreetMap (2015). www.openstreetmap.org. Available online; accessed on April-2016.
- Pasetto, D. (2013). *Reduced order models and Data Assimilation for hydrological applications*. PhD thesis, Università degli Studi di Padova, Dipartimento di Matematica.
- Pasetto, D., Finger, F., Rinaldo, A., and Bertuzzo, E. (2016). Real-time projections of cholera outbreaks through data assimilation and rainfall forecasting. *Submitted to Advances in Water Resources*.
- Porta, M., Lenglet, A., de Weerd, S., Crestani, R., Sinke, R., Frawley, M., Van Herp, M., and Zachariah, R. (2014). Feasibility of a preventive mass vaccination campaign with two doses of oral cholera vaccine during a humanitarian emergency in South Sudan. *Royal Society of Tropical Medicine and Hygiene*. doi:10.1093/trstmh/ztu153.
- Righetto, L., Bertuzzo, E., Casagrandi, R., Gatto, M., Rodriguez-Iturbe, I., and Rinaldo, A. (2011). Modelling human movement in cholera spreading along fluvial systems. *Ecohydrology*, 4:49–55.
- Rinaldo, A., Bertuzzo, E., Mari, L., Righetto, L., Blokesch, M., Marino, G., Casagrandi, R., Murraye, M., Vesenbeckhe, S. M., and Iturbef-Rodriguez, I. (2014). Reassessment of the 2010–2011 Haiti cholera outbreak and rainfall-driven multiseason projections. *PNAS*, page 6602–6607.
- Ross, S. (2010). *A first course in probability*. Pearson Education, Inc., 8 edition. Available online; accessed on 14-July-2016.
- Shaman, J., Karspeck, A., Yang, W., Tamerius, J., and Lipsitch, M. (2013). Real-time influenza forecasts during the 2012-2013 season. *Nature Communication*, 4(2837). doi:10.1038/ncomms3837.
- SSNBS (2010). Southern Sudan Counts: Tables from the 5th Sudan Population and Housing Census, 2008. Technical report, Southern Sudan Centre for Census Statistics and Government of Southern Sudan, Juba, South Sudan.
- SSNBS (2010). Statistical Yearbook for Southern Sudan 2010. Technical report, Southern Sudan Centre for Census Statistics and Evaluation, Juba, South Sudan.
- SSNBS (2012). Key indicators for south sudan. Technical report, South Sudan National Bureau of Statistics.
- SSNBS (2015a). Population Projections for South Sudan 2015 - 2020. Technical report, South Sudan National Bureau of Statistics.
- SSNBS (2015b). Population projections for South Sudan by County 2015 - 2020. Technical report, South Sudan National Bureau of Statistics.

-
- SSNBS (2015c). Population Projections for South Sudan by Payam From 2015 - 2020. Technical report, South Sudan National Bureau of Statistics.
- Sudan Tribune (2015). South Sudan's Kiir appoints governors of 28 new states. www.sudantribune.com. Available online; accessed on April 2016.
- Swerdlow, D. L., Malenga, G., Begkoyian, G., Nyangulu, D., Toole, M., Waldman, R. J., Puhr, D. N. D., and Tauxe, R. V. (1997). Epidemic cholera among refugees in Malawi, Africa: treatment and transmission. *Epidemiology and Infection*, 118(3). doi:10.1017/S0950268896007352.
- ter Braak, C. (2006). A Markov Chain Monte Carlo version of the genetic algorithm Differential Evolution: easy Bayesian computing for real parameter spaces. *Springer Science & Business Media*, (16):239 – 249. doi:10.1007/s11222-006-8769-1.
- Treccani (2016). Sud Sudan. <http://www.treccani.it/enciclopedia/sud-sudan/>. Available online; accessed on 15-May-2016.
- Ujjiga, T. T., Wamala, J. F., Mogga, J. J., Othwonh, T. O., Mutonga, D., Kone-Coulibaly, A., Shaikh, M. A., Mpairwe, A. M., Abdinasir, A., Abdi, M. A., Yoti, Z., Olushayo, O., Nyimol, P., Lul, R., Lako, R. L., and Rumunu, J. (2015). Risk Factors for Sustained Cholera Transmission, Juba County, South Sudan, 2014. *Emerging Infectious Diseases*, 21(10):1849–1852. doi:10.3201/eid2110.142051.
- UN (2015). World Population Prospects: Key findings and advance tables. Technical report, United Nations.
- UNHCR (2016). Global Focus for South Sudan. Technical report, United Nations High Commissioner for Refugees.
- UNMISS (2015). Weekly Flight Schedule Effective June 2010. Technical report, United Nation Mission In South Sudan.
- Upton, G. and Cook, I. (2014). *A dictionary of statistics*. Oxford University Press, 3 edition. doi:10.1093/acref/9780199679188.001.0001. Available online; accessed on 14-July-2016.
- USAID (2005). Juba Assessment: Town Planning and Administration. Technical report, United States Agency for International Development, Juba.
- Vrugt, J. A. (2016). Markov chain Monte Carlo simulation using the DREAM software package: Theory, concepts, and MATLAB implementation. *Environmental Modelling & Software*, 75:273 – 316.
- Vrugt, J. A., ter Braak, C., Diks, C., and Schoups, G. (2012). Hydrologic data assimilation using particle Markov chain Monte Carlo simulation: Theory, concepts and applications. *Advances in Water Resources*, 51:457–478.
- VUVM (2011). World Maps of Köppen-Geiger climate classification. www.koepen-geiger.vu-wien.ac.at. Vienna University of Veterinary Medicine - Institute for Veterinary Public Health. Available online; accessed on 15-July-2016.
- Wesolowski, A., Prudhomme O'Meara, W., Eagle, N., Tatem, A., and Buckee, C. (2015). Evaluating Spatial Interaction Models for Regional Mobility in Sub-Saharan Africa. *PLoS Comput Biol*, 11(7). doi:10.1371/journal.pcbi.1004267.
- WHO (2010). Weekly Epidemiological Record, No. 13, 26 March 2010. Technical report, World Health Organization.
- WHO (2015a). South Sudan cholera outbreak updates. Technical report, World Health Organization. Available online; accessed on February 2016.

WHO (2015b). South Sudan health situation reports. Technical report, World Health Organization. Available online; accessed on February 2016.

WHO & UNICEF (2015). Joint Water Supply and Sanitation Monitoring Programme: 25 years of progress on sanitation and drinking water. 2015 update and MDG assessment. Technical report, World Health Organization and UNICEF. isbn:9789241509145.

World Atlas (2016). Africa - South Sudan. www.worldatlas.com. Available online; accessed on 15-May-2016.

WorldPop (2013). <http://www.worldpop.org.uk/>. Available online; accessed on March 2016.

Xia, Y., Bjørnstad, O., and Grenfell, B. (2004). Measles Metapopulation Dynamics: A Gravity Model for Epidemiological Coupling and Dynamics. *The American Naturalist*, 164(2).